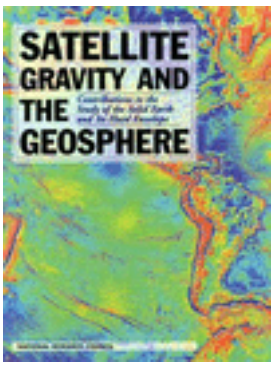

Satellite Gravity and the Geosphere: Contributions to the Study of the Solid Earth and Its Fluid Envelopes

Committee on Earth Gravity from Space, National Research Council

ISBN: 0-309-53866-1, 126 pages, 8.5 x 11, (1997)

SATELLITE GRAVITY AND THE GEOSPHERE

Contributions to the Study of the Solid Earth and Its Fluid Envelope

Committee on Earth Gravity from Space
U.S. Geodynamics Committee
Board on Earth Sciences and Resources
Commission on Geosciences, Environment, and Resources
National Research Council

National Academy Press
Washington, D.C.1997

NOTICE: The project that is the subject of this report was approved by the Governing Board of the National Research Council, whose members are drawn from the councils of the National Academy of Sciences, the National Academy of Engineering, and the Institute of Medicine. The members of the committee responsible for the report were chosen for their special competences and with regard for appropriate balance.

This report has been reviewed by a group other than the authors according to procedures approved by a Report Review Committee consisting of members of the National Academy of Sciences, the National Academy of Engineering, and the Institute of Medicine.

This study was supported by Grant No. NAG 5-3105 between the National Academy of Sciences and the National Aeronautics and Space Administration. Any opinions, findings, conclusions, or recommendations expressed in this publication are those of the author(s) and do not necessarily reflect the view of the organizations or agencies that provided support for this project.

Library of Congress Catalog Card Number 97–67450

International Standard Book Number 0-309-05792-2

Additional copies of this report are available from:
National Academy Press
2101 Constitution Ave., NW
Box 285
Washington, DC 20055
800-624-6242
202-334-3313 (in the Washington Metropolitan Area) http://www.nap.edu

Cover art by Walter Smith, National Oceanic and Atmospheric Administration.
The cover is a color shaded relief image of the Earth's gravity anomaly field. Warm colors (yellow-orange-red) indicate stronger than normal gravity, whereas cool colors (cyan-blue-violet) indicate weaker than normal gravity. Highlights are illuminated from the northwest. The image combines data from EGM96 over land areas with data derived from satellite altimetry (Smith and Sandwell, 1995a) over ocean areas.

Printed in the United States of America
First Printing, September 1997
Second Printing, March 1998

COMMITTEE ON EARTH GRAVITY FROM SPACE

JEAN O. DICKEY, *Chair,* Jet Propulsion Laboratory/California Institute of Technology, Pasadena
CHARLES R. BENTLEY, University of Wisconsin, Madison
ROGER BILHAM, University of Colorado, Boulder
JAMES A. CARTON, University of Maryland, College Park
RICHARD J. EANES, University of Texas, Austin
THOMAS A. HERRING, Massachusetts Institute of Technology, Cambridge
WILLIAM M. KAULA, University of California, Los Angeles
GARY S. E. LAGERLOEF, Earth and Space Research, Seattle, Washington
STUART ROJSTACZER, Duke University, Durham, North Carolina
WALTER H. F. SMITH, NOAA Geosciences Laboratory, Silver Spring, Maryland
HUGO M. VAN DEN DOOL, NOAA Climate Prediction Center, Camp Springs, Maryland
JOHN M. WAHR,* University of Colorado, Boulder
MARIA T. ZUBER, Massachusetts Institute of Technology, Cambridge

Staff

ANNE M. LINN, Senior Program Officer
VERNA J. BOWEN, Administrative Assistant

* Resigned as a committee member on December 1, 1996; served as consultant to the committee through the end of the study.

U.S. GEODYNAMICS COMMITTEE

Staff

BOARD ON EARTH SCIENCES AND RESOURCES

Staff

COMMISSION ON GEOSCIENCES, ENVIRONMENT, AND RESOURCES

Staff

THE NATIONAL ACADEMIES

National Academy of Sciences
National Academy of Engineering
Institute of Medicine
National Research Council

The **National Academy of Sciences** is a private, nonprofit, self-perpetuating society of distinguished scholars engaged in scientific and engineering research, dedicated to the furtherance of science and technology and to their use for the general welfare. Upon the authority of the charter granted to it by the Congress in 1863, the Academy has a mandate that requires it to advise the federal government on scientific and technical matters. Dr. Bruce Alberts is president of the National Academy of Sciences.

The **National Academy of Engineering** was established in 1964, under the charter of the National Academy of Sciences, as a parallel organization of outstanding engineers. It is autonomous in its administration and in the selection of its members, sharing with the National Academy of Sciences the responsibility for advising the federal government. The National Academy of Engineering also sponsors engineering programs aimed at meeting national needs, encourages education and research, and recognizes the superior achievements of engineers. Dr. William A. Wulf is president of the National Academy of Engineering.

The **Institute of Medicine** was established in 1970 by the National Academy of Sciences to secure the services of eminent members of appropriate professions in the examination of policy matters pertaining to the health of the public. The Institute acts under the responsibility given to the National Academy of Sciences by its congressional charter to be an adviser to the federal government and, upon its own initiative, to identify issues of medical care, research, and education. Dr. Kenneth I. Shine is president of the Institute of Medicine.

The **National Research Council** was organized by the National Academy of Sciences in 1916 to associate the broad community of science and technology with the Academy's purposes of furthering knowledge and advising the federal government. Functioning in accordance with general policies determined by the Academy, the Council has become the principal operating agency of both the National Academy of Sciences and the National Academy of Engineering in providing services to the government, the public, and the scientific and engineering communities. The Council is administered jointly by both Academies and the Institute of Medicine. Dr. Bruce Alberts and Dr. William A. Wulf are chairman and vice chairman, respectively, of the National Research Council.

www.national-academies.org

Preface

For the past three decades, it has been possible to measure the Earth's static gravity field from satellites. Such measurements have been used to address many important scientific problems, including the internal structure of the Earth and geologically slow processes such as mantle convection. In recent years, improved accuracy of satellite gravity measurements has made it possible to resolve the time-varying component of the global gravity field. These temporal variations are caused by dynamic processes that change the mass distribution in the Earth, oceans, and atmosphere, and could potentially be used to study a new class of important scientific problems.

The Committee on Earth Gravity from Space was formed under the auspices of the National Research Council's U.S. Geodynamics Committee to undertake the following tasks:

1. evaluate the potential for using satellite technologies to measure the time-varying component of the gravity field;
2. assess the utility of an improved global gravity field in general, and the time-varying component in particular, for addressing problems of interest to the earth science, natural hazards, and resource communities; and
3. determine what complementary data are needed to increase the usefulness of satellite-derived gravity data.

With regard to the first charge, the committee reviewed approximately a dozen mission concepts that were planned or envisioned by investigators in the United States and Europe. We grouped the missions into broad categories and developed a "generic" mission scenario for each category. In the course of our investigation it became clear that future technological refinements might yield more information than is currently feasible, so we expanded our list of generic mission scenarios to include future possibilities as well as current ones.

We investigated the trade-offs in orbit design that affect the spatial and temporal resolution of the mission, and chose the altitudes for our generic missions. Mission resolutions were estimated assuming a white-noise error source in the measurements and an isotropic distribution of errors over the Earth. These assumptions simplified the committee's work and left the results generic and not tied to a specific mission proposal. The white noise levels we chose were calibrated initially so that the results corresponded closely with more detailed mission simulations in the published literature (reviewed in Chapter 2). We then adjusted the noise levels to reflect what we thought was currently feasible or likely from future technology,

and asked the scientists and engineers involved in the design of current missions to review our estimates. Based on that review, we made some refinements in the white noise levels and added recommendations about ancillary acceleration and tracking data. We believe that this process has yielded results that are sufficiently generic to be broadly useful, but that also accurately reflect the capability of current technology.

The committee addressed its second and third charges by focusing on two classes of scientific problems: (1) fields of study that would be significantly advanced by a dedicated satellite gravity mission, and (2) fields that would benefit from improved gravity data but that would also require ancillary data to interpret the results. The committee also considered phenomena that move mass, but that are not currently amenable to study with satellite gravity data because of small size, high speed, or difficulty in isolating the relevant geophysical signal. A large number of natural hazards fall into this category. With a few exceptions, these phenomena are not discussed in this report

Because relatively little has been written on the application of the time-varying component of the gravity field to scientific problems, it was necessary for the committee to conduct a substantial amount of original research and to develop forward models. I would like to extend my appreciation to the committee, which undertook the demands of this study with collegial enthusiasm and a remarkable ability to work across disciplines. Each member made an important and unique contribution to the report Special thanks go to Richard Eanes, who had the time-consuming and difficult task of generalizing a dozen proposed or envisioned gravity missions into generic mission classes, and John Wahr, who modeled (and remodeled) all the time-varying phenomena discussed in this report. Although John had to leave the committee in December 1996 to honor a previous commitment, he continued, as a consultant, to complete the final model runs on behalf of the committee. The committee also expresses it sincere appreciation to the staff of the Board on Earth Sciences and Resources, and particularly to Anne Linn, Study Director of this project, for a job superbly done.

Finally, I would like to thank the individuals who made presentations to the committee or who provided input to the study. They include Knut Aagaard, Peter Bender, Srinivas Bettadpur, Bruce Bills, David Bromwich, Frank Bryan, William F. Budd, Steve Castles, Ben Chao, T.C. Chen, Tom Clark, Oscar Colombo, Ab Davis, Mike DiPirro, Danon Dong, Mario B. Giovinetto, Arnold Gordon, Brad Hager, Gordon Hamilton, K.H. Ilk, Yu Jin, Masao Kanamitsu, Günther Können, Steve Marcus, Marcia McNutt, Mark Meier, Bill Melbourne, P.C.D. Milly, Mery Molenaar, RS. Nerem, Lauri Newman, Denis O'Brien, Ho Jung Paik, Erricos Pavlis, Dick Rapp, Mark Richards, Rick Rosen, Suranjana Saha, Jae Schemm, Peter Shirron, Dave Smith, Detlef Stammer, Court Stevenson, Byron Tapley, Jim Titus, Kevin Trenberth, Michael Watkins, Raymond Willemann, and Victor Zlotnicki.

Jean o. Duckey

Chair

Contents

Satellite Gravity and the Geosphere

Contributions to the Study of the Solid Earth and Its Fluid Envelope

Executive Summary

The Earth is a dynamic system constantly undergoing change. As the processes of change affect the Earth's topography—the heights of land, ice, and ocean surfaces—they also modify the distribution of mass within the Earth and consequently alter its gravitational field. The unique contribution of gravity is to discriminate among causes of variation in topography—for example, between thermal expansion and mass inflow as sources of a rise in sea level. Studies of the Earth's static and temporally varying gravity field can yield improved understanding not only of the Earth's interior, but also of its external envelope—its ice, water, and air. However, time-varying effects are three to four orders-of-magnitude smaller than the static field variations, so dense temporal and spatial coverage and highly accurate measurements are necessary. These can be obtained only from space.

The static (i.e., essentially constant in historic time) gravity field is affected by processes over a wide range of scales, from global (10,000 km) for mantle convection to regional (30 km) for tectonic, magmatic, and sedimentary processes. An improved knowledge of the static gravity field would help to resolve deep crustal and mantle structure and to understand plate tectonic processes, such as the structure and thermal state of ridges and trenches and the patterns of mantle convection. Additionally, a more accurately known geoid would lead to an improved mapping of the dynamic topography of the ocean, which would in turn allow an improved determination of ocean circulation and an enhanced understanding of ocean dynamics. An improved gravity field would also lead to better orbits and reference geoids for the lower-altitude-altimeters dating back to the 1985 Geosat mission.

The much smaller time-dependent component of gravity is also affected by processes on a wide range of scales, most of them entailing lateral transfers of water. Determining and understanding these transfers is a high priority of geophysicists studying climate and related phenomena; indeed, second only to studies of the radiative balance of the atmosphere. Processes causing large enough transfers to be measurable include ocean circulation, annual cycles of snow pack and groundwater, post-glacial rebound, sea-level rise, and possibly melting of the ice sheets.

In the past two decades, the earth-science community has called for improved measurements of the global gravity field (e.g., Nerem et al., 1995; National Aeronautics and Space Administration [NASA], 1987; National Research Council [NRC], 1979, 1982.) The Committee on Earth Gravity from Space concurs in that call and offers the following new findings, which address the committee's charge to examine new technological advances, the new scientific questions that could be addressed by a state-of-the-art gravity mission, and the benefits of complementary data (see Preface for details). Our findings were based on the consideration of five generic mission scenarios, new modeling results, and a literature review.

BENEFITS OF A DEDICATED SATELLITE GRAVITY MISSION

Fields of study that would be significantly advanced by a dedicated satellite gravity mission include the following:

- ***Ocean Dynamics.*** Ocean heights measured by current satellite altimetry are approaching ~10 mm accuracy, from which the horizontal pressure gradient uncertainty increases with decreasing length scale. Nevertheless, present geoid slope errors are much larger at resolutions shorter than about 3000 km. This prevents the accurate measurement of absolute surface pressure gradients from which ocean currents are computed A satellite gravity measurement can eliminate the geoid uncertainty in horizontal pressure gradients at much shorter scales (to about 300 km). It would also allow recomputation of accurate altimetric orbits for past satellites, back to 1985, permitting studies of long, global-sea-level time series. A time-varying gravity measurement would allow the determination of seafloor-pressure variations over the world's oceans at spatial scales of a few hundred kilometers or longer. This would be useful for inferring variable deep ocean currents and, when combined with altimetry measurements of sea-surface variations, would place a powerful constraint on models of ocean circulation.
- ***Continental Water Variation*** (including snow pack and groundwater). Seasonal and annual variations in groundwater and soil-moisture levels can potentially be measured with a high level of accuracy at subcontinental length scales. More accurate detection of these variations would be of great value in forecasting conditions for agriculture, as well as developing scientific insight into hydrologic cycles. Gravity data would also be valuable for monitoring secular water-level decline in aquifers.
- ***Sea-Level Rise.*** Measurement of the ocean geoid would enable determination of the nonsteric component (i.e., caused by the addition of water to the oceans) of sea-level rise. In addition, estimates from tide gauges would be much improved by more accurate knowledge of post-glacial rebound (see below).

  Changes in the masses of the Antarctic and Greenland ice sheets are the major unknown contributions to sea-level rise. Gravity measurements (particularly in combination with a laser-altimeter mission) would yield a much-improved determination of those contributions.
- ***Post-Glacial Rebound.*** Accurate gravity measurements, especially at long wavelengths, would lead to major improvement in the knowledge of mantle rheology and its lateral variations.

Fields of study that would benefit from improved gravity data but that require ancillary data to increase the usefulness of the gravity data include the following:

- ***Structure and Evolution of the Crust and Lithosphere.*** Gravimetry is an important contributor, supplementing the findings of geology, seismology, and topography. Satellite gravity could help to validate and adjust conventional terrestrial gravity; however, GPS-located airborne gravimetry, which provides higher spatial resolution than satellite techniques, is more appropriate in areas lacking gravimetry.
- ***Mantle Dynamics and Plumes.*** The factors currently limiting progress in this field are our understanding of the relationship among gravity anomalies, seismic tomography, and mantle convection, and our ability to simulate realistic convection scenarios on a computer. However, refinement of the gravity field may eventually place tighter constraints on the problem.

Atmospheric dynamics is an area of special consideration. Accurate measurement and modeling of surface atmospheric pressure, a direct measure of the atmospheric mass, is needed to unravel the atmospheric gravity signal from the hydrologic and glacial signals of interest. Although pressure measurements in most areas are sufficiently accurate to permit advances in hydrology and glaciology, some areas of interest (e.g., Antarctica) have few barometers. It is possible to use gravity measurements to learn more about the atmosphere, but extending barometric networks would provide the best return on available resources.

The contributions that a gravity mission could make to the study of these processes are discussed in more detail below, following the discussion of mission designs considered in this report

MISSION SCENARIOS AND MEASUREMENT TECHNIQUES

All satellite gravity missions are constrained by fundamental trade-offs in temporal and spatial resolution that depend on orbital altitude, ground-track pattern, and mission lifetime. We considered three mission designs which could be built, launched, and operated at a reasonable cost (order $100M) today, and two mission designs which require further techno

logical development. These designs offer high resolution at lower cost than other systems described in the past, due to improved technologies and the fact that very low orbits and expensive "drag-free" designs are no longer called for.

Two broad categories of mission designs, gravity gradiometry and satellite-to-satellite tracking, were considered. Both of the categories were subdivided into "generic" missions, based on the technology used and the mission duration. Gravity gradiometry, which measures the differences in acceleration of two masses within the same spacecraft, was divided into two missions:

- ***Spaceborne Gravity Gradiometry (SGG).*** An SGG mission would yield a significant improvement over current results to degree 155 (250 km wavelength) at an orbital height of 400 km and to degree 215 (180 km wavelength) at 300 km. However, currently estimated accuracies are poorer than for the satellite-to-satellite tracking missions for degrees less than 25 (1600 km wavelength). The launch vehicle allowable within a reasonable cost cap limits the size of the dewar for current gradiometer technology to one sufficient for only a year lifetime. Hence the SGG mission is of limited value for the study of temporal variability.
- ***Extended Spaceborne Gravity Gradiometry (SGGE).*** A mission using a larger launch vehicle and/or more miniaturized gradiometer could extend the lifetime to five years, and thus would permit the detection of temporal gravity variability on seasonal and interannual time scales. However, the accuracy would have to be improved to be competitive with the satellite-to-satellite tracking missions.

Satellite-to-satellite tracking utilizes differential tracking of two satellites and thereby measures orbital perturbations; accelerometers are required to remove atmospheric drag effects. Three missions were considered:

- ***High-Low Microwave Tracking (GPS).*** In the immediate future, such a mission would depend on the Global Positioning System (GPS) for the high satellite. A mission flown at an altitude of 400-500 km would yield significant improvements over the best current Earth-gravity models at harmonic degrees less than 25 (1600 km wavelength), whereas a mission flown at 300 km would be useful for degrees up to 30 (1300 km wavelength). A system much more accurate than GPS would be of great value to geodesy and gravimetry and is technically feasible, but probably much more expensive than tolerable for these applications.
- ***Low-Low Satellite-to-Satellite Microwave Tracking (SST).*** The SST mission is highly accurate at long and moderate wavelengths (10,000 to 1600 km), at which it produces more accurate geoid heights and gravity anomalies than the SGG, SGGE, and GPS missions. Also, the mission lifetime (estimated to be five years) permits the effective determination of many important time-varying effects.
- ***Low-Low Satellite-to-Satellite Laser Interferometry (SSI).*** The anticipated results from the SSI mission are the best of the five scenarios studied. They are an order of magnitude better than the SST results at all wavelengths considered and two orders of magnitude better than SGG at long wavelengths. However, both SST and SGG involve mature technologies, whereas SSI requires additional development (e.g., order of magnitude improvements are needed in accelerometer accuracy and laser-cavity thermal noise at low frequencies) and proof-of-concept, which would delay a mission some years compared with the other techniques.

OCEAN DYNAMICS AND HEAT FLUX

- The SGG, SST, and SSI missions at an orbital altitude of 400 km offer dramatic improvements in the knowledge of the absolute dynamic topography and surface circulation that can be obtained from satellite altimetry. The most significant improvement will come at basin scales (300-3000 km), at which the geoid determination will be virtually eliminated as an error source. The orbital height needed to resolve smaller-scale phenomena, such as western boundary currents, would need to be impractically low. *In situ* techniques, such as airborne or shipborne gravimetry, both with GPS positioning and controlled acceleration environment, appears more practical. Studies in ocean regions with a strong barotropic component will benefit from knowledge gained from the static geoid. These include the recirculation cells in the subtropical gyres of the western Atlantic, the Kuroshio Current, the Agulhas Current, and the Antarctic Circumpolar Current.
- Most of what is known about the ocean occurs in the upper 500 meters. Studies suggest that uncertainties in the deep circulation and heat and mass transport will be reduced by a factor of two or more in oceanographic regions that are data sparse. Part of this reduction comes from an improvement in estimates of

surface currents. For example, the geostrophic advective terms in the mixed-layer heat budget would be resolvable with an uncertainty of less than 10 Wm^{-2}.

- The combination of altimetry and gravity will allow the separation of the steric and mass components of sea-level rise. This separation will substantially increase the usefulness of sea-level measurements in testing ocean models and constraining ocean circulation.
- Interesting and detectable signals that indicate changes in sea-floor pressure averaged over spatial scales of a few hundred kilometers and larger are expected. These will allow the detection of abyssal ocean current variations with seasonal to interannual time scales. Detection of these phenomena requires a multi-year mission lifetime and high accuracies at long wavelengths. These requirements give priority to SST or SSI over an SGG-type mission.

SOLID EARTH PROCESSES

- Satellite gravity measurements from four of the five generic missions (SGG, SGGE, SSI, and SST) would constrain properties of mantle convection on scales as small as 200 km (half wavelength). An accuracy of ~10^{-2} mGal would be met for resolutions larger than 300-400 km, which would permit small, though important, variations in thermal structure to be characterized, thus helping to distinguish between various models of mantle structure. A one-mGal accuracy at length scales of 500-1000 km would resolve discrepant estimates of the depths of continental roots and would also help to distinguish between models of mantle flow. Gravity resolution of approximately 1 mGal over length scales of order ~120 km would help constrain the depths of origin of hotspot mantle plumes, which are a major source of intraplate volcanism and enhanced heat flow.
- The best satellite missions for regional tectonics are SGG, SSI, and SST. In a 300-km orbit, the SGG missions provide marginally better resolution than the SST mission for resolutions finer than 300 km.
- The recent availability of gravity data from former communist nations will help elucidate interesting geologic structures in remote regions such as the Himalayas and the Tibetan Plateau. Satellite gravity can help to put these data on a unified datum. Satellite gravity data could be used elsewhere also to calibrate existing terrestrial and marine gravity measurements, improving their continuity across political boundaries and shorelines by several milliGals, which would significantly improve the accuracy of the global terrestrial gravity database.
- The SST and SSI missions would provide the data needed to resolve differences between models of lower-mantle viscosity and to separate the effects of post-glacial rebound from the effects of other processes on sea-level rise, such as changes in ice sheets, groundwater, and surface water. These applications require the highest accuracy at the longest wavelengths. Only SST and SSI fulfill this need. A multi-year mission is essential.
- Improvements in the application of gravity data to studies of the crust and lithosphere require scales appreciably smaller than 200 km. Differential GPS measurements can contribute to these surveys by accurately controlling the altitudes of airborne gravimetry.

WATER CYCLING

Gravity missions can provide estimates of changes in water storage over spatial scales of several hundred kilometers and larger that would be accurate to 10 mm or better. These would benefit the Global Energy and Water Cycle Experiment (GEWEX) directly and would be useful to hydrologists for connecting hydrological processes at traditional length scales (tens of kilometers and less) to those at longer scales. The main measurables related to these processes are groundwater and snow pack. Improved knowledge thereof would enhance agricultural productivity by assessing water available for irrigation. Water storage is important also to meteorologists because of the effect of soil moisture on evapotranspiration. SST and SSI missions are more accurate than SGG missions at long wavelengths and thus are more useful than SGG for hydrology applications.

SEA-LEVEL RISE AND GLACIOLOGY

- The sources of global sea-level rise (between 1.0 and 2.5 mm/yr over the last century) are uncertain; most, but not all, of the likely mechanisms involve the redistribution of mass from the continents to the ocean. Gravity measurements can help to discriminate between these sources through the continual monitoring of geoid changes, not only on global scales, but also on regional and basin scales. From an SST or SSI type mission (five-year mission assumed), an increasing mass of water in the ocean equivalent to 0.1 mm/yr of sea-level rise can be measured.

- Gravity changes in Greenland and Antarctica reflect changes in ice-sheet mass, but there are other phenomena that need to be evaluated to recover the mass loss to the oceans: secular post-glacial rebound, interannual variability in snowfall, and the effect of atmospheric pressure variations. (a) Post-glacial rebound could be partly separated from ice-mass changes with the aid of a network of GPS receivers on the land surface, models of rebound that use improved determinations of mantle viscosity provided by the gravity mission, and comparisons with satellite laser altimetry. (b) Separation of interannual mass changes from true secular changes will be aided greatly by the continually improving calculations of mass input to the ice-sheet surfaces from measurements of moisture-flux divergence around the perimeters of the ice sheets. (c) The removal of pressure effects over Antarctica and other remote areas will become more effective as the number of automatic weather stations in the interior of the continent increases. (d) Gravity measurements would be most effective in combination with the observations planned for NASA's Laser Altimeter Mission. Together, an accuracy of 0.1 mm/yr in the determination of the contribution of the ice sheets to sea-level change should be attainable.
- Satellite gravity measurements are capable of yielding valuable information about the mass balance of individual drainage systems within the Antarctic ice sheet, as well as of the ice sheet as a whole. Glaciologists could use such information to test models of ice dynamics, which are essential to the prediction of future sea-level change.
- Satellite gravity could be used to study secular, interannual, and seasonal changes in the mass of ice and snow in regions characterized by a large number of glaciers and ice caps. A prime example is the glacier system that runs from the Kenai Peninsula in southern Alaska down to the coastal ranges of the Yukon and British Columbia.
- Accurate evaluation of post-glacial rebound models, together with improved ocean circulation models, should remove significant errors from old tide-gauge records, thus gaining almost a century of sea-level data.

THE DYNAMIC ATMOSPHERE

- The atmosphere is currently the best measured fluid of any the Earth's subsystems. This fact is key in unraveling the effects of the other subsystems (such as the hydrological cycle and the mass balance of the Antarctic ice sheet) involved in gravity variations. With increasing accuracy in gravity measurement, precise knowledge of the uncertainty in atmospheric surface pressure on seasonal, annual, and secular time scales becomes increasingly important.
- Reliable, extended-range forecasting, which would require interactive coupling between the atmosphere and the water in soils and the ocean, would benefit from hydrological constraints and improved understanding of ocean dynamics.
- Gravity measurements with high temporal and spatial resolutions may improve the atmospheric databases and aid in the verification of models in areas where atmospheric measurements are lacking. But it would be much more effective to have a global network of barometers, sufficient to remove the atmospheric signals from the gravity data.

A TOOL FOR SCIENCE

All five mission scenarios considered in this report offer significant improvements in the static gravity field that are necessary for several important applications. These include:

- An improved reference frame for defining position coordinates.
- Better calculation of orbits for other remote-sensing applications, such as altimetry and synthetic-aperture-radar interferometry.
- A more accurate geoid, the equipotential surface to which land elevations ideally refer and to which ocean circulation is referred.
- The adjustment and datum correction of regional terrestrial, marine, and airborne gravity-survey data.

As shown in the examples above, satellite gravity measurements can provide unprecedented views of the Earth's gravity field and, given sufficient duration, its changes with time. Not only can they provide a truly global integrated view of the Earth, they have, at the same time, sufficient spatial resolution to aid in the study of individual regions of the Earth. Together with complementary geophysical data, satellite gravity data represent a "new frontier" in studies of the Earth and its fluid envelope.

1

Introduction

SCIENTIFIC OVERVIEW

The Earth is a dynamic system—it has a fluid, mobile atmosphere and oceans, a continually changing distribution of ice, snow, and groundwater, a fluid core undergoing hydromagnetic motion, a mantle undergoing both thermal convection and rebound from glacial loading of the last ice age, and mobile tectonic plates. These processes affect the distribution of mass in the Earth and produce variations in the Earth's gravitational field on a variety of spatial and temporal scales (Figure 1.1). Highly accurate measurements of the Earth's gravity field made with appropriate spatial and temporal sampling can thus be used to better understand the processes that move mass within the Earth, and on and above its surface.

In this report the Committee on Earth Gravity from Space explores the scientific questions that could be addressed with a better global gravity field. Traditionally, the gravity field has been treated as essentially steady-state, or "static," over human lifetimes because over 99% of the departure of the field from a rotating fluid figure of the Earth's mass, mean radius, and moment-of-inertia is static in historic time. The static field is dominated by irregularities in the solid Earth caused by convective processes that deform the solid Earth on time scales of thousands to millions of years. Spaceborne gravity measurements have already led to dramatic advances in recent years in the understanding of the structure and dynamics of the core and mantle, the thermal and mechanical structure of the lithosphere, ocean circulation, and plate tectonics. The substantial improvements in the accuracy of static field measurements that would result from the satellite gravity missions we discuss in this report would allow geophysically important smaller-scale features to be resolved and, by improving the geodetic reference frame, would greatly enhance other types of satellite measurements as well.

Nevertheless, it is not in the improved measurement of the static field that we envision the most dramatic advances arising from the next generation of gravity satellites, but in the examination of the remaining 1% of the departure of the gravity field, which is caused by processes that vary on time scales ranging from hours to thousands of years. Temporal variations are caused by a variety of phenomena that redistribute mass, including tides raised by the Sun and Moon, and post-glacial rebound (i.e., creep in the mantle in response to the geologically recent removal of ice sheets) (Figure 1.2). The hydrosphere-oceans, lakes, rivers, groundwater—is the source of much of the irregular variations in the time-varying mass distribution from sub-daily (tides) to long-term (aquifer depletion). Variations of mass within the atmosphere are manifested as surface pressure and contribute significantly at seasonal and other time scales. The cryosphere—the part of the Earth's surface that is perennially frozen—also has seasonal and interannual variations, as well as a long-term secular effect. Particularly exciting is the potential to study sea level changes, post-glacial rebound, deep circulation of the

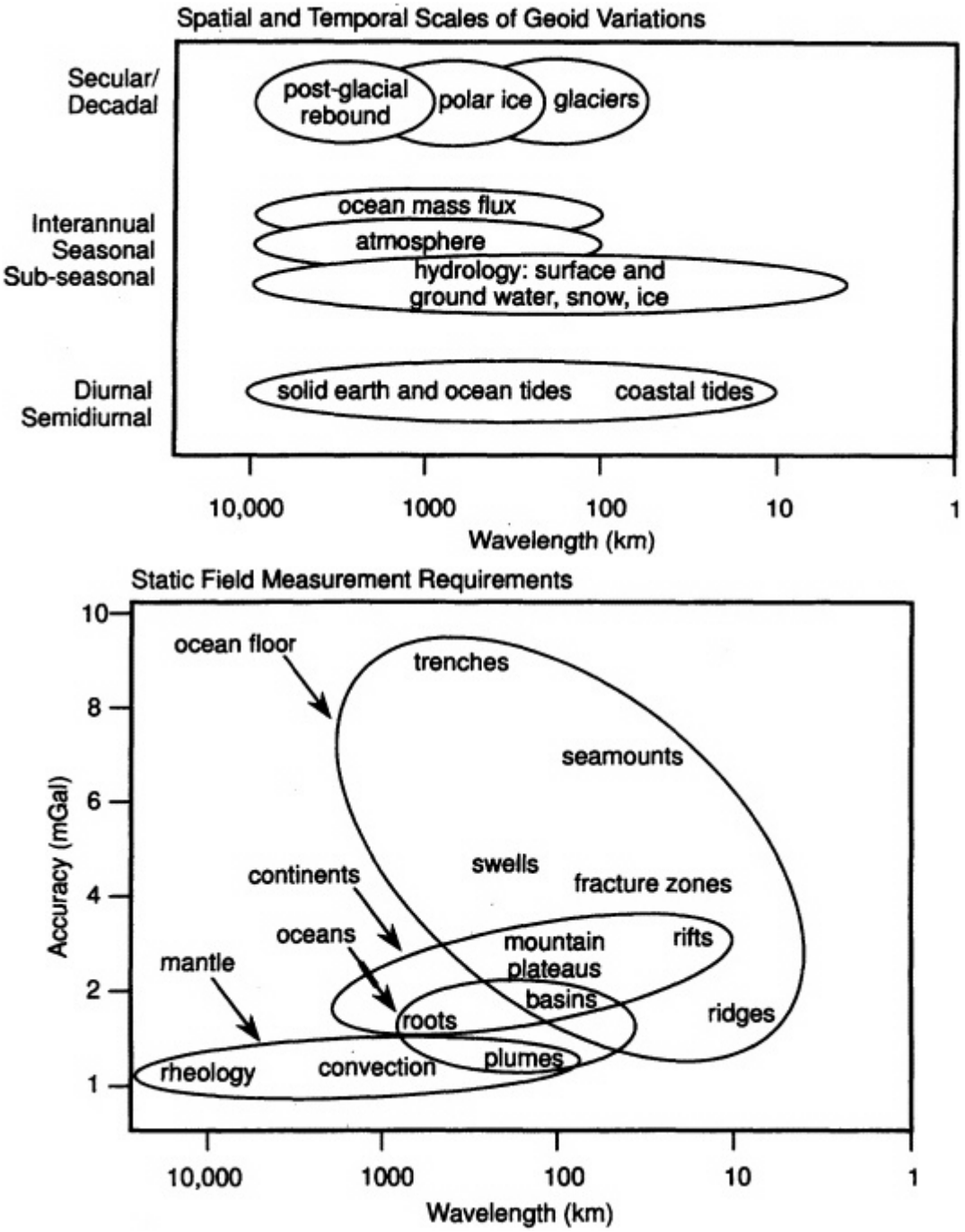

FIGURE 1.1
(Above) Geophysical phenomena that cause measurable temporal and spatial variations in the Earth's gravity field. Adapted from Bettadpur and Tapley (1996a). (Below) Summary of requirements for static gravity-measurement accuracy as a function of wavelength, adapted from NASA (1987).

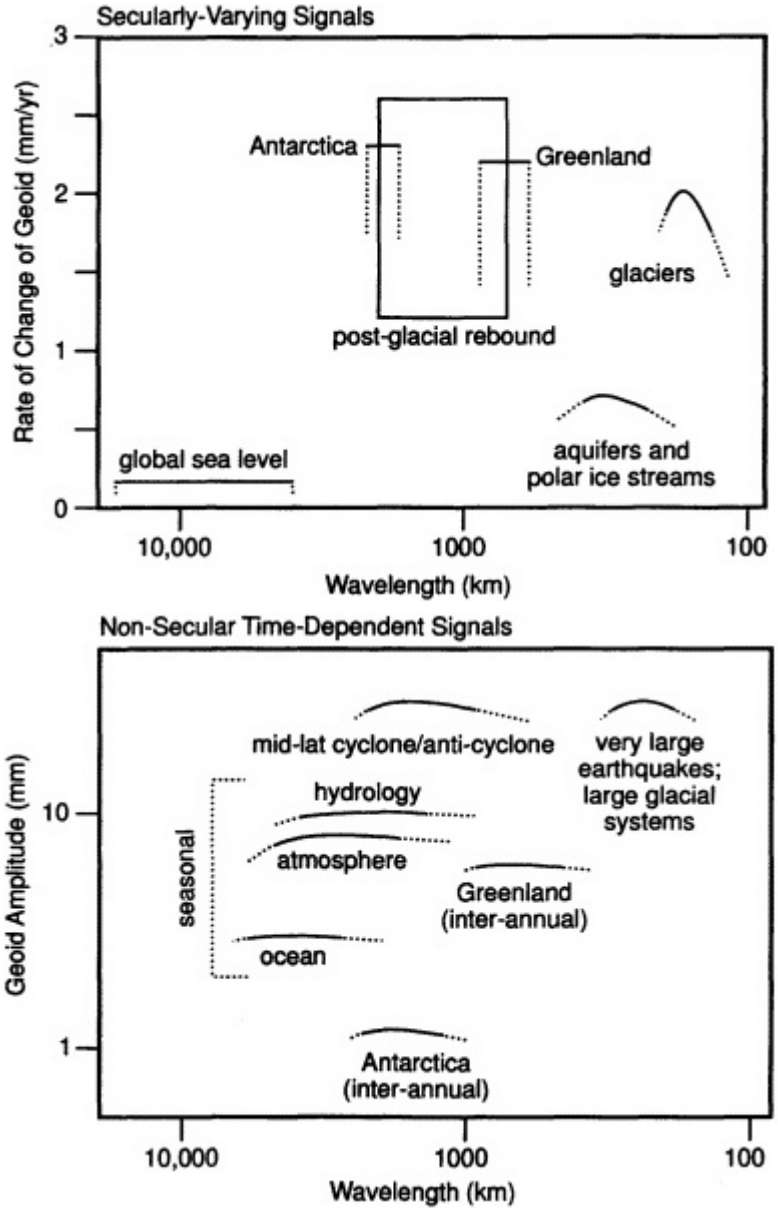

FIGURE 1.2

(Above) This figure indicates some of the expected sources of variability in the Earth's gravity field that would appear to vary linearly in time over a few years of observations. Each mechanism is represented in the figure by the amplitude of its contribution to the rate of change in the geoid (given on the y axis), and by the typical horizontal wavelengths that characterize its contribution to the geoid (the x-axis). For localized mass anomalies (e.g., aquifers, glaciers, etc.), we have chosen the approximate radius of the anomaly as the measure of the horizontal resolution. There can be a considerable spread in the geoid contributions within any one of the indicated categories. For example, there are many glacier systems around the globe, some that cause a notable secular change in the geoid and some that do not. The curve in the figure that represents the effects of glaciers is meant to indicate a crude upper bound of the likely effects of the different glacier systems. (Below) Similar to above figure, except that these are the sources of geoid variability that would not appear to vary linearly in time over a few years.

oceans, and changes in groundwater levels. Many of these have application to issues of importance to society like global change and the availability of natural resources.

The phenomena that produce static and temporally-varying gravity field signatures occur at spatial scales ranging from a few kilometers to tens of thousands of kilometers (Figures 1.1 and 1.2). At the longest spatial scales, large-scale processes such as sea-level change, mantle convection, and ocean and atmosphere circulation are important, whereas studies of lithospheric features (e.g., ridges, fracture zones, swells, trenches), ice-sheet flow and mass-balance, western boundary currents, and aquifers require resolutions of about 500 km or better. High resolutions, of course, require relatively low satellite orbits. On the other hand, determination of temporally varying phenomena improves as the time span of the measurements increases. Consequently, as we discuss further in this report, there are trade-offs to be evaluated, in selecting orbital parameters for a specific mission, that depend on the particular purposes and goals of that mission.

Throughout much of this report we consider gravity effects expressed as a spectrum with amplitudes as functions of wavelength, as in the previous paragraph and in Figures 1.1 and 1.2. However, the most significant influence on the magnitude of a variation in the gravity field is the causative mass. Figure 1.3 is a schematic representation of the masses that cause various features of the gravity field. This representation allows a rough comparison of magnitudes, which makes it evident that the static gravity field must be determined precisely in order to infer the much smaller time-varying effects.

In this report we identify the terrestrial mass variations that produce gravity signals usefully detectable from space and show how improved gravity-field data can be used to achieve a better understanding of a wide variety of earth-science processes. There is perhaps no other kind of experiment that can simultaneously advance the study of so many different levels of the Earth, from the asthenosphere through the atmosphere.

THE ATMOSPHERE AS A POTENTIAL SOURCE OF NOISE FOR TIME-DEPENDENT APPLICATIONS

A gravity satellite would determine the Earth's gravity field at regular time intervals. Because gravity is caused by mass, the satellite results would provide information on time-dependent changes in the Earth's mass distribution. However, inverting gravity data to calculate a mass distribution is an inherently nonunique process. It is impossible, using gravity data alone, to determine uniquely both the depth-dependence and the latitude- and longitude-dependence of a density anomaly.

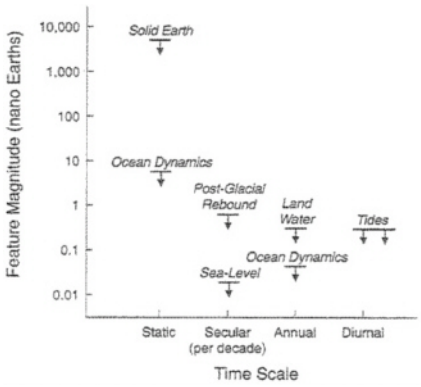

FIGURE 1.3
Estimates of the masses associated with deviations of the Earth's gravity field from a fluid equilibrium state. The unit of mass shown is the "nano-Earth," 10^{-9} of the Earth's total mass, or approximately 6×10^{15} kg. The time variations shown represent the mass involved in a periodic (annual or diurnal) motion, or the mass which flows during a decade (secular motion). Note that time-varying gravity field signals are caused by mass flows which are 3 to 5 orders of magnitude smaller than the solid Earth sources of static field anomalies. Temporal variations at periods other than annual or daily are not shown. These generally involve even smaller masses, and are likely to have continuous frequency spectra difficult to schematize in this figure.

Most of the non-secular variability in mass can be assumed to occur in a thin layer at the Earth's surface, consisting of the atmosphere, the oceans and, on the continents, the groundwater plus the water/snow/ice on the Earth's surface. This layer of variable mass is thin enough that gravity data could be used to determine unambiguously the change in mass, integrated vertically through that layer, as a function of latitude and longitude, but the vertical location of the mass anomalies cannot be inferred.

Over a continental region, for example, one could not distinguish between changes in the atmosphere and changes in the continental water-bearing layer. Whether the gravity data would be more useful for studying the atmosphere or the continental water would depend on which is better known from independent data. In most cases, it is the atmospheric mass that is better known. Pressure fields are accurate to about 0.1-0.3 mbar for seasonal periods, and perhaps 0.5 mbar at non-seasonal periods, which translates into about 1-3 mm equivalent water thickness for seasonal periods and to about 5 mm at non-seasonal periods. As will be apparent in later chapters, this level of inaccuracy would sometimes be the largest source of error in a hydrological or glaciological estimate. Except in a few cases, however, it is not likely to seriously limit the scientific value of those estimates. Precise knowledge of the atmospheric surface pressure uncertainty on seasonal, annual, and secular time scales becomes increasingly important as gravity measurements become increasingly accurate.

There are a few areas, such as parts of the Southern Hemisphere, where the atmospheric pressure errors may be larger than the uncertainties in the hydrological estimates. In that case, mass anomalies derived from satellite gravity observations could be useful for learning more about atmospheric pressure variations.

The atmospheric pressure uncertainties may be larger still over much of the ocean. However, as will be discussed in Chapter 4, uncertainties in atmospheric pressure, whatever their amplitude, are not apt to be a limitation for oceanic studies.

HISTORY OF SATELLITE GRAVITY

Over the first three decades of space techniques, the emphasis of gravimetry was to obtain a more detailed determination of spatial variations in the Earth's static gravity field (Table 1.1). All of these variations also affect the elevation of the Earth's surface, which is usually easier to measure than the gravitational field. However, there are differences of effect reflecting the depths of the causative density variations, and hence their nature. Consequently, since the inference of isostasy well over a century ago, gravity has always been analyzed in conjunction with topographic elevation.

While measurement accuracy steadily improved, the need to lower orbits to obtain better resolution was always frustrated by the greatly increased expense of maintaining orbits against atmospheric drag (see Nerem et al., 1995 and references therein). As measurements became more precise, it became possible to detect temporal variations in the gravity field, which are typically less than 10^{-6} g in amplitude. The first significant temporal measurement was in 1983, when it became possible to measure secular variations in the gravity field associated with changes in the overall shape of the Earth probably arising from a combination of post-glacial rebound and changes in the mass of polar ice (Table 1.1). Temporal variations in ocean tides have been incorporated into gravity field determinations since 1987. Today, scientists are exploring processes that vary over seasonal, interannual, decadal, and secular (i.e., varies linearly over the mission lifetime) changes in the gravity field.

The development of new technologies, such as satellite laser ranging systems with sub-centimeter accuracy, high-accuracy Global Positioning System (GPS) receivers designed for use onboard orbiting satellites, and the successful operation of several geodetic satellite missions (e.g., Laser Geodynamics Satellite [LAGEOS] 1 and 2) has led to new advances in gravity modeling and interpretation (Nerem et al., 1995). However, many of the goals of the earth-science community have not been achieved due to the lack of a dedicated gravity mission. Several mission concepts have been studied and advanced over the last two decades, but none has been realized. Although these missions did not fly, they stimulated a vigorous development of gravity instruments and left a legacy of an improved understanding of the accuracy and resolution required to meet the goals of the scientific community. Three important factors have come into play:

1. the availability of new low-cost (e.g., on the order of $100 M) mission designs;
2. the need to improve the geodetic reference system for other satellite measurements; and
3. the realization that there are significant temporal variations of longer wavelengths measurable from higher altitude orbiters, which would allow nontraditional and interdisciplinary applications to be addressed.

Two categories of mission designs are currently being considered: (1) gradiometry in a single satellite; and (2) tracking between two satellites. The Spaceborne Gravity Gradiometer (SGG) combines pairs of accelerometers in close proximity along a common axis to measure components of the gravity gradient tensor along the axis of each pair. By combining three pairs in

TABLE 1.1 Milestones in Gravitational Satellite Geodesy

Year	Event	Implications
1958	Determination of the oblateness from tracking of Sputnik	• Definitive determination of the Earth's oblateness: the largest difference of the real Earth from fluid equilibrium
1959	Determination of the "pear shape" (odd zonal harmonic) of the Earth	• First determination of a gravity term not associated with rotation • Showed that the Earth has major density variations not associated with isostatic topographic compensation, as predicted by Jeffreys (1952)
1963	Longitudinal variations from camera tracking included in gravity field determination	• Confirmed the "$10^{-5}/l^2$" rule for the decline in magnitude of variations in gravity with harmonic degree l; ±27 meters rms error in the geoid
1965	Doppler tracking from U.S. Navy TRANET network included in gravity field determination	• Significantly improved gravity-field accuracy to ± 12 meters rms error in the geoid
1968	Effective satellite-to-satellite tracking, i.e., Earth to lunar satellite	• Mapped the front-side field of the Moon to better accuracy than contemporary measurements of the Earth
1975	The first altimetric satellite Geodetic Satellite Mission (GEOS-3)	• Measured sea-level height at the 1-m level, an order-of-magnitude improvement in the ocean geoid
1979	Incorporation of laser ranging data into gravity field solutions	• Significantly reduced systematic error and improved accuracy of the geopotential field
1979	Gravity field of Mars determined from Mariner Orbiters	• Showed a gravity field twice as great in its irregularities as predicted from the Earth's field, and the dominance by a great high over the Tharsis province, a planet-scale locus of high topography, volcanism, and tectonism
1981	Gravity field of Venus determined from Pioneer Orbiter	• Showed a gravity field of much greater geoid:topography ratio than the Earth's, implying depths of compensation greater than 100 km
1983	Generation of marine gravity field from Seasat data	• Revealed major uncharted tectonic features of the ocean floor (Haxby et al., 1983)
1983	Detection of the change in the Earth's oblateness (dJ_2/dt) from high LAGEOS spacecraft	• Implied an increasing spin rate consistent with the long-term post-glacial motion of matter toward the rotation axis
1987	Incorporation of tidal variations in gravity-field determinations	• Provided important constraints on ocean-tide solutions and improved the accuracy of the static field
1987	Analysis of monthly gravity data from LAGEOS and complementary atmospheric pressure data	• Linked seasonal variations of the geopotential with atmospheric pressure variations
1993	Comprehensive solution incorporating altimetry, surface gravimetry, and GPS tracking (Joint Gravity Model [JGM3])	• Determined the gravity field to the 70th degree, plus tides, to an estimated geoid accuracy of ±0.5 meters
1995	Mass of asteroid 243 Ida determined from Galileo spacecraft Doppler tracking	• Bulk density consistent with "rubble-pile" model of asteroids
1995	Inference of tidal Love number of Venus from Magellan Doppler tracking	• The high value (0.27) indicated that Venus has a completely fluid core, consistent with the absence of an energy source for a Venusian magnetic field
1995	Geodesy Satellite altimetry (ERS-1 acquired; Geosat declassified)	• Led to a global map of the oceanic gravity field with a resolution of 20 km
1996	Measurement of the ellipsoidal fields of the Galilean satellites	• Moments-of-inertia indicated big iron cores in Ganymede and Europa, a modest core in Io, and no core in Callisto

orthogonal directions, the trace of the gradient tensor can be measured. Existing technologies permit missions of one-year duration, whereas five-year duration missions utilizing improved miniaturization and cryogenic techniques are expected around 2010. Three types of tracking between satellites are considered in this report: (1) high-low GPS tracking; (2) low-low microwave tracking between two satellites (SST); and (3) low-low laser interferometry between two satellites (SSI). There are tradeoffs between mission lifetime, altitude, and resolution (e.g., long missions are higher altitude and have lower resolution than short missions), and between temporal and spatial sampling.

The compact size, low weight, and low power consumption of the instrumentation proposed for future gravity missions allows the use of newly available low-cost launch vehicles. The development of compact, highly accurate accelerometers and gradiometers eliminates the need for the expensive "drag-free" system included in many of the earlier gravity-mission designs. In all of the current gravity-mission proposals, modern, highly capable, compact GPS flight receivers will provide access to the rich information content of the dual-frequency navigation signals of the GPS constellation. These improvements will allow several types of gravity missions to be flown at low cost.

The proposed missions will have different capabilities and thus will have application to different scientific problems. In discussing the scientific issues, we note the accuracies that could be obtained by each type of gravity mission.

"GRAVITY" AS USED IN THIS REPORT

Newton's laws of motion apply to inertial reference frames, whereas terrestrial motions are observed in a non-inertial coordinate system rotating with the Earth. In accordance with standard practice among geodesists, we will use the term "gravity" to mean the combination of Newtonian gravitational attraction with the effect of the Earth's rotation at a point stationary with respect to the Earth's surface; it has the physical dimension of acceleration. The rotational effect is included in the definition of the standard ellipsoidal model of the reference gravity field for the Earth. "Gravity anomalies" are departures from this reference model at points fixed relative to the Earth and are thus identical to the anomalies of attraction only, the rotation being common to both the reference field and the observed values. The "anomalous potential" is the difference between the potentials of the real and reference gravity fields, consequently, gravity anomalies are related to the gradient of the anomalous potential. The "geoid" is the equipotential surface of the real gravity field that coincides, on average, with mean sea level. A "gravity mission" is an observational satellite program designed to sense these gravity anomalies.

There are three different ways that deviations from the reference gravity-field model are commonly expressed; each has its convenience. "Gravity anomalies" are anomalies in the magnitude of the acceleration and, from long habit, are commonly expressed in milli-Galileos (mGal). One mGal = 10^{-5} m/s^2 and is approximately 10^{-6} of the total gravity acceleration. "Deflections of the vertical" are anomalies in the direction of gravity, measured as angles and conveniently described in micro-radians (μrad), a slope of 1 μrad being a 1 mm rise in a 1 km run. "Geoid anomalies" or "geoid heights" are elevations of the geoid above or below the standard ellipsoidal reference shape of the Earth and are conveniently measured in meters. Root-mean-square (rms) magnitudes are about 42 m for geoid height, 30 mGal for gravity anomaly, and 30 μrad for deflections of the vertical with respect to a hydrostatic figure.

Geoid anomalies can be calculated from gravity anomalies, and vice versa. Spatial derivatives of the anomalous potential in different coordinate directions are related to one another through Laplace's equation. By combining these two relations, one can relate horizontal derivatives (slopes) of the geoid to gravity anomalies, and thus obtain the convenient result that a 1 mGal gravity anomaly approximately corresponds to a 1-μrad slope in the geoid. Furthermore, at mid-latitude values of the Coriolis parameter, a slope of 1 μrad in the dynamic ocean height implies a surface-current velocity of 0.1 m/s. This is important for oceanographers to bear in mind, because if a gravity anomaly as determined by a satellite mission has an uncertainty of x mGal, it means that the slope of the geoid is also uncertain by x μrad, hence that the calculated slopes of the oceanic dynamic topography will also be uncertain by x μrad. In this way, the gravity anomaly uncertainties described in this report may be scaled into uncertainties in derived ocean circulation.

ORGANIZATION OF REPORT

In this report we evaluate the capabilities of the next generation of satellite gravity missions for improving the global gravity field and explore the scientific questions that could be addressed with better gravity data. The applications of the static field are important; however, they have been discussed extensively in the literature (e.g., National Research Council [NRC], 1979, 1982; National Aeronautics and Space Administration [NASA], 1987; Nerem et al., 1995). Here, we summarize and update these findings. In contrast, application of the time-varying field to geophysical processes is an emerging frontier of science and requires significantly more detail in this report. Because little systematic work has been done in this area, it was necessary to develop forward models to determine which phenomena could be detected from space. The models are described in Appendix B.

In Chapter 2 (Mission Scenarios and Measurement Techniques), we describe the measurement techniques needed to advance the state of the art in gravity research. Here, we focus on the expected results of five possible missions, which are described in a generic format, and illustrate the trade-offs between mission duration and spatial resolution. In Chapter 3 (The Gravity Field as a Tool for Science) we describe the utility of gravity data (e.g., the geoid) to a broad range of scientific disciplines. In the remainder of the report we examine what new insights can be gained with improved gravity measurements, with an emphasis on understanding "processes." Both static (i.e., constant in historic time) and time-varying phenomena are described. Within the time-varying category, we distinguish among those that are secularly-varying and those that are expected to fluctuate, some shorter and some longer than one mission lifetime. The focus of Chapter 4 (Ocean Dynamics and Heat Flux) is oceanic processes, with a particular emphasis on ocean circulation and the ocean's role in global change. Chapter 5 (Solid Earth Processes) contains a discussion of mantle convection and plumes, tectonics and crustal deformation, post-glacial rebound, and earthquakes. Monitoring of one of the most important renewable resources, water, is discussed in Chapter 6 (Water Cycling). In Chapter 7 (Sea-Level Change) we consider how rates of sea-level rise can be constrained using space geodetic measurements, an issue of profound concern to coastal societies. Chapter 8 (The Dynamic Atmosphere) is a description of the synergistic benefits of space gravity measurements when studied with more conventional meteorological data and, on the other hand, the need for accurate atmospheric pressure data to deconvolve other sources of gravitational variations. Finally, in Chapter 9 we summarize our conclusions.

2

Mission Scenarios and Measurement Techniques

The path of an Earth-orbiting satellite departs from a simple Keplerian ellipse because of various perturbing forces acting on the satellite. These include the effects of atmospheric drag and solar radiation pressure, in addition to the gravitational attractions of the Sun, Moon, and Earth. By observing the motion of a satellite one obtains information about the forces acting on it, including the anomalies in the Earth's gravity field. Models of the Earth's gravity field are combined with models of these other forces in order to predict the path of a satellite, and the predictions are compared against the observations. As observational data are refined the model parameters are adjusted, yielding improved gravity field models. The history of this process is shown in Table 1.1 of Chapter 1.

Two kinds of errors can be introduced into the estimated gravity field model during this force modeling process. The first might be said to introduce a "bias," or a "systematic error," or to affect the "accuracy" of the estimated gravity field. The second might be called a "random error," or "noise," which limits the "precision" of the gravity field estimates. Both will affect how far an estimated gravity field model departs from the "true" gravity field of the Earth. The first kind of error occurs when there are systematic biases in the measured quantities, or when non-Earth-gravitational perturbations are erroneously attributed to the gravity field. These errors make the estimated gravity field model inaccurate. The second kind of error occurs because the quantities of interest can only be measured with a finite precision, and noise in the observations makes the estimated gravity field imprecise.

In this chapter we describe some scenarios for satellite missions that could improve our knowledge of the Earth's gravity field. Some of these involve mature technologies that are probably feasible now; others envision using emerging technologies that may be ready to fly at some time in the future. All are discussed in a generic form. The literature on specific missions proposed in the past or for the future gives more technical details, and is cited where appropriate. At the end of this chapter there is a table summarizing the generic mission scenarios referred to in the subsequent chapters.

We estimate the ability of each of our generic missions to resolve the gravity field using standard techniques in spherical harmonic analysis. Spherical harmonic analysis of functions defined at points on a sphere is analogous to Fourier analysis of functions defined at points on the real line. We use a convolution theorem and assumed statistical distributions to obtain relationships among mean square values averaged over the surface of a sphere, called "variances." The square roots of these quantities are the root-mean-square (rms) average values, which we call "amplitudes." A constituent of a function with harmonic degree l has a wavelength of 40,000 km/l. A graph of constituent variance or amplitude versus l is a "degree spectrum," analogous to the power and amplitude spectra of one-dimensional functions. We characterize the resolution capabilities in terms of the rms amplitude of the

uncertainty in an areal average of the gravity or geoid anomaly; we illustrate this as "precision" versus a "resolution," the latter being the square root of the area. Precisions have units of geoid height or gravity anomaly and resolutions have units of length. Degree amplitude spectra are dimensionless and represent the amplitude of a quantity relative to the total amplitude of the Earth's gravity field. Details of these methods are given in Appendix A.

Our characterization of the resolution of these generic missions is essentially an analysis of how the error in a measured quantity will map into an error in the gravity field model. As such, it is a study of errors of the second kind, that is, of the "precision" of the derived gravity field model. However, we also discuss what ancillary measurements are required in order to facilitate a correct modeling of the non-gravitational signals, so that type-one errors will be reduced or eliminated. These missions are expected to make a significant improvement in the gravity field at short wavelengths, that is, at frequencies of many cycles per revolution of the satellite orbit. Most of the nongravitational modeling errors are confined to frequencies of one or a few cycles per revolution, that is, at very long wavelengths where the gravity field is already well known. Thus a spectral separation of the two kinds of errors is also possible. In the chapters following this one, we will compare the size of gravity field signals associated with various scientific problems against the resolution and error estimates obtained here. In effect, this means that the "error" estimates obtained here are treated as though they were "departure from the truth." This treatment is justified by the spectral separation noted above and in the later error analysis review. These have shown that by placing accelerometers and/or GPS receivers onboard the spacecraft, one obtains the necessary data to separate the gravitational and non-gravitational signals.

SATELLITE OBSERVATIONS OF THE GRAVITY FIELD

Since the beginning of the satellite era in 1957 the tracking of orbiting satellites has been done from sites on the surface of the Earth, first optically, and later by Doppler and laser techniques. In the 1980s, a new dimension was added to these methods with the development and maturation of GPS of the U.S. Department of Defense, and the Global Navigation Satellite System (GLONASS), developed by the former USSR. Both these systems involve a constellation of high altitude satellites broadcasting navigation information which may be used by a receiver to determine its position both accurately and precisely. Virtually continuous tracking data obtained from high-quality GPS receivers onboard the low-altitude Ocean Topography Experiment (TOPEX/Poseidon) and GPS Meteorology Satellite (GPS/MET) have proven valuable in improving the resolution of the currently available Earth gravity field models (Tapley et al., 1996a; Lemoine et al., 1996).

The accurate determination of the long-wavelength (few thousand kilometers and longer) components in current gravity field models is largely due to extensive satellite tracking data. Medium- and shorter-wavelength components are constrained by combining satellite tracking data with heterogeneous data sets of land and marine gravity anomaly surveys and satellite altimetry. A dedicated spaceborne gravity mapping mission has long been seen as the means to improve the accuracy and resolution of Earth gravity field models. Such a mission would provide data of global extent and homogeneous quality, without the geographic or geopolitical limitations of altimetry and surface gravity anomaly surveys.

Most of the mission scenarios we describe in this report would improve the sensitivity to the gravity field by using various forms of satellite-to-satellite tracking. These include both a "high-low" scenario, in which a low-altitude satellite tracks its position with respect to the high-altitude GPS and/or GLONASS systems, and "low-low" scenarios, in which two low-altitude satellites track one another's motions. In another category are the "gradiometer" missions, which measure spatial gradients (derivatives) of the gravity field. If the distance separating the two spacecraft in a low-low mission is small (a few hundred kilometers), the mission will be particularly sensitive to differences in gravity over that distance. Because differentiating a signal will amplify its short-wavelength components more than its long-wavelength components, both the low-low tracking and the gradiometer scenarios could yield enhanced resolution of gravity field components between a few hundred and a few thousand kilometers.

TRADE-OFFS IN SPACECRAFT MISSION DESIGN

The ability of a satellite-borne instrument to provide measurements of the anomalous gravity field of the Earth depends on its orbital altitude. This is due to the attenuation of the gravitational potential with altitude, shown in Figure 2.1 (top panel) and described

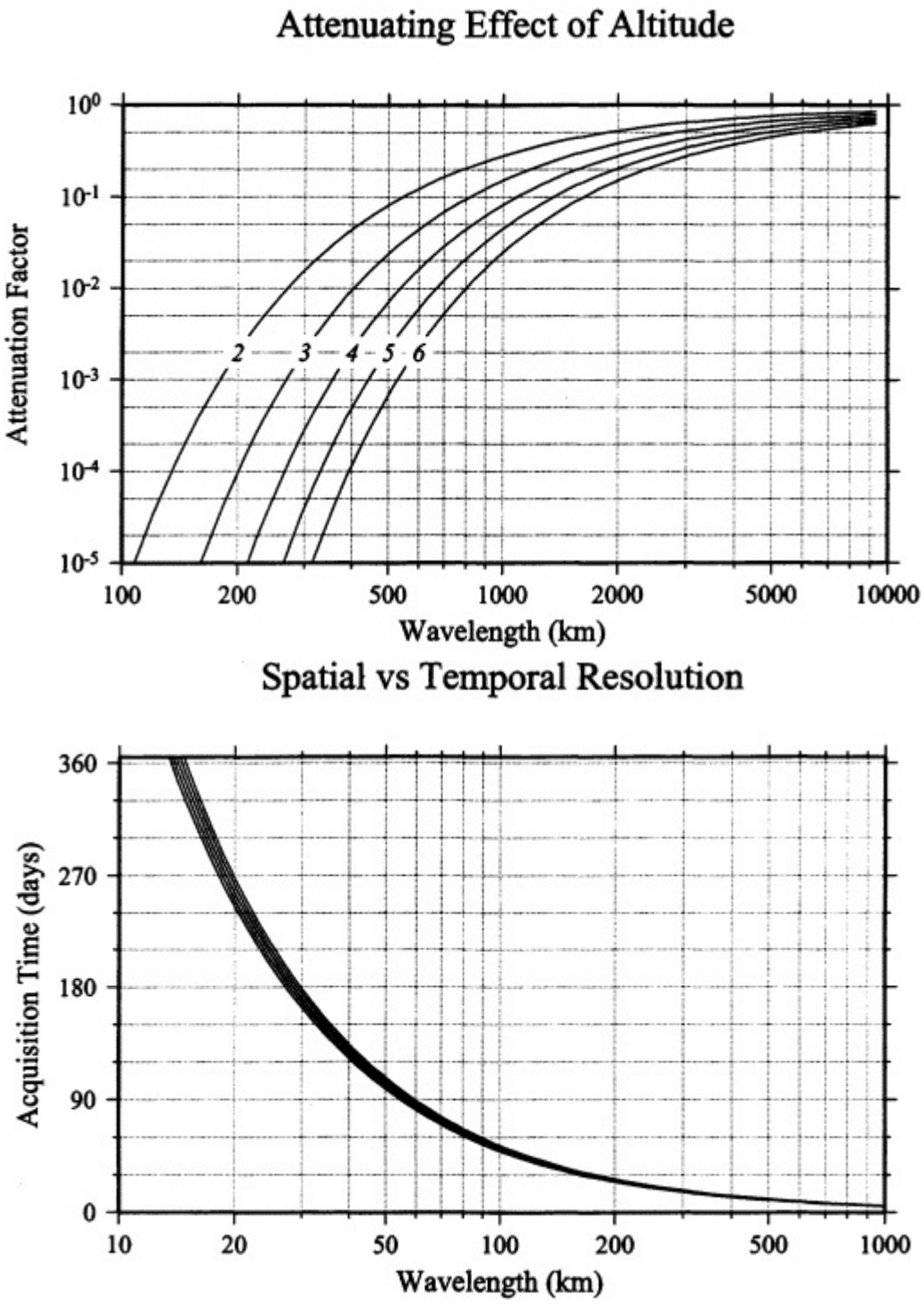

FIGURE 2.1
Top panel: The attenuation of gravitational potential with orbital altitude. Numbers labeled 2 through 6 denote orbital altitudes of 200 through 600 km, respectively. Bottom panel: The time required to acquire a ground-track pattern that will resolve a given across-track wavelength. Curves are drawn for the same orbital altitudes as in the top panel.

in Appendix A, section A.4. Most dedicated geopotential mapping mission scenarios call for low-altitude orbits (250 to 600 km) in order to maximize sensitivity to anomalies in the gravity field.

The altitude of the orbit is linked to the mission lifetime. The density of the atmosphere increases exponentially with decreasing altitude, so that the effect of the dissipative atmospheric drag accelerations becomes very significant at low altitudes. This drag will cause the orbital altitude to decay and eventually the satellite will re-enter the lower atmosphere, unless it is periodically boosted to a higher altitude by burning fuel carried onboard. The duration before re-entry, or the satellite mission lifetime, is dependent upon the initial altitude of injection, the ballistic characteristics of the satellite, the onboard fuel-carrying capacity, and the ambient drag conditions, which, in turn, depend upon the phase of the solar cycle. While predictions of orbit lifetime differ widely, in general satellites in the 250 to 350 km altitude range will last approximately 6 to 12 months in orbit, while those in 400 to 600 km altitude may last up to 2 to 5 years or more, depending upon the solar activity (Figure 2.2). Through these considerations, there are direct links between the observability of the geopotential, the mission's lifetime, the launch time table, and the weight and cost of the satellite.

At the range of altitudes discussed here, the spacecraft typically makes 15 to 16 revolutions of the Earth every day, at speeds of approximately 7.5 km per second. With measurements taken every few seconds, a dense sampling of the perturbative effects of the anomalous potential may be obtained along the satellite's ground track. The spatial sampling ability of any mission is thus limited by the across-track separation or the distance between two adjacent ground traces of the satellite's trajectory. Following Nyquist sampling requirements, resolution of an across-track anomaly of a given wavelength requires the satellite ground tracks

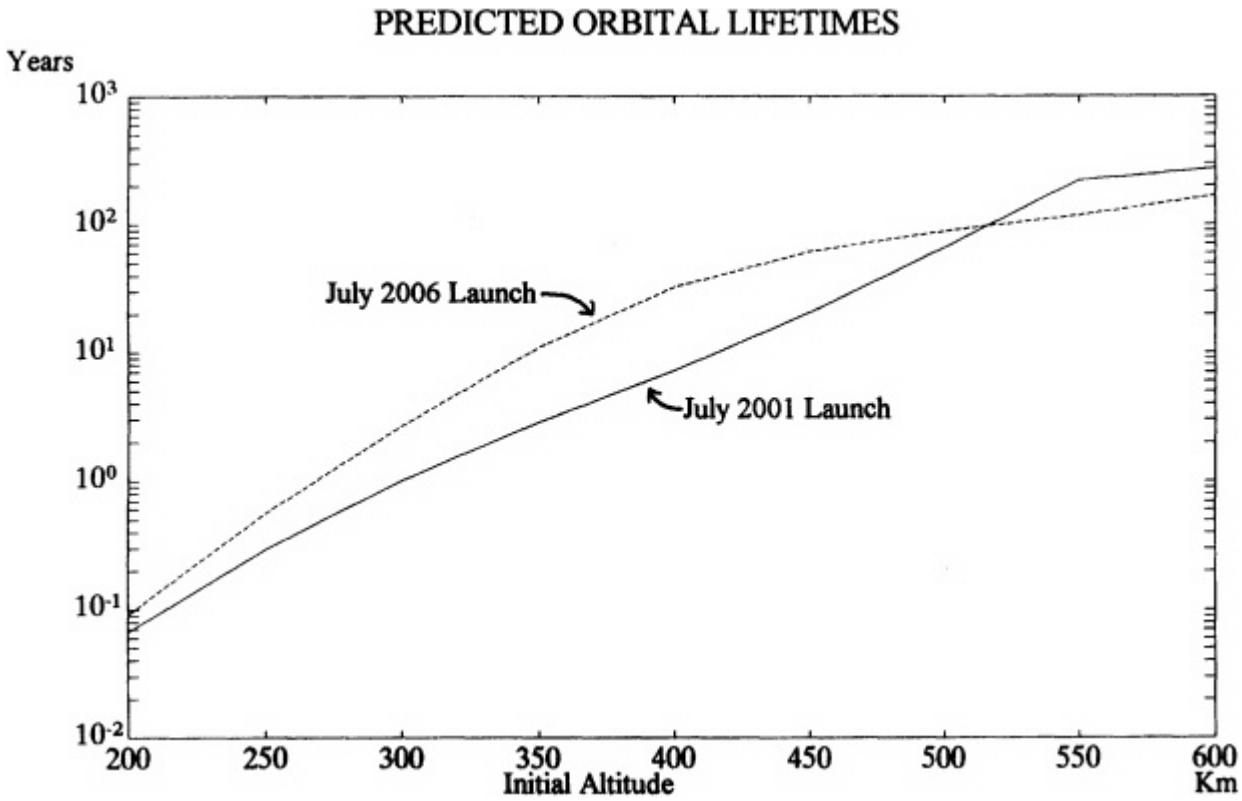

FIGURE 2.2
Orbit lifetime as a function of initial altitude and solar cycle. Polar circular orbits, A/M = 1 m^2/77 kg. Computed by L.K. Newman, NASA Goddard Space Flight Center.

to be separated by half that wavelength or less. Thus an increase in the desired resolution requires a concomitantly denser sampling of the globe by the satellite ground tracks. However, this also means that the same geographical location can be sampled again only after a longer duration. Figure 2.1 (bottom panel) shows the acquisition time required to resolve a given across-track wavelength at the equator, where the track separation is largest. To resolve a spatial wavelength of λ the satellite must make at least $2l$ revolutions around the Earth, where l = 40,000 km/λ. At an orbital altitude of 400 km, the satellite makes 15.5 revolutions per day, and so the orbit repeat time R must be at least 80,000 km/15.5l days. Figure 2.1 (bottom panel) shows the trade-off between λ and R. An orbital repeat time of R limits the shortest period temporal oscillation that can be resolved to $T = 2R$. There is thus a trade-off between the spatial and temporal resolutions that might be obtained from an orbit design, such that the product Tλ is roughly 10,000 km-days. (While it might seem that l revolutions are sufficient to resolve degree l, in fact $2l$ are required [Jekeli and Rapp, 1980].)

The mission design also affects the science capability in other ways. To separate properly the time-varying gravitational effects from the static gravity field, it is necessary that a long record of measurements be available. An ideal mission design might call for low altitudes for desired high values of signal-to-noise ratios; long lifetimes to ensure adequate separation of the static and time-varying parts of the gravity field; and low weights to reduce launch and mission costs. These requirements are not all mutually compatible and potentially influence the science returns from a geopotential mapping mission. A mission flown continuously at altitudes below 300 km, as aspired to 15 years ago, becomes much more expensive because of the launch costs to put such mass in orbit. It now appears preferable that a satellite mission be placed at a higher altitude, where it would stay in orbit for several years, while resolving the longer wavelength components of the geopotential over that time scale, after which the natural decay of its orbit would allow it to resolve the shorter wavelengths over the last few months. As a further example, if the observing instrument must be cooled to superconducting temperatures, the current state of the technology limits the liquid helium dewar life, and hence the mission lifetime, to approximately 9 months. In such a case, it becomes necessary to fly at the lowest practical altitude, in order to maximize the resolution of the geopotential, while obtaining a snapshot (in time) of the gravity field.

MISSION SCENARIOS

GPS

The simplest concept for the mapping of the Earth's gravity field from space involves a single low altitude satellite, carrying a GPS or GLONASS receiver. Also onboard might be a high precision accelerometer, in order to properly model the effects of atmospheric and other non-gravitational accelerations upon the motion of the satellite. Failure to model these latter effects adequately will reduce the accuracy with which the geopotential models may be estimated from satellite tracking data. Such a scheme, making measurements of the satellite position, will be referred to hereafter as "GPS." Examples of such mission concepts are described in Reigber et al. (1996) and Clark et al. (1996).

SST and SSI

Another gravity-field-mapping scheme involves the measurement of the differences in satellite orbital perturbations over baselines of a few hundred kilometers (typically 100-600 km). These measurements may be made by placing two satellites in the same orbit but separated from each other by a few degrees, so that, in effect, one satellite "chases" the other. Mutual tracking between the two satellites then provides the information on the differential accelerations acting on the two satellites.

Two scenarios for making such measurements are considered in this report. In one, a microwave link between the two satellites is used to measure the line-of-sight range-rate (time derivative of the inter-satellite distance); this will be called Satellite to Satellite Tracking, "SST." In the other, the inter-satellite tracking is done using laser interferometry; hereafter called Satellite to Satellite Interferometry, or "SSI." Both these mission concepts are expected to carry high precision accelerometers at the center of mass of each of the satellites. This ancillary measurement is necessary to enable the effect of differential non-conservative accelerations on the inter-satellite orbit perturbations to be modeled accurately. Some examples of such missions are discussed by Fischell and Pisacane (1978), Pisacane et al. (1982), Yionoulis and Pisacane (1985), Keating et al. (1986), Bender (1992), Frey et al. (1993), Davis et al. (1996), and Chao et al. (1996).

Our SST mission scenario characterizes the current capabilities of a mature technology using a microwave sensor. Our SSI mission scenario envisions some

future engineering developments (e.g., reduction of thermal noise in the laser cavity), which might allow a laser to achieve an order of magnitude improvement in sensitivity over the current microwave design. The necessary developments are being studied as part of the European Space Agency's Cornerstone Project LISA, a laser interferometer space antenna intended to observe gravitational waves.

SGG and SGGE

When a satellite of finite extent is in orbit under the influence of purely gravitational accelerations, only its center of mass is in free fall. An accelerometer rigidly attached to such a satellite at a point displaced from the center of mass will measure only the acceleration relative to the center of mass. The difference in the acceleration measurements between two such collinear accelerometers, divided by the (short) baseline distance, yields a measurement of the gradient of gravitational acceleration along the baseline. This concept, extended to include three mutually orthogonal baselines (typically a few centimeters long) within the satellite, forms the basis of gravity gradiometry. Such a gravity gradiometer is likely to use a cryogenic super-conducting technology to ensure very high precisions of differential acceleration measurements. This concept is referred to hereafter as a Spaceborne Gravity Gradiometer, or "SGG." Examples of such mission concepts are described by Morgan and Paik (1989), European Space Agency (ESA) (1991, 1996), Rummel and Schwintzer (1994), and Bills and Paik (1996).

Current engineering constraints limit the time that a cryogenic SGG can be kept cold to something on the order of 9 to 12 months. It is conceivable that future technological advances will make it possible to operate an SGG for a much longer period of time. Such an extended SGG we refer to as "SGGE."

PREVIOUS STUDIES

The study of the capabilities and requirements of satellite gravity missions has a long history in the geodetic literature. These studies describe the signals in the various measurements, the nature of the principal error sources, and their effects on the resolution of the estimated gravity field. These error analyses have ranged from the approximate, rule of thumb techniques assuming white noise measurement errors, to fully rigorous numerical simulations of diverse random and systematic measurement and model errors.

The GPS mission concept is the only one for which real data have been analyzed and incorporated into a gravity field model. Two such examples are GPS tracking of TOPEX/Poseidon and GPS/MET satellites (Tapley et al., 1996a). The data from these satellites have been incorporated into the JGM3 (Tapley et al., 1996) and the EGM96 (Lemoine et al., 1996) models and have proven the value of high-density GPS tracking. Future GPS tracking missions should yield results that are enhanced by lower flight altitudes and will most likely carry an accelerometer to reduce the errors due to mismodeled non-gravitational accelerations. Several studies have been conducted on the use of the GPS concept for improvements in the gravity field models. Simulations for the Shuttle-GPS Tracking for Anomalous Gravitation Estimation experiment (Jekeli and Upadhyay, 1990) showed that 2-degree-mean anomalies could be estimated to 5 mGal. In the Aristoteles configuration (Schrama, 1991), tracking a Sun-synchronous satellite in a 250-km orbit yields a 1-mGal cumulative point-value error up to spherical harmonic degree 70 or so. The Polar Orbiting Platform Satellite-Geopotential Recovery Mission simulations (Reigber et al., 1987) showed errors ranging from 3 to 8 mGal depending on the duration of the mission. It is clear from all these results, however, that a gravity-mapping mission that includes only GPS tracking will not provide a "quantum leap" improvement in modeling the Earth's gravity field. Its most significant contribution would be at the longest wavelengths. In this sense it could be complementary to other gravity-mapping techniques.

The studies of SST missions have appeared in the literature in step with the various past proposals for such space missions. Early simulations focused on the Geopotential Research Mission scenario (Keating et al., 1986), using Fourier analysis of the inter-satellite range-rate signals (Kaula, 1983; Wagner, 1983) to determine that gravity field models of high degree and order could be resolved using this technique. Other studies (Douglas et al., 1980) used a local gravity inversion technique to show that with 1 μm/s range rate, the 1-degree-mean anomalies could be determined to near 1 mGal precision. All of these studies assumed satellite altitudes of 160 km, which required some form of drag compensation or frequent orbit maneuvers to raise the altitude for any reasonable mission lifetime.

Simulation studies of the gravity gradiometer mission concepts are more recent and have focused on ESA's Aristoteles mission scenario. This mission calls

for a gradiometer and a GPS receiver onboard the spacecraft. Consortium for Investigation on Gravity Anomaly Recovery (CIGAR) (1996) presents a review of the considerable literature devoted to this mission. Extensive study of a gradiometer mission with a 0.01 Eötvös (1 E = 10^{-9} s^{-2}) precision has been made by the European geodetic community. Under the somewhat restrictive assumption of total loss of gradiometer signal at frequencies below 5 mHz (27 cycles per revolution) along a 200-km altitude Sun-synchronous orbit, Visser et al. (1994) showed that 100-km-mean anomalies could be recovered to 5 mGal or better from such a mission, with high-low GPS tracking playing an integral part in determining the long wavelength features of the gravity field.

Using an approximation based on white-noise measurement errors, Rapp (1989) showed that 1-degree-mean anomalies could be determined to 2, 3, and 5 mGal with mission altitudes of 160, 200, and 240 km, respectively. The corresponding precisions expected for 0.5-degree anomalies were 7, 9, and 11 mGal, respectively. Rummel and Schrama (1991) pointed out that the precisions at half-wavelengths less than 100 km would be approximately 1 mGal in the presence of white-noise measurement errors. CIGAR (1990) and Visser et al. (1994) showed that the effects of bandwidth limitations on measurements at frequencies less than 5 mHz and of polar data gaps due to the Sun-synchronous orbit are significant, and they recommended the use of GPS tracking and *a priori* constraint to reduce the estimation errors as well as to handle numerical instabilities in the data-inversion process. Kahn and von Bun (1985) pointed out that a 0.001-E instrument in a 160-km orbit could further improve the determinations of 0.5 degree mean anomalies to 3 mGal. Only a few rigorous numerical simulations of the gravity gradiometer problem have been carried out to high degree and order, due to limitations on computer time. Bettadpur (1993) reported supercomputer simulations to degree and order 100, taking into account orbit, white and colored measurement noise, and drag-mismodeling errors. He showed that the alignment of the sensitive axis of the accelerometer and the reduction of the accelerometer cross-talk factors were important for removing both the mean and the episodic (short-period) errors arising from variations in drag acceleration. The computing issues in gravity gradiometry were addressed by Balmino and Barriot (1991). A more comprehensive analysis of the Gravity Field and Steady-State Ocean Circulation Mission (ESA, 1996), based on a measurement accuracy of 0.001 E, addressed the need for an improved gravity field in such diverse areas as geodesy, geodynamics, oceanography, and orbit determination.

ERROR ESTIMATES FOR MISSION SCENARIOS OF THIS REPORT

All the mission concepts discussed here will yield observations with some limited precision. To determine definitive error estimates for a specific mission, it would be necessary to have a detailed engineering summary of the mission, including the spectra of all the errors, and to combine these with full numerical simulations of the estimation of the gravity field. Such a complete analysis is beyond the scope of this report. Instead, we make some simplifying assumptions that allow us to use analytical expressions to relate errors in the mission data to errors in the coefficients of the gravity field model. The error amplitudes we give are root-mean-square average values; that is, they are the square roots of the expected variances and may be thought of as "one-sigma" errors. Our approach and assumptions are outlined here; further details are in Appendix A.

Degree Amplitude Error Spectra

We begin with the assumption that the orbit will distribute errors in the observed quantity isotropically over the surface of a sphere surrounding the Earth at the altitude of the satellite orbit. In practice, no real orbit can distribute errors in this way; the ground track pattern is always least dense at the equator and most dense at the highest latitudes reached by the orbit. The actual orbits in real missions are likely to be very slightly elliptical and may be Sun-synchronous in order to simplify the design of the solar power systems. Sun-synchronicity requires the orbital plane to be inclined approximately 6 to 8 degrees from the polar axis so that small areas over the poles will not be covered by the satellite's ground track pattern. However, the assumption of isotropic error distribution permits us to convert the power spectral density (PSD) of the error in the time series of observables into the spatial covariance of the observable error over a sphere at satellite altitude. Once we have this, we can proceed with an error propagation analysis that treats the mean square values of errors averaged over a spherical surface. The error estimates we obtain by this method

will be average values; they may somewhat underestimate the errors at the equator and overestimate the errors at the maximum latitude reached by the satellite, and they will certainly underestimate the errors over polar gaps, if the orbit is not polar.

We used the method of Jekeli and Rapp (1980) to convert the PSD for errors in the time series of the observable into the spatial covariance of observable errors distributed over a sphere. This method assumes that the PSD of the errors is white. In reality, the data from an actual mission will likely have non-white PSDs, that is, correlated errors. We expect this to affect our error estimates primarily at the lowest degrees.

The Jekeli and Rapp method requires us to select a duration over which the data are analyzed, *D*. *D* must be chosen to be long enough that the assumption of spatially isotropic error distribution is justified. For example, if one wants to estimate the error in a spherical harmonic coefficient of degree *l*, then *D* must be long enough that the satellite makes at least 2*l* revolutions around the Earth during the time *D*. We chose *D* = 90 days. At the altitudes we simulated, a satellite makes about 15.6 revolutions per day and 1400 revolutions in 90 days; thus our calculations should be good to *l* = 700. We found that none of our simulated missions could resolve 1 > 300, so it would have been safe to have used any duration greater than about 40 days. Our resolution estimates for D = 90 can be rescaled to any *D′* > 40 by multiplying our resolved amplitudes by • (*D*/*D′*) to obtain resolved amplitudes for a different duration. Later chapters discuss time variations in the gravity field and assume that a five-year mission can obtain an independent sample of the gravity field every *D* days.

The above process results in a covariance function for the errors in the observable that is distributed isotropically over the sphere at satellite altitude. Next, we make the assumption that all the forces on the satellite apart from the Earth's gravity field can be correctly modeled so that the signal in the observed quantity is caused entirely by the Earth's gravity field. This allows us to relate the covariance of the error in the observable at satellite altitude to the covariance of the errors in the coefficients of the gravity-field model. For the SGG and SGGE missions we need the spatial derivatives of the field (Appendix A, equation A.16), which are well known; an elegant so-called "Meissl Scheme" solution has been given by Rummel and van Gelderen (1995). We follow previous studies in making the approximation that the errors in the recovered gravity field can be estimated from the errors in the second radial gradient only. The SST and SSI missions need a relation involving the range-rate observable—this has been derived from an energy integral by Jekeli and Rapp (1980). This expression requires specification of the angular separation between the two spacecraft (δ in equation A. 15 of Appendix A); we assumed a separation of two degrees. For the GPS case no analytic scheme was available, so we used the error predictions from numerical simulations for the white noise case reported by Bettadpur and Tapley (1996b). There, the observation data were assumed to be the double-differenced ranges between one ground receiver, one satellite receiver, and two GPS satellites. In practice, this would be derived from pair-wise differencing of the GPS carrier phase measurements between the two GPS satellites and the two receivers. The results from this study were appropriately scaled to reflect various altitude, noise level, and mission durations.

The white-noise levels we assumed for the missions were as follows: for the GPS mission, a 1 cm rms error in the double-difference range data. For the SST, a PSD of 0.5 (micron/s)/√Hz in the microwave measurement of line-of-sight range-rate. For the SSI, a PSD of 0.05 (micron/s)/√Hz in the interferometer measurement of line-of-sight range-rate. For the SGG and SGGE missions, we assumed that the error source was predominantly the error in the second radial-radial derivative of potential, and we assumed a PSD for this error of 0.001 E/√Hz. These measurement-noise levels were chosen to yield gravitational parameter precisions that are representative of those expected from contemporary mission designs.

Figures 2.3-2.6 show the degree amplitude spectra (the rms amplitude of the errors in the geoid, σ_l) we obtained by this method for our GPS, SST, SSI, and SGG mission scenarios at altitudes of 200, 300, 400, and 500 km. Also shown are the error amplitudes for a current state-of-the-art gravity field model, EGM96 (Lemoine et al., 1996), reflecting the current status of knowledge based upon tracking data (predominately satellite laser ranging), surface gravity-anomaly measurements, and satellite altimetry. The figures show that a 90-day GPS mission provides an improvement over the current knowledge of the long-wavelength components of the mean gravity field, but the errors rise rapidly with increasing degrees. For a fixed altitude, the SST errors are lower than SGG errors at degrees less than 100 or so. The well-known insensitivity of SGG data to the long-wavelength geopotential is an inherent property of the gradient data type. We have not included the data from the onboard GPS receiver in our simulation for SGG. Had we done

so, the SGG error amplitudes at any degree would be approximately equal to the minimum of the SGG and GPS error amplitudes shown in Figures 2.3-2.6. Note that this would serve to reduce the errors in a gradiometer-derived gravity model at the low degrees where the GPS mission has smaller errors, though the resulting SGG +GPS errors would still be larger than the SST or SSI errors below degree 100. The SGG errors are smaller than SST errors at higher degrees. In all cases, the errors from SGG and SST become greater than the errors in current gravity models at degrees greater than 200 for missions at an altitude of 300 km, and degree 120 for the 500-km missions. Because the SSI is essentially an SST with an order-of-magnitude greater precision, it out-performs all the other missions. It would provide improved knowledge of the gravity field to harmonic degree 140-300, depending on its orbital altitude.

Precision Versus Resolution

We used the degree amplitudes in Figures 2.3-2.6 to derive resolution estimates that are more understandable physically. These are shown with a resolution length on the horizontal axis and a precision amplitude on the vertical axis: geoid-height precisions in Figures 2.7-2.10 and gravity-anomaly precisions in Figures 2.11-2.14. These precisions represent the expected (average behavior over the sphere) root-mean-square uncertainty (one sigma error) in a regionally averaged estimate of the geoid height or gravity anomaly. The regional averaging is a Gaussian-weighted average on a spherical cap and the resolution length is the side of a square of the same area as a circle of the radius at which the Gaussian weight function has 1/2 its maximum amplitude. Calculation of these resolution estimates (Appendix A, section A.8) follows established methods for the propagation of degree variances. Some previous workers (Kahn and von Bun, 1985; Jekeli and Rapp, 1980) have used a simple spherical-cap average, but this operation is known to have significant sidelobes; a superior error estimate can be obtained by using the Gaussian smoothing operator (Jekeli, 1981, 1996).

These precision-versus-resolution estimates are calculated from the degree variances of the errors obtained above, but with two adjustments. The first adjustment applies only to the SGG and SGGE cases. The SGG and GPS curves in Figures 2.3-2.6 show that at very low degree the gravity field coefficients determined from an SGG gradiometer will be less certain than those obtained from a GPS mission. For this reason, an SGG mission should include a GPS receiver onboard the spacecraft, and the low-order field should be constrained by the GPS data, as discussed above. Therefore, we calculated the resolution of the SGG and SGGE missions by using degree variances that comprised the lesser of the SGG and GPS degree variances.

The second adjustment was applied to the degree variances used to calculate the resolution estimates for all the missions, but was applied in making estimates only of the static field, not the time-varying field. Figures 2.3-2.6 show that at high degree, the errors in the gravity-field coefficients determined from all the missions exceed the expected gravity-field signal and the error estimates of the current gravity-field model EGM96. At these high degrees, the satellite missions do not usefully constrain the gravity-field model. In practice, a new gravity-field model would be estimated from a satellite gravity mission by using the mission data to update an existing model. If this were done, the uncertainties in the new model coefficients at high degree would be the same as they had been in the starting model, since the satellite mission would not have provided additional constraint at these degrees. (In the language of inverse theory, at high degrees the *a posteriori* model error would equal the *a priori* model error because the *a priori* model error is smaller than the data error.) To represent such modeling, we calculated the resolution estimates for the static field for all the missions by taking the lesser of the degree variances of the mission error estimates and the EGM96 error estimates. We did not apply this constraint in modeling the time-varying field resolution because no *a priori* information about error bounds is available for the time-varying field.

Figures 2.7-2.10 show the precision of the averaged geoid height resolved by the generic GPS, SGG, SST, and SSI missions, each flying at altitudes of 200, 300, 400, and 500 km, respectively, and, for comparison, the precision that can be obtained from the current gravity-field model EGM96. At long wavelengths, the SGG, SST, and SSI geoid-height precision curves are approximately parallel, with SSI being the most accurate, SST being an order of magnitude less accurate than SSI, and SGG being two orders of magnitude less accurate than SSI. At intermediate wavelengths there is a gradual degradation of precision with decreasing wavelength that is dependent on the altitude of the mission; there is an upward trend at 300-km resolution for a 200-km altitude, and at 400-km resolution for a 500-km altitude.

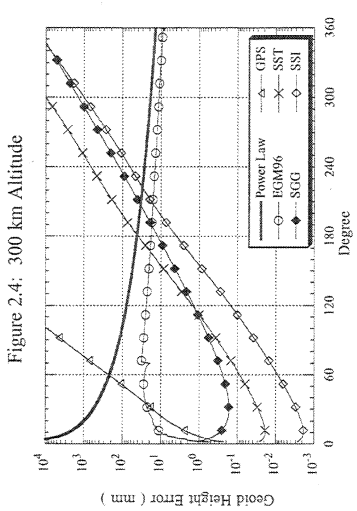

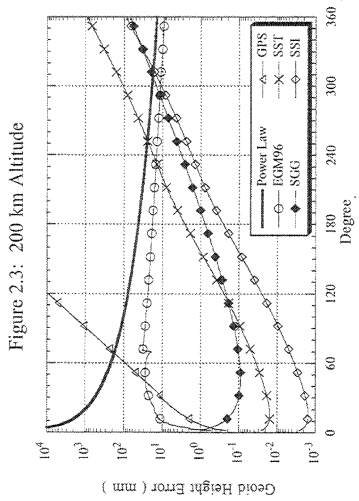

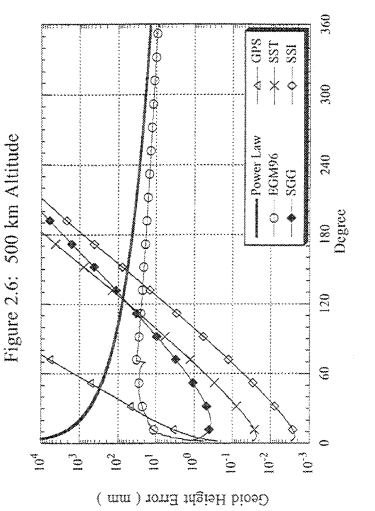

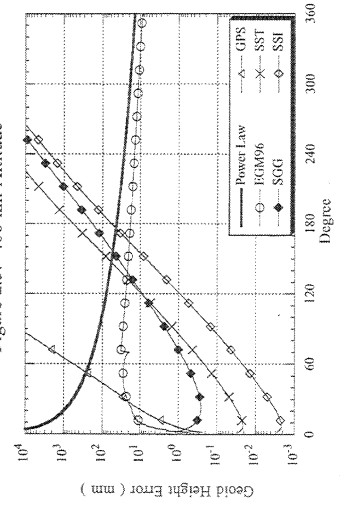

FIGURES 2.3-2.6
Geoid height error spectrum by degree for 90-day EGM96 and white noise generic missions at altitudes of 200, 300, 400, and 500

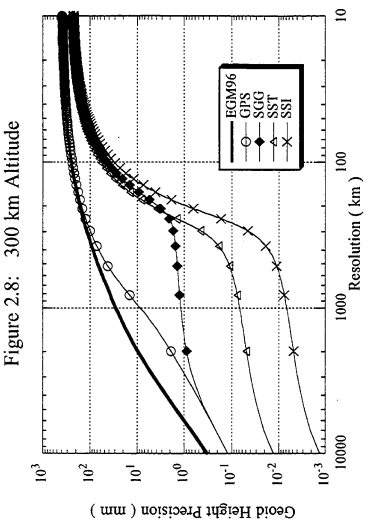

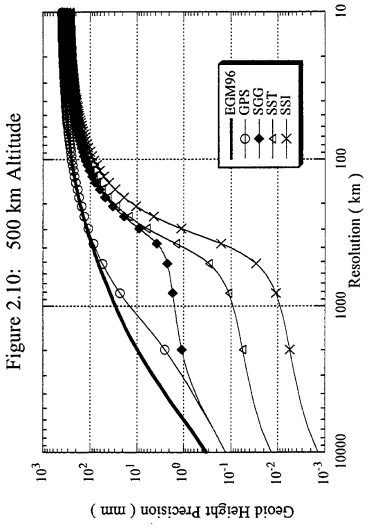

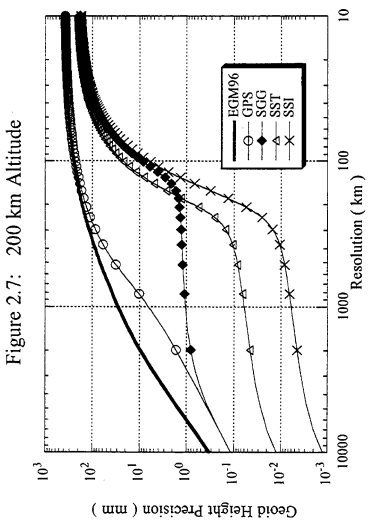

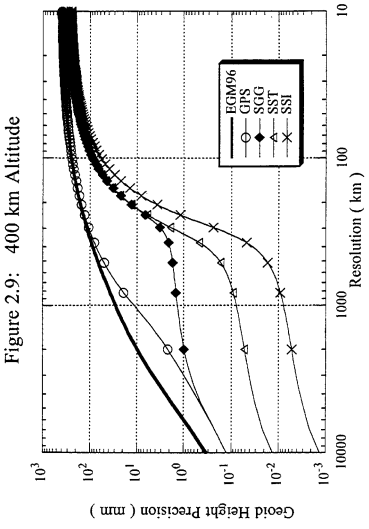

FIGURES 2.7-2.10
Geoid height precision vs. resolution for 90-day EGM96 and white noise generic missions at altitudes of 200, 300, 400, and 500 kilometers.

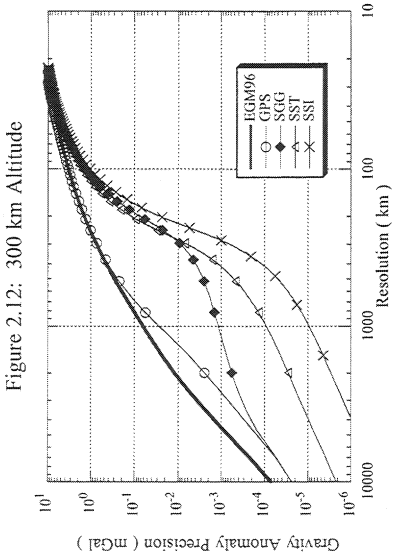

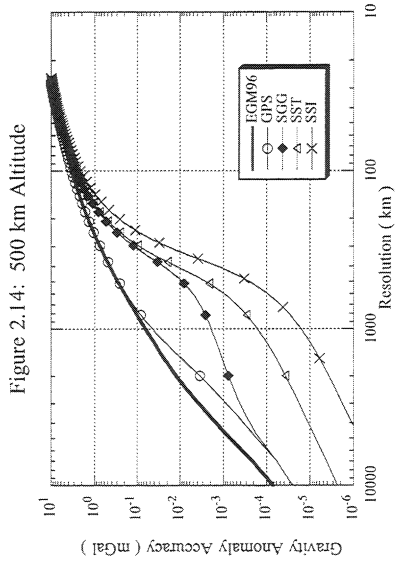

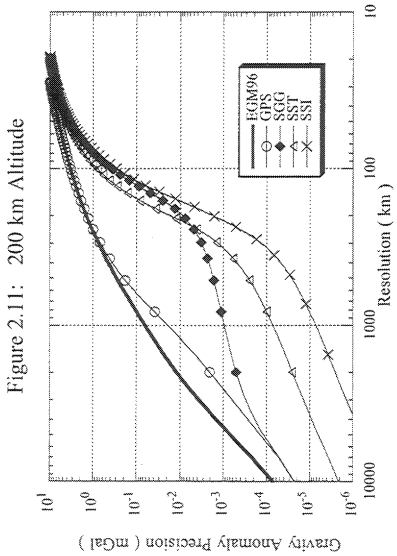

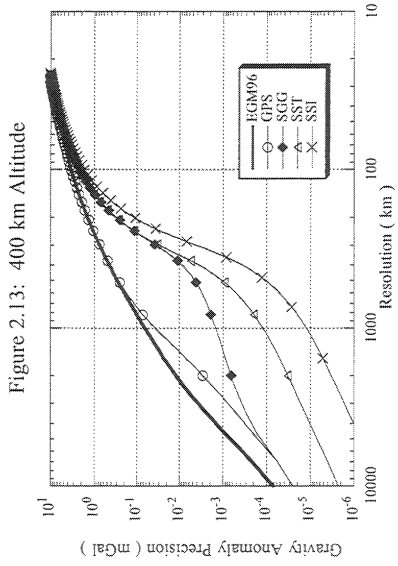

FIGURES 2.11-2.14
Gravity anomaly precision vs. resolution for 90 day EGM96 and white noise generic missions at altitudes of 200, 300, 400, and 500 kil

These upward trends occur where the satellite mission ceases to provide new information about the gravity field and the *a priori* constraint on the error takes over. Similar trends can be seen in the illustrations of gravity-anomaly precision versus resolution in Figures 2.11-2.14.

The error and resolution estimates obtained in this section are not meant to be a definitive representation of the errors realizable from actual missions. In addition to the idealizations and approximations mentioned above, there are other reasons why actual missions would be different. However, in spite of the approximations in our error-estimation technique, we feel that the gravity errors presented here are close enough to the results of more rigorous error analyses that they adequately reflect the character of the errors expected from each of the four generic missions. In particular, the variations of the errors with increasing altitude and decreasing spatial resolution should be quite accurate.

Although we have not simulated the error effects of non-gravitational or rotational influences, we do not think these will bias our results as SST and SSI missions are expected to be flown with high-precision accelerometers onboard, and the SGG missions are expected to reject these influences with careful common-mode rejection and precise alignment of the accelerometers. In addition, rigorous numerical simulations reported by Bettadpur and Tapley (1996a) indicate that, for the SST and SSI missions, the aliasing effects of low-frequency (82 cycles/revolution) accelerometer and measurement errors are greatly reduced by adjusting appropriate bias parameters simultaneously with the gravity model parameters.

Time-dependent signals in the Earth's gravity field introduce additional complications. Our simulations have assumed that the gravity field signal is constant over a 90-day period. Inspection of Figure 1.2 shows that there will be variations over this time period. The secular post-glacial rebound signal would show a change of 10^{-10} of gravity over 90 days with a mostly known spatial pattern. Mid-latitude cyclonic circulations in the atmosphere could generate signals of 10^{-9} of gravity if they varied significantly over 90 days, but these signals would also be manifest in atmospheric pressure and could be removed. Signals from very large earthquakes would also approach 10^{-9} of gravity, but would be at wavelengths too short for these missions to resolve. These issues are discussed further in the following chapters. The key to isolating these signals is that many of them have known spatial patterns (post-glacial rebound) or can be correlated with other observations (atmospheric pressure). Since a mixture of secular, seasonal, and interannual signals is expected, longer missions will be better able to separate these than shorter missions.

STANDARD GENERIC MISSIONS

In this chapter we have shown the effects of varying orbital altitude by modeling errors at 200, 300, 400, and 500 km altitudes. In the following chapters we will show resolution diagrams that, for clarity, use only one altitude. We have adopted 400 km as a "standard" altitude for all missions except the SGG mission, which we show at 300 km. This is because we expect the SGG mission lifetime to be limited to 9 months by the helium dewar technology, and therefore we expect the SGG to fly at the lowest possible altitude that will allow the mission to last 9 months without carrying and burning fuel. The other missions are expected to carry fuel to re-boost their orbits; we therefore suppose that they can fly at an average altitude of 400 km for as long as 5 years. It is possible that these other missions could begin or end in a lower (300-km) orbit to increase their resolution of the static field. Our standard mission designs are summarized in Table 2.1. Note that the technologies for the SGG and SST missions are mature and ready for implementation.

In the following chapters, resolution diagrams will use the standard designs and the 90-day error estimates if the discussion is independent of time, or 5 years of independent 90-day estimates if the discussion is of time-varying constituents of the gravity field. Further details of modeling time-dependent resolutions are given in Appendix B.

CONCLUSIONS

1. There are tradeoffs between mission lifetime, altitude, and resolution. Long missions are higher and have lower resolution than short missions. Also, tradeoffs exist between temporal and spatial sampling. For example, a mission at a height of 160-170 km, which would be best for 60-km resolution (l = 350), would be a costly mission of short duration. A mission at an altitude of 400 km with a resolution capability such as we have modeled would be able to achieve its optimal spatial resolution with an orbit repeat period on the order of 40 days.

TABLE 2.1 Summary of Generic Missions

Mission	Primary Measurement	Ancillary Equipment	Altitude (km)	Duration (years)	Readiness
GPS	high-low tracking by double-differenced phase	accelerometer	400	5	current
SST	low-low microwave tracking	accelerometer	400	5	mature
SGG	cryogenic gradiometer	GPS receiver	300	0.75	mature
SSI	low-low laser tracking	accelerometer	400	5	future?
SGGE	gradiometer	GPS receiver	400	5	future?

2. The contributions of GPS tracking of a low satellite lie at long wavelengths. Such a mission flown at an altitude of 400-500 km would yield significant improvements over the current EGM96 results at harmonic degrees less than 25, whereas a mission flown at 300 km would contribute significant improvements at degrees up to 30.
3. The strength of the SGG mission is its high resolution, with significant improvement over the EGM96 results for degrees up to 155 at a height of 400 km and up to 215 at a height of 300 km. The short lifetime (less than one year) would limit the study of temporal variability.
4. A strength of the SST mission (the low-low mission with microwave tracking) is its high precision at long and intermediate wavelengths, hence better geoid height and gravity anomaly precisions than the SGG mission (Figures 2.7-2.10). Also, the mission lifetime (estimated to be 5 years) permits the determination of a greater range of time-varying effects.
5. The anticipated results from the SSI mission (the low-low mission with laser interferometry) are the best of the four scenarios studied. They are an order of magnitude better than the SST results at all wavelengths considered and 2 orders of magnitude better than the SGG results at long wavelengths. Technological development is required for SSI, however, whereas the technology needed for SGG and SST is mature.
6. Precision tracking by GPS is needed on all missions.

3

The Gravity Field as a Tool For Science

In the chapters following this one we address specific fields of research that we believe will particularly benefit from a satellite gravity mission. In this chapter, we mention some of the ways in which gravity field data are vital to the basic infrastructure of science. The gravity field is an essential part of the reference frame used for locating points on the Earth. The gravity equipotential surface, called the "geoid," is essentially equivalent to the "mean sea level" to which elevations on land are referred and the shape that the ocean surface would have if there were no currents flowing. The direction of gravity determines the directions of "horizontal" and "vertical" and anomalies in the direction ("deflections of the vertical") affect the location of points on land by classical astronomic surveying. Gravity anomalies also perturb the orbits of Earth satellites and accurate gravity field models are required to correctly locate the position of an orbiter above the Earth. The limiting factor in the accuracy of some remotely sensed data is the uncertainty in the orbit produced by uncertainty in the gravity field. For example, synthetic-aperture-radar interferometry would be enhanced if the spacecraft's orbit could be computed with an across-track accuracy of a few centimeters; satellite altimetry would have improved accuracy if orbits could be computed with a radial error under 30 mm. In this chapter we discuss some of the ways in which accurate gravity-field information is a vital part of the Earth reference frame and the value a satellite mission would have in the calibration and validation of existing data from gravity-field surveys.

REFERENCE FRAME (1): THE FOUNDATION FOR MEASURING THE CHANGING EARTH

The gravity field has conventionally played a critical role in the definition of reference frames that provide the basis for measurement of periodic and stochastic motions in the Earth's atmosphere, hydrosphere, lithosphere, and deep interior. Indeed, the establishment of precise geodetic reference frames is necessary to quantify the dynamic Earth system. The global gravity field is useful as the fundamental reference for two reasons: (a) the conformance of mean sea level to a (nearly) equipotential surface allowed a height reference system based on the geoid to be established worldwide before the advent of satellite-based positioning systems; and (b) the only directions that could be defined globally were the directions of plumblines, which are perpendicular to the equipotential surface. With the advent of spaced-based measurements of positions that use range or range-rate determinations (and are thus independent of the angle relative to the direction of gravity), both of these reference-frame issues have become moot to some degree. It is now possible to position points geometrically without any direct reference to the gravity field. However, there is still a need to realize a coordinate system through some means, and the gravity field is a natural basis. Moreover, many countries would like to have a geoid model that is sufficiently accurate to be combined with satellite positioning to

give direct estimates of elevations above sea level, without traditional leveling surveys.

To define an instantaneous coordinate system for the Earth, six parameters are needed (assuming that scale is not a serious issue with the measurement system): three translations and three rotations. Nearly all measurement systems derive their orientation from the rotation axis of the Earth or a suitably averaged measure of this axis. However, the rotation axis of the Earth moves by several meters every year with respect to the crust of the Earth due to atmospheric, oceanic and, to a lesser extent, solid-Earth dynamical motions. In practice, the current definitions of the orientations of coordinate systems are based on the minimization of the difference in orientation between coordinates at different times.

For some measurement systems based on monitoring of extraterrestrial sources such as quasars, the same applies to translations (i.e., the system is not sensitive to translations of the coordinate system because the observed objects are so distant that the frame can be arbitrarily translated between measurements). However, systems that make measurements of Earth-orbiting bodies cannot be freely translated because the bodies are orbiting around the center of mass of the Earth. For these measurement systems, the gravity field plays a critical role in the definition of the coordinate system. Of particular significance in this regard is that these types of systems can make absolute measurements of the changes in heights of points independently of the orientation of the coordinate system. Thus the gravity field provides the center of the coordinate system for making measurements of phenomena such as post-glacial rebound. Of concern is the possible motion of the center of mass of the Earth with respect to the center of figure, but these motions (expected to be <10 mm) are themselves geophysical signals. In a fully consistent analysis of measurements to Earth-orbiting satellites, the coordinates of the site and changes in the first-degree harmonic terms of the gravity field should be estimated in the same solution. These gravity-field coefficients can be estimated equivalently as translations of the coordinate system with time. In this case, the measurement is of changes of the center of figure relative to the center of mass.

It is clear that a major limitation in detecting subtle but important changes in the Earth, particularly those that arise from coupled interaction of discrete parts of the geosystem, is the accuracy of the absolute reference frame. Establishing even more accurate reference coordinate systems will be required in future efforts to characterize the Earth quantitatively as a complex system.

REFERENCE FRAME (2): THE GEOID, FLUID CIRCULATION, AND SATELLITEALTIMETRY

As stated in the Introduction, the "gravity" experienced on the rotating Earth combines the effects of attraction and rotation. If the fluids of the atmosphere and oceans were to cease their motions and come to rest in a state of hydrostatic equilibrium upon the (uniformly rotating) solid Earth, then surfaces of constant pressure within the fluids would conform to equipotential surfaces of the gravity field. In that condition, the interface between the oceans and the atmosphere would lie on a particular equipotential surface called the "geoid." Since the geoid is defined as an equipotential of gravity, it can be extended through areas on land occupied by rock; it is not restricted to the oceans only. The shape of the geoid is approximately an ellipsoid. A reference ellipsoidal shape is adopted for the Earth, and "geoid anomalies" are defined as displacements of the geoid above or below the ellipsoid; these have root-mean-square amplitudes of about 30 m. (This mean ellipsoid differs from the hydrostatic figure by 29 m rms.) The geoid defines the "mean sea level" to which heights on land have been classically referred, as discussed above.

Since the fluids in the atmosphere and oceans are in motion with respect to the solid Earth, the actual position of the sea surface is vertically displaced from the geoid through a dynamic equilibrium involving the fluid motions. These departures are on the order of 1-2 m and are referred to as dynamic heights. Through the techniques of satellite altimetry, one can measure the shape of the ocean surface with respect to the ellipsoid (that is, the combined effects of the geoid plus the dynamic displacement) with an accuracy currently approaching 40-50 mm (Fu et al., 1994). The current limit on accuracy is the ability to model the orbital height of the altimeter satellite above the ellipsoid; the distance between the altimeter and the ocean surface has a precision of 20-30 mm, and its absolute accuracy depends on corrections for delays in the atmosphere, which are known or can be modeled to a few centimeters. Thus, satellite altimetry measures the sum of the geoid anomalies plus the dynamics of fluid circulation with an accuracy much better than is needed to study either one; however, it cannot separate the two effects.

The trade-off between spatial and temporal resolution discussed in Chapter 2 applies to all satellite remote-sensing missions, including satellite altimetry. Most satellite altimeters are operated in "exact repeat" orbits, which sacrifice spatial resolution to achieve temporal resolution. For example, the NASA/Centre Nationale d'Etudes Spatiales' TOPEX/Poseidon spacecraft measures the sea-surface height every 10 days along a pattern of ground tracks spaced 315 km apart at the equator. This allows oceanographers to study the time variations in sea-surface height, which are caused by variations in the ocean circulation. The absolute circulation cannot be studied without independent knowledge of the geoid. In Chapter 4 we describe the science that could be done by combining a dedicated satellite gravity mission with a satellite altimeter sea-height mission.

Two satellite altimeters have operated in "geodetic" orbits in which the sea-surface elevation is measured only once along a densely-spaced network of ground tracks. Over an 18-month period in 1985-1986 the U.S. Navy's Geosat surveyed the ocean height with a track spacing of approximately 5 km at the equator, whereas in an 11-month period in 1994-1995, the European Space Agency's European Remote-Sensing Satellite-1 (ERS-1) surveyed the ocean height with a track spacing of approximately 8 km at the equator. These data have been combined to produce a map of the variation of gravity over the oceans (Smith and Sandwell, 1995a; Sandwell and Smith, 1997); however, this map is not a correct characterization of gravity because of errors and oceanographic dynamic effects (Smith and Sandwell, 1995b). Marks (1996) found root-mean-square differences of 3 to 5 mGal between the Smith-Sandwell gravity field and the best available marine gravity surveys, with coherency only at wavelengths exceeding 20 km or so. This level of resolution (about 90% of the total signal) is sufficient to allow reconnaissance of ocean-floor tectonic features, but it is not as accurate as could be achieved with state-of-the-art marine (Bell and Watts, 1986) or airborne (NRC, 1995) gravimetry.

DATA CALIBRATION AND VERIFICATION: GIVING OLD DATA NEW VALUE

Conventional gravity surveys on land, at sea, and in the air are made with gravimeters, which yield only relative values and so must be calibrated by "known" values to yield complete information. In many cases this has been done inaccurately, or the "known" values have been in error. Furthermore, when surveys are contributed to data banks, the documentation about calibration and reference frames (including the standard ellipsoidal gravity model to which anomalies are referred) is frequently not supplied. When one attempts a global synthesis of the various data in data banks, a peculiar patchwork quilt emerges, with significant discrepancies at the borders between countries and land surveys. Errors in marine surveys are particularly large, as evidenced by the discrepancies at their crossings (Wessel and Watts, 1988). The relative changes in gravity measured by all these surveys over short horizontal distances (less than a few hundred kilometers) are potentially very accurate—much more accurate than a satellite mission could achieve—so one would like to be able to tie these surveys together into a seamless regional or global synthesis.

A satellite gravity mission would provide spatially (nearly) uniform coverage and error distribution, and it would allow correct calibration of archival survey data, adding enormous value to existing data. As the resolving power of the satellite data increases, so would the statistical reliability of the calibration. An important calibration of gravity survey data could be made with a satellite mission that has a resolution of a few hundred kilometers and a precision of 1 mGal.

The calibration problem is particularly severe for marine data. Marine gravimeters are calibrated when the ship is in port, and recent investigations of the accuracy of these data suggest that incorrect port calibrations are a major source of error (Wessel and Watts, 1988; Smith and Sandwell, 1995c). A typical situation is shown in Figure 3.1, where a sequence of shipboard gravity measurements is plotted against the distance the ship traveled between ports (bottom panel). This example is a 1985 cruise of the *R/V Conrad* between two ports on the South China Sea. For comparison, the gravity anomalies estimated from satellite altimetry by Smith and Sandwell (1995a) are also shown (bottom panel, dotted). The difference between the two profiles (top panel) shows a linear trend starting out around 42 mGal and decreasing by more than 1 mGal per day of the cruise. Shipboard gravimeters do not drift this rapidly; the difference is most easily explained by supposing that the shipboard data were calibrated to one wrong value in the port of origin and a different wrong value in the port of arrival, producing the apparent drift. (Superimposed on this linear drift are short-wavelength differences. These are expected, due to a variety of effects: real short-wavelength signals that can be measured by the ship

board gravimeter but not by a satellite; errors in the shipboard data due primarily to navigational errors in the Eötvös correction [Wessel and Watts, 1988]; and errors in the satellite data due to the dynamic ocean topography.)

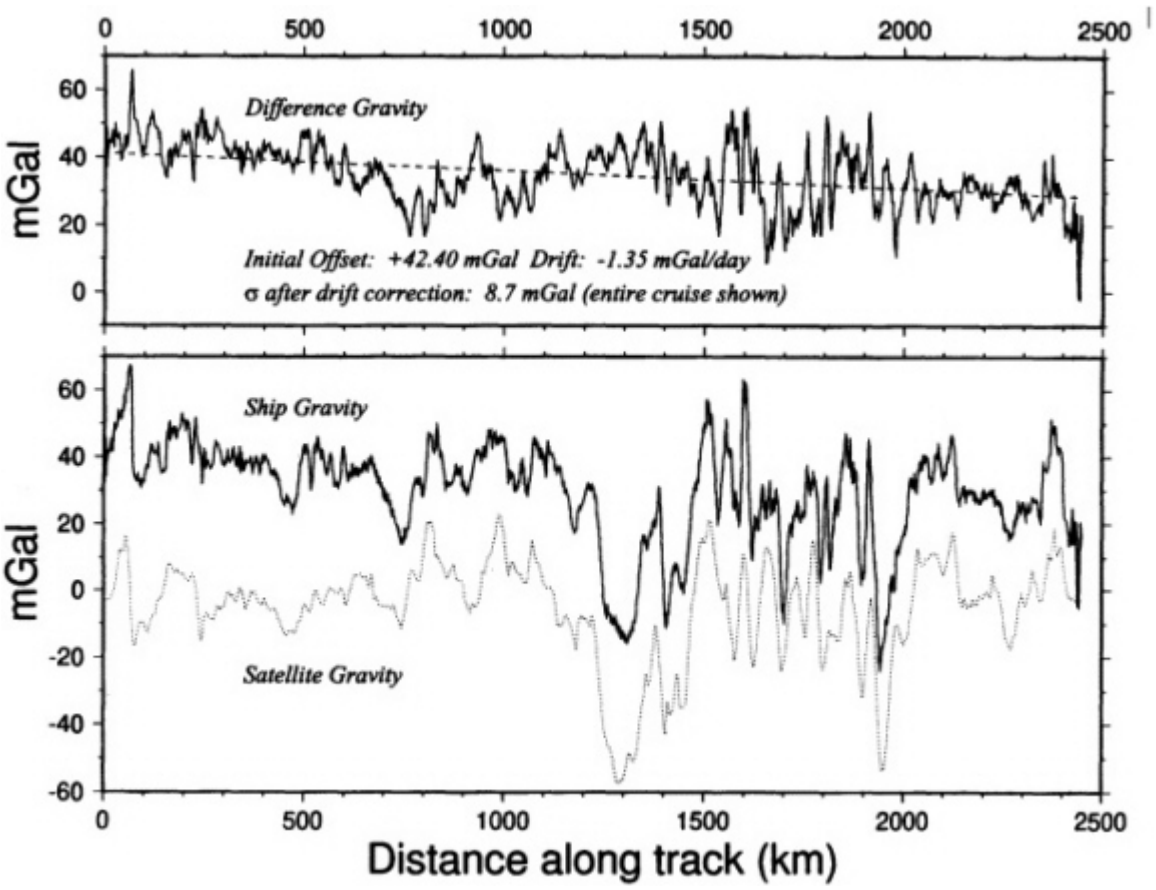

FIGURE 3.1
Gravity anomaly versus distance traveled for a ship survey (bottom panel, solid line) and gravity anomaly estimated from satellite altimetry (bottom panel, dashed line) for comparison. Top panel: the differences between the two appear to show a linear trend, probably due to errors in calibrating the ship instrument to correct values in port. Figure from Smith and Sandwell (1995c).

Calibration errors as large as those shown in Figure 3.1 are detectable—but not correctable—either through examination of errors at crossing ship tracks (Wessel and Watts, 1988) or through comparison with gravity anomalies estimated from satellite altimetry, as shown here. Wessel and Watts (1988) estimated corrections for the mean level and apparent drift of marine survey data by minimizing the errors at crossing ship tracks. This left the global mean value of their data set after correction undetermined, since any constant could then be added to all the marine surveys without adding a crossing error; they found their global mean differed from other gravity fields by 9 mGal. Their technique would also leave wavelengths longer than the typical distance between port calls poorly determined. Although Figure 3.1 seems to suggest it, one should not try to fix the marine data simply by adjusting them to a gravity field derived from satellite altimetry, because that field has errors caused by assuming that the sea-surface height determined by the altimeter is the geoid height One ultimately would like to use the correctly calibrated marine gravity data to make a gravimetric geoid that can be compared with the altimeter-derived sea

surface to study the oceans. Use of the satellite data shown in Figure 3.1 to correct the shipboard data would not yield a geoid measurement that is independent of altimetry. Therefore, only a satellite gravity mission, such as investigated in this report, can adequately calibrate and validate the existing marine gravity database.

CONCLUSIONS

Satellite gravity measurements are useful for complementing and supporting other types of measurements. All four mission scenarios considered in this report offer significant improvements in measuring the static gravity field, which is vital in a variety of fundamental ways. These include:

1. Determination of the reference frame for defining position coordinates;
2. Calculation of orbits for other remote sensing applications (e.g., altimetry, synthetic-aperture-radar interferometry);
3. Determination of the geoid as the hydrostatic reference level to which absolute ocean circulation is referred (this is discussed further in Chapter 4); and
4. Verification and calibration of regional and shorter-scale terrestrial, marine, and airborne gravity-survey data.

4

Ocean Dynamics and Heat Flux

STATIC FIELD

The primary direct benefit of an improved static geoid for ocean circulation studies is in the determination, in conjunction with precise-satellite altimeter measurements, of the geostrophic surface currents. These, in turn, can become the basis of calculations of such quantities as near-surface advective heat transport, can be assimilated into general circulation models (GCMs), and can be used with *in situ* data in inverse calculations of mass, heat, salt, and other transports at intermediate and deep levels. The importance of determining the deep ocean circulation derives from its role in regulating the Earth's climate on decadal and longer time scales (Box 4.1). It is therefore fundamentally important to the understanding and prediction of future climate change that the dynamical and thermodynamical processes of the ocean be studied and modeled. With the advent of satellite systems, we are now able to obtain nearly synoptic global measurements of key variables such as surface temperature, sea level, and wind stress. Satellite altimetry measures sea level, which is a parameter for both ocean currents and heat storage. As is discussed below, a precise gravity model is necessary to obtain full benefit from altimetry in determining the mean surface circulation.

The surface geostrophic velocity is proportional to the slope of the dynamic topography, which is the departure of the sea-surface elevation (measured by altimetry) from the static marine geoid. (Assuming that the geoid is static, a change in the sea-surface elevation equals a change in the dynamic topography, so the altimeter data are widely used to study temporal oceanic variability on all scales.) The geostrophic calculation will be valid where the uncertainty of the marine geoid is negligible compared to the magnitude of the undulations of the mean dynamic topography. As shown below, the latter can be estimated with dynamic heights derived from historical oceanographic-atlas data, such as that of Levitus et al. (1994) and Levitus and Boyer (1994), or from a state-of-the-art numerical ocean general circulation model, such as the Parallel Ocean Circulation Model (POCM) described by Semtner and Chervin (1992) and Stammer et al. (1996). Figure 4.1 indicates that this condition is satisfied to about degree 20-25 (1600-2000 km wavelength) with the EGM96 geoid errors. The state of the art of gravity modeling and existing satellite tracking is not likely to offer significant reductions in geoid error to improve oceanographic calculations at shorter wavelengths. In contrast, the satellite gravity missions will offer major improvement to degree 100 or greater (~400 km and shorter wavelength), with the exception of the GPS scenario, which will not provide significant improvement for oceanographic purposes.

The classical method for computing dynamic topography is to integrate the specific volume of sea water vertically to obtain the steric height, or vertical separation between isobaric surfaces. It is generally assumed that the slopes of deep isobaric surfaces are small, so that the variation of the steric height of the sea surface relative to a deep surface nearly represents

the variation of the sea surface relative to the geoid. When the deep surface also has a slope, which it generally does, then that slope must be added to the steric estimate for the surface in order to obtain the absolute dynamic topography. In this context, we refer to the barotropic component of the pressure field as that which is the same at all levels. Determining a reference-level pressure field, or barotropic term, is a long-standing problem in dynamical oceanography. The World Ocean Circulation Experiment (WOCE) is producing a global, but still very sparse, network of conventional transoceanic sections and measured deep ocean currents. Efforts are under way to use observations to constrain models of ocean circulation. However, because of the limited array of observations in the deep ocean and the lack of direct control of the circulation by the atmosphere, our knowledge of deep ocean pressure and circulation will retain significant uncertainty.

BOX 4.1 THE OCEAN'S ROLE IN GLOBAL CHANGE

The ocean influences climate change on seasonal, interannual, and longer time scales in a variety of important ways. Half of the solar radiation reaching the Earth's surface is first absorbed by the ocean (Peixoto and Oort, 1992). The ocean stores or transports this heat before it is eventually released to the atmosphere through evaporation and longwave radiation, providing the major source of energy for atmospheric motions and thus for the Earth's climate (NRC, 1994). Surface currents influence the exchange of heat across the air-sea interface and thus indirectly influence how the oceans regulate climate change. The moderation of the northern European climate by the warm waters carried in the Gulf Stream and North Atlantic Current is a well known example. Conversely, a southward shift in the flow axis of the North Atlantic is believed to have been responsible for cooling events in the geologic past.

Changes in the deep circulation caused by warming in the polar latitudes can also affect the primary productivity of the oceans by changing the area and intensity of upwelling of water from deeper layers (IPPC, 1996). This would have profound impacts on fish species production—marine mammals and sea birds, in turn, would be affected as centers of food production shift

Finally, the El Niño-Southern Oscillation (ENSO), which occurs when warming in the eastern and central tropical Pacific Ocean becomes coupled with a seesaw in atmospheric mass, is the most significant source of interannual variability in weather and climate (IPCC, 1996). ENSO events, which occur every 3 to 10 years, have far-reaching climatic and economic consequences. For example, it has been estimated that improved forecasts of ENSO events could lead to savings in agricultural production that exceed $100 million per year in the United Stares alone (Subcommittee on Global Change Research, 1997).

The question is whether such a calculation will be as good an estimate for the surface dynamic height as that obtained from a gravity mission coupled with satellite altimetry. Put another way, will a gravity mission offer substantially new information about the ocean given what we already know? As shown below, the answer is "yes" for spatial scales ranging from 300 to 3000 km. The observed sea-surface elevation is the sum of the geoid and the ocean dynamic height signals. While the problem is usually viewed as the ocean being the unknown, it is equally valid to state that a geoid can be estimated with an ocean model and an altimeter (Ganachaud et al., 1997). At present, it seems that our knowledge of the ocean provides a better estimate of the geoid than *vice versa*.Figure 4.2 shows the differences between an ocean model and a mean surface determined by altimetry and the JGM3 gravity model. Biases as large as 20-30 cm over large expanses are clearly spurious in the geoid and not the model, particularly the large >50 cm anomaly near Indonesia, because otherwise they would imply vigorous circulation features that are known to be absent from the real ocean.[1] A spaceborne estimate of dynamic height can be used as a reference from which the pressure field and velocity at all depths can be determined from the steric calculations. Ganachaud et al. (1997) considered

[1] The JGM3 gravity model (Tapley et al., 1996b) used by Rapp et al. (1996) in the analysis shown in Figure 4.2 is a predecessor of the EGM96 model discussed throughout this report. EGM96 differs from JGM3 over the oceans in that marine gravity anomalies estimated from altimetric data were included in EGM96. These additional data cause EGM96 to partially absorb dynamic topography signals into the EGM96 geoid at degrees larger than 70 (the maximum degree included in JGM3). It is necessary to have a precise geoid model obtained independently from altimeter measurements to obtain a better measure of the ocean circulation. An investigation similar to that of Rapp et al. (1996), but using the EGM96 gravity model is under way and the results are expected to be somewhat different (R. Rapp, personal communication).

this problem very rigorously using the accuracy of heat fluxes derived from inverse methods, and concluded that the JGM3 model coupled with altimetry did not reduce the uncertainty of the heat flux estimates, but that a more precise geoid could reduce uncertainties by as much as a factor of two in large data-sparse regions, such as the Antarctic Circumpolar Current (ACC) and portions of the Pacific. Such calculations were based on box-inverse methods set up such that the unknown quantities were computed at the same locations where high quality hydrographic data had been collected, densely along track, with large gaps between cruise profiles. Minster and Legrand (1996) argue that errors will be larger when the estimates are computed in the large gaps between cruises, and that the technique chosen by Ganachaud et al. (1997) must make a single barotropic correction at all depths between each station pair, rather than allow a vertical profile of velocity corrections (which introduces a non-linearity in the problem). While they also find small reduction in total heat and mass transport errors, they argue that the primary benefit from a gravity mission will be improved estimates of upper-ocean baroclinic transports rather than the reference velocity and barotropic terms.

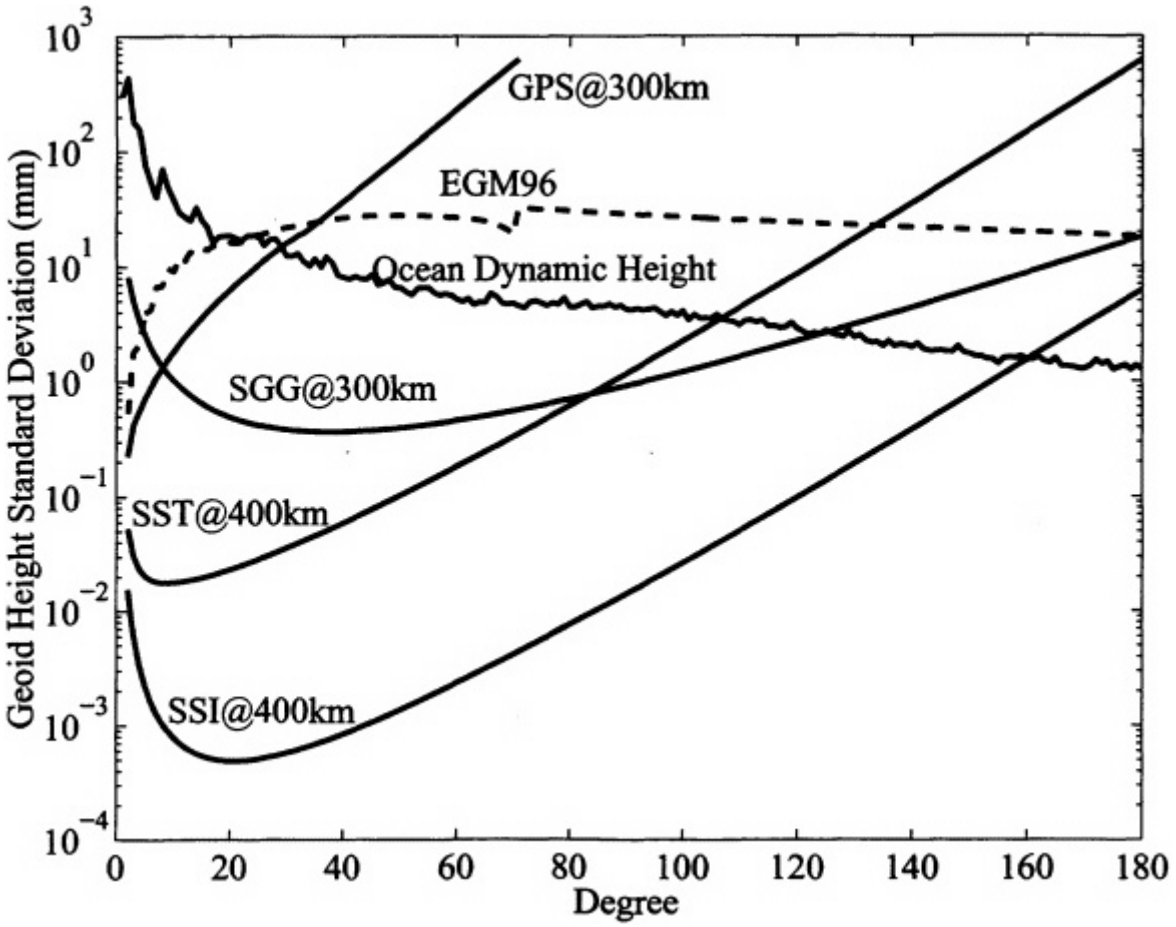

FIGURE 4.1
Geoid height and mission error spectra from Figs. 2.3-2.6 based on 90-day missions (see Chapter 2), plotted along with the degree spectrum of mean ocean surface dynamic height derived from the Parallel Ocean Circulation Model, POCM-4B, (Stammer et al., 1996). The degree variances were based on an orthonormal expansion (Rapp et al., 1996) to degree 20 and spherical harmonic expansion for degree 21 and higher (Courtesy of R. Rapp, Ohio State University). The EGM96 errors exceed the oceanographic signal higher than about degree 20-25. All missions except GPS will yield significant improvement in the static marine geoid.

Hasselmann and Giering (1996) suggest that data assimilation with a coupled ocean-atmosphere general

circulation model (GCM) is a preferred approach to the box inverse-closure methods employed by Ganachaud et al. (1997). Indeed, we can expect that various GCM, assimilation, and inverse methods and data sets will continue to improve and reduce the uncertainty of the mean circulation estimates and deliver high-resolution gridded analyses. A major difficulty at present, however, is understanding the uncertainties of GCM simulations, which impedes our ability to assess the relative improvement to be gained from a gravity mission.

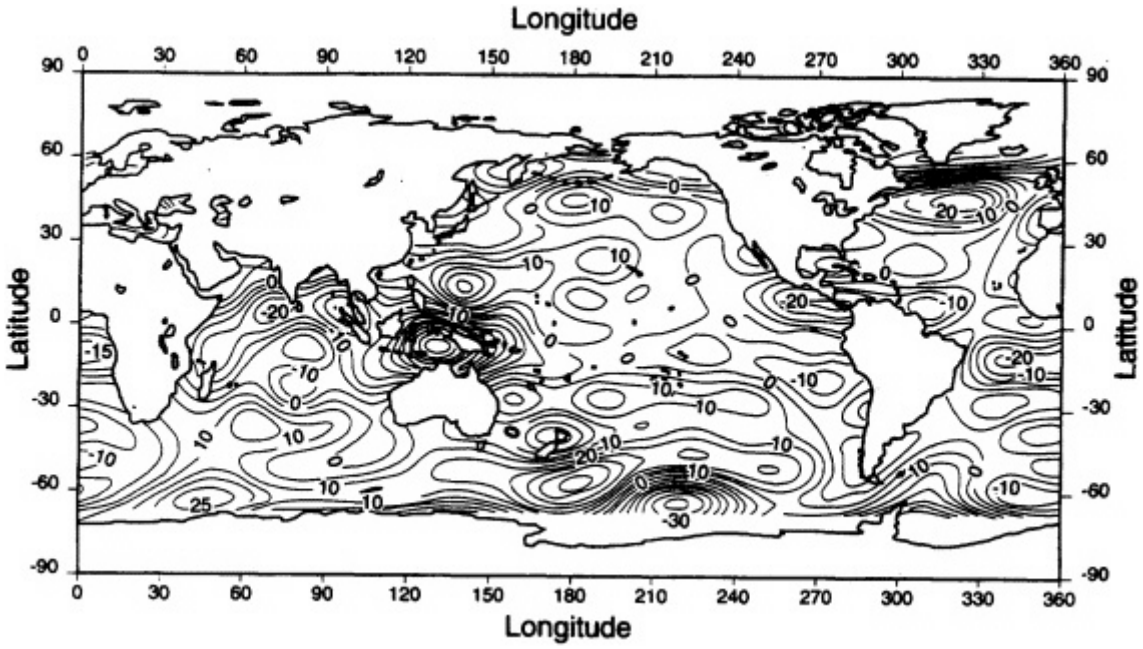

FIGURE 4.2
Difference in cm between the dynamic topography derived from TOPEX/Poseidon and JGM3 geoid model and a numerical general circulation model (from Rapp et al., 1996). Note the large discrepancies, particularly around Indonesia, which are the result of geoid model errors.

Another important source of error is the contemporaneousness of measurements (Ganachaud et al., 1997). Oceanographic data collected over several decades to estimate a mean sea surface do not represent the same state of the ocean, in the presence of significant interannual to interdecadal variability, as a few years of satellite altimeter data. Likewise, higher frequency ocean variability can cause estimates of steady-state properties from individual temperature and salinity hydrographic sections to be uncertain by tens of percent (Wunsch, 1996). These uncertainties must be carried through inverse calculations as error sources. Satellite gravimetry with simultaneous altimetry provides a significant advantage by providing a snapshot of the state of the surface dynamic topography. This will then serve as a datum for all co-registered altimeter data obtained before and after a precise gravity mission from which the absolute as well as time-varying surface geostrophic flow can be computed.

To further evaluate the potential payoff for a gravity mission, it is useful to examine the scales over which we are likely to obtain important new information. Since we are dealing with two measurement systems—the altimeter to measure sea level and the gravity mission to derive the geoid—both must have errors smaller than the static ocean signal we wish to measure. Ideally, we would like each error to be at least an order of magnitude smaller than the mean dynamic topography signal. That is generally the case for the altimeter, except for the longest resolution lengths. If the two errors are of the same order, we cannot distinguish them and the errors are compounded as the root sum square. If one is an order of magnitude smaller than the other, it is effectively eliminated as an error source. Thus, another practical criterion for geoid-slope accuracy is that it be an order of magnitude better than the satellite-altimeter accuracy and thus be eliminated as an error source over the range of spatial scales of interest.

An estimated mean-slope error for altimetry is plotted versus separation distance as a line in Figure 4.3. This assumes that a 10-mm uncertainty in the dif

ference between two mean height measurements is attainable by altimeter systems in the near future, taking into account tropospheric, ionospheric, tidal, wave-height, orbit-error, and other corrections. Figure 4.3 also shows the gravity-anomaly uncertainty for EGM96[2] and for 400-km-altitude 90-day missions of the SGG, SST, and SSI concepts. The right-hand axis gives the equivalent surface-slope accuracy (1 mm/km is equivalent to 10^{-6} = 1 mGal/g). The EGM96 error exceeds the altimeter error at horizontal resolutions shorter than about 3000 km by 1 to 2 orders of magnitude. With the advent of any of the gravity missions, the situation reverses and the gravity error becomes insignificant for a range of resolutions of importance to oceanography. The geoid-error curves for SGG, SST, or SSI missions indicate they will provide at least an order of magnitude lower contribution than altimetry to the total error budget for the estimation of geostrophic currents on spatial scales greater than ~400 km; the SST and SSI missions offer additional orders of magnitude improvement over SGG. At shorter scales, the SGG, SST, and SSI geoid-slope errors increase rapidly, crossing the altimeter-slope error curve at resolutions of 200-300 km; SGG and SSI provide the best small-scale accuracy. The payoff for the static ocean problem appears to be in the range of about 300-3000 km where the gravity error is dominant without a gravity mission and becomes insignificant with a gravity mission. Uncertainties in inverse calculations are of the same order as altimeter errors (Ganachaud et al., 1997). As noted above, GCM uncertainties have not been quantified, but they are not likely to be smaller than those of inverse calculations or altimetry. Consequently, in this 300-3000 km scale range, the gravity mission offers substantially better geoid information than can be inferred from altimetry and an ocean model. The improved geoid data could therefore be used to improve the ocean model.

Ocean geostrophic currents are dependent on surface slope, so the ability to resolve currents accurately will be limited by slope error. As indicated in Figure 4.3, this will require ~10^{-9} slope accuracy on basin-wide current (denoted BASIN) scales >1000 km. The slope resolution required for the 500-1000 km [width] scales of the ACC and 50-100 km scales of typical Western Boundary Currents (WBC) are likewise shown. The SGG, SST, and SSI gravity-mission concepts will allow BASIN and ACC scales to be resolved accurately. At the short WBC scales, the gravity uncertainties will be near the same order as the dynamic height slope, which may limit the accuracy of WBC estimates. It may turn out that airborne gravimetry has advantages in regions such as this because of its ability to resolve smaller scales. On the other hand, our gain of knowledge from the satellite gravity mission will be greater for basin scales and regions where there are few conventional data, such as the Antarctic Circumpolar Current.

Eliminating the gravity model as a significant source of surface-slope uncertainty over these spatial resolutions allows a number of issues to be addressed. The dynamic-topography surface determined by altimeter and gravity measurements represents the sum of the barotropic and steric height terms, and from this the total surface geostrophic current can be calculated. The regions where the barotropic component is strong but difficult to obtain will benefit significantly. The recirculation cells in the western subtropical gyres are presently poorly defined because they are significantly barotropic (Marchese and Gordon, 1996). In the western Atlantic, these circulations have transport volumes 2 or 3 times that of the Florida Current. The seasonal and interannual variability of these recirculation cells influences the large-scale heat transport and climate variability of the North Atlantic. Such recirculations exist in the North Pacific Kuroshio Current, the Agulhas Current, and possibly the weaker Brazil Current of the South Atlantic. The Antarctic Circumpolar Current is estimated to be about 30% barotropic (A. Gordon, personal communication). This current tends to appear in several narrow parallel filaments about 50 km wide, rather than as a broad flow. The gravity missions considered here will not resolve the individual filaments but will provide constraints for the transport sum across these filaments over 300-km and larger widths.

As noted above, time changes in the geostrophic circulation can be studied by altimetry without the benefit of an accurate geoid. However, both the mean and variable components are essential for heat and freshwater budget calculations. Budgets of the upper ocean mixed layer are balanced by the net flux of heat and water across the air-sea interface. Estimates of these fluxes have large errors and are important climatological variables. Divergences of surface temperature and salinity are important terms in these balances. Thus, accurate determination of surface currents is critical to closing both the heat and freshwater budgets

[2] The EGM96 error values at wavelengths shorter than about 570 km are not useful in oceanographic studies because these error estimates are derived from the surface gravity anomaly estimates used in EGM96 at spherical harmonic degrees above l=70. The anomaly estimates were derived from altimeter sea level data. See Footnote 1.

of the coupled ocean-atmosphere system. For example, an uncertainty in the net surface flux of less than 10 Wm^{-2} is desirable for climate studies. Sea-surface-temperature anomalies in the mid-latitude North Pacific have significant climatological variations on interannual to decadal time scales that may be related to changes in advection. Typical sea-surface-temperature gradients are of the order of 10° C per 1000 km. Assuming a 50m-deep mixed layer, the implied uncertainty in the surface current requires a slope error equivalent to about 0.05-mGal gravity error at around 40 degrees latitude (see Chapter 1). In the tropics, the uncertainty will need to be an order of magnitude smaller for similar temperature gradients. It can be seen from Figure 4.3 that the altimeter and various gravity-mission uncertainties at 300-1000 km resolution will be smaller in either case. Thus we can expect to calculate the advective terms in the heat budget of the mixed layer to better than 10 Wm^{-2} with the proposed gravity missions.

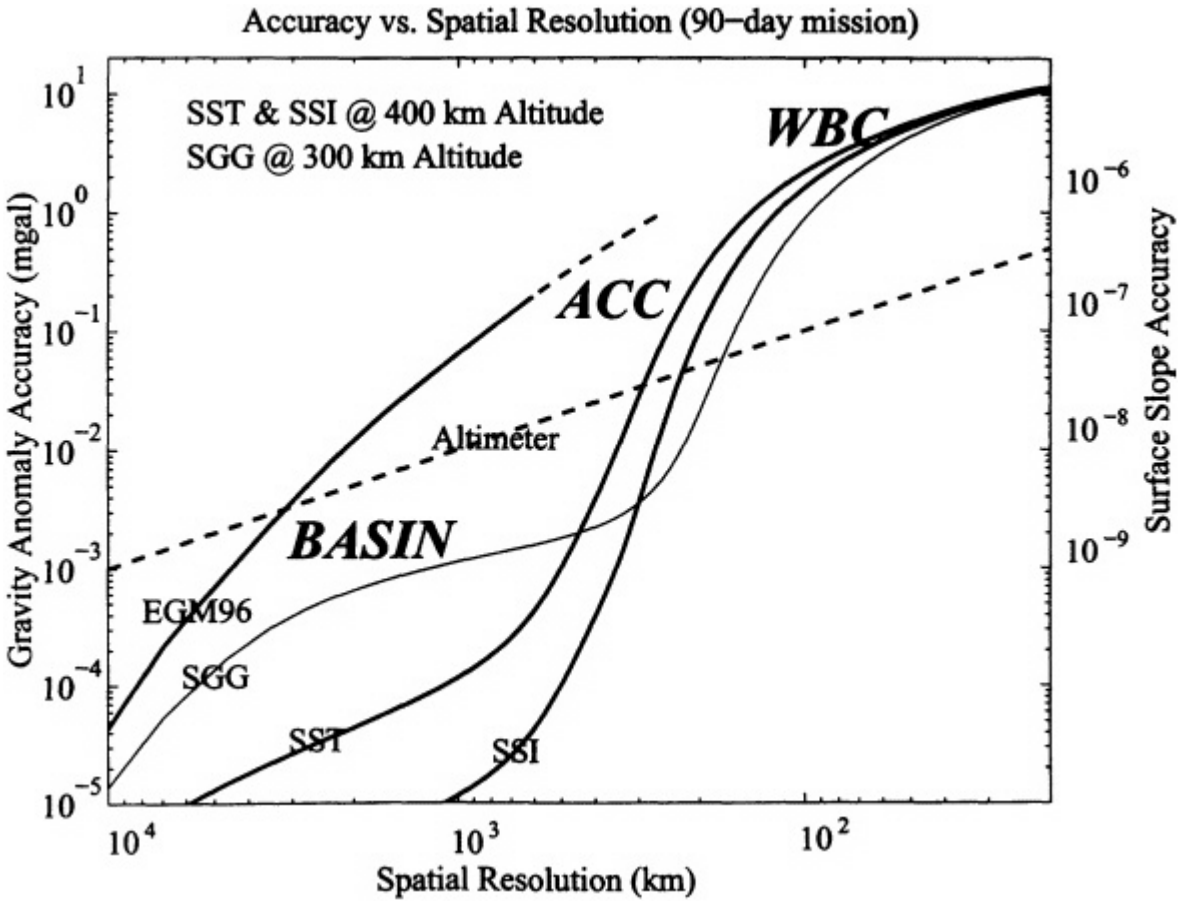

FIGURE 4.3
Errors versus spatial resolution for the SGG 300-km mission, the SST and SSI 400-km missions, and the EGM96 gravity model (see Chapter 2). The surface-slope scale is shown on the right-hand axis and the approximate slope magnitude and spatial scales of basin-wide currents (BASIN), the Antarctic Circumpolar Current (ACC) and Western Boundary Currents (WBC) are indicated. The dashed line indicates the slope error versus separation distance assuming a 10-mm uncertainty in altimeter height differences. The payoff for the static ocean problem appears to be in the range of about 300 to 3000 km where the gravity error is dominant without a gravity mission and becomes insignificant with a gravity mission.

TIME-DEPENDENT MEASUREMENTS

Most of what is known about the ocean occurs in the upper 500 meters. Time-dependent gravity measurements have the potential to provide a global estimate of

processes that occur deeper in the water column. For example, gravity measurements could revolutionize ocean circulation studies in at least two ways. The first is that they will allow a reasonably direct way of estimating bottom pressure variations, and thus variations in oceanic mass and deep ocean currents, from space. (Currently, oceanographers rely on indirect integrative constraints, such as those based on ^{14}C tracer measurements [Broecker and Peng, 1982]. Such tracer measurements are limited in that they cannot resolve changes in ocean circulation but indicate the time it takes for a water mass to move along an unknown trajectory.) The second is that, when combined with altimetry from a mission such as TOPEX/Poseidon, gravity measurements will allow the separation of steric changes in sea level associated with changes in density from nonsteric changes. Thus the combination of gravity and altimetry places a powerful constraint on models of ocean circulation. At the end of this section we discuss the important issue of the accuracy with which different geophysical effects may be separated.

The Earth's gravity field is mostly determined by the density distribution within the solid Earth. The total mass of the ocean, for example, is only about 0.02% of the mass of the solid Earth. However, because the ocean is far more mobile than the solid Earth, it provides significant contributions to time-dependent variations in gravity (see Figure 4.4 for the annual variation). As a result, observations of time-dependent gravity can provide information about changes in the total vertically-integrated mass in oceanic water columns. Even in the presence of horizontal mass and pressure and surface topography differences that propel ocean currents, the ocean can be treated theoretically as being hydrostatic in the vertical direction. This assumption is valid at spatial scales greater than 10 km because vertical accelerations on these scales are small compared with gravity. Because the ocean is very nearly hydrostatic, variations in gravity are directly related to time-varying bottom pressure. Satellite gravity observations function, in effect, as a global network of bottom pressure gauges providing estimates of pressure changes over spatial scales of a few hundred kilometers. The accuracy of these measurements increases with increasing spatial and temporal scales, the former because of the smaller uncertainties in the satellite-gravity measurements at larger scales, and the latter because of the availability of multiple samples. Improvement in the sensitivity of the measurements at longer periods, as well as the research community's interest in seasonal and longer time scales suggests that a multi-year mission is desirable.

Bottom Pressure and Mass

To illustrate the accuracy in bottom pressure that could be achieved with a gravity mission, we consider the annual cycle, which is of particular interest because of its high amplitude (<= 7.5 mbar, Tsimplis and Woodworth, 1994) and broad spatial scales. Figure 4.5 depicts estimates of the degree amplitudes of several annually-varying signals, including signals from the ocean, together with the uncertainties of the generic SGGE, SST, and SSI missions (these results are estimated as described in Appendix B, equation B5 for the degree variance of equivalent water thickness. The improvement in variance estimation in the 5-year data set is a result of improved sampling). The water thickness results can be converted to bottom pressure by noting that a 10 mm increase of water corresponds to a 1 mbar increase of pressure. For Figure 4.5 we assumed a 5-year mission length and a 400-km satellite altitude. The 5-year SGG case is labeled as SGGE in this figure. This figure shows that after 5 years of data, the degree amplitudes of the annually-varying ocean signal are larger than the uncertainties of SST at all degrees below 25 (corresponding to half-wavelengths larger than 800 km) and are larger than the uncertainties of SSI at degrees less than 40+ (corresponding to a 500-km half-wavelength). By contrast, the oceanic signal lies well below the SGGE error bars, even assuming a 5-year mission. Figure 4.6 shows that if the objective is to determine the annually-varying signal one year at a time, the SST and SSI uncertainties are still well below the oceanic signal at low degrees.

As described in Appendix B, however, a degree amplitude comparison does not do full justice to a satellite's ability to detect geographically fixed signals. Direct observations of the annual cycle of bottom pressure fall in the range of 0.5-5 mbar (Cartwright et al., 1987; Woodworth et al., 1996). The usefulness of the missions to detect geographically fixed signals can be better assessed using the results shown in Figures B.1-B.4 in Appendix B. Figure B.2 shows that with 5 years of data, the annual variation of bottom pressure can be determined over a square with a side of length 500 km with a precision of 0.1 mbar for SSI and of 1 and 3 mbar, respectively, for SST and SGGE. At longer (1000 km) scales, the detection limit for SSI approaches an astonishing 0.01 mbar, while the detection limit for SST is 0.1 mbar. The limit for SGGE remains above 1 mbar for squares of up to 2000 km. This result suggests that accurate determination of the annual cycle of bottom pressure may be difficult with SGGE.

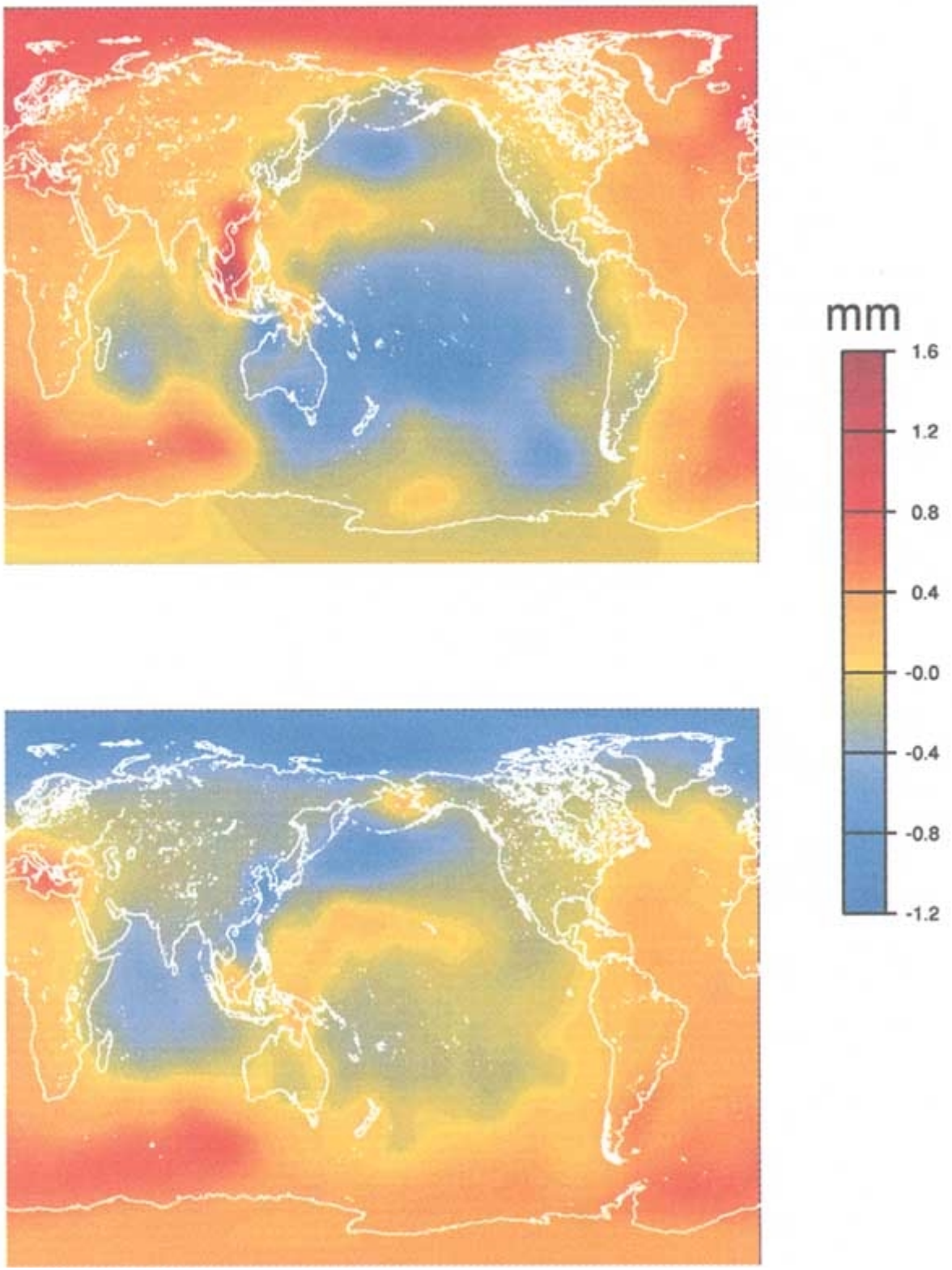

FIGURE 4.4
The annually-varying contributions to the geoid from oceanic variability, as estimated from output from NCAR runs of the Los Alamos POP ocean general circulation model. Top panel: the amplitude of cosine(ωt), where ω = 1 cycle/yr and t = 0 on January 1. Bottom panel: the amplitude of sine(ωt).

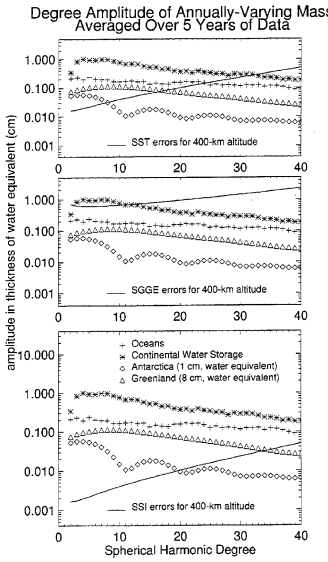

FIGURE 4.5
The degree amplitudes in mass, expressed as the thickness of a water layer, for the annually-varying terms (averaged over 5 years of data) from continental hydrology, oceanography, and changes in Antarctic and Greenland ice mass, computed as described in the text (see Appendix A; conversion to equivalent thickness of water is described in Appendix B). To estimate the Antarctic and Greenland contributions, we assumed annually-varying changes in thickness of 1 cm and 8 cm, respectively, for the two ice sheets, which are in reasonable agreement with the results of Bromwich et al. (1993, 1995).

Currently, less than 20 direct measurements of bottom pressure are available from *in situ* gauges. These are generally distributed at a few "choke points," primarily in the Southern Ocean. Even at these locations current technology limits the periods detectable by the measurements to 12 months or less because of compression effects on sensor accuracy performance that result from the high pressure of the benthic environment (Woodworth et al., 1996). Thus, the current suite of *in situ* bottom pressure measurements represent a complementary data set that could provide "ground truth" for the time-dependent gravity data. Its use in this capacity, however, may be limited to deployments with sufficient spatial coverage.

Gravity data provide a direct estimate of the change of total mass within an oceanic basin or large sea. These data could open up a completely new set of applications of which we can suggest only a few possibilities. The semi-enclosed Arctic Ocean, for example, is subject to an enormous increase in freshwater input during summer due to continental runoff. The residence time of the freshwater along the continental shelves at the southern margins of the Arctic Ocean is likely to be a month or longer. The increase in mass could potentially raise the geoid by 15 mm. Gravity data could provide an important constraint on this increase, and thus on the residence time of the freshwater (see, for example, Aagaard and Carmack, 1989).

Another example is determining changes in the oceanic conveyor belt that supplies deep and bottom water to the major ocean basins. Deep geostrophic currents are proportional to the gradient of bottom pressure. Thus, gravity measurements provide the possibility of directly estimating changes in the poleward and equatorward transports in the lower limb of the conveyor. At this time, we can only put forward "back of the envelope" calculations in support of this statement. However, choosing scales from the North Atlantic, formation rates of North Atlantic Deep Water suggest basin-averaged meridional velocities of ~2×10^{-3} m/s. Integrated zonally across 4000 km, this meridional transport implies a pressure difference across the basin of approximately 1 mbar, corresponding to a surface slope of 2×10^{-9}. The accuracy versus spatial resolution comparison in Figure 4.3 shows that the SST and SSI missions are sufficiently accurate to measure annual and secular variations in this transport if the variations are assumed to be 10% or greater of the mean transport.

Steric Changes

Another way in which gravity measurements can contribute to improved understanding of ocean circulation is through their complementary relationship to altimetry and *in situ* measurements of temperature and salinity. The difference between the observed sea level

and the bottom pressure variations will equal the change in sea level due solely to changes in density (the steric effect). Figure 4.3 was introduced above to illustrate the improvement in the static gravity field. It also shows, however, that for spatial scales greater than 400 km all three missions (SGG, SST, and SSI) will improve the accuracy of bottom pressure variations to such an extent that determination of the time-dependent steric effect will be limited by the accuracy of altimetry rather than gravity. This improvement extends down to scales of 250 km for SSI.

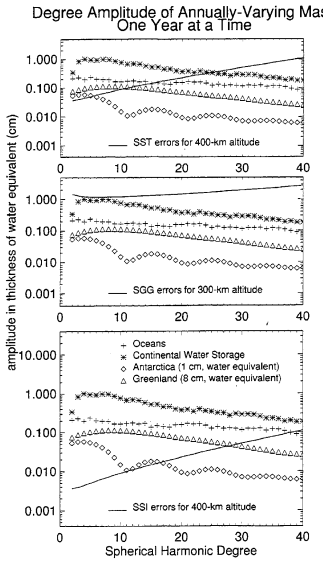

FIGURE 4.6
The degree amplitudes in mass, expressed as the thickness of a water layer, for the annually-varying terms (using 1 year of data) from continental hydrology, oceano- graphy, and changes in Antarctic and Greenland ice mass.

Knowledge of bottom-pressure and steric variations would provide powerful constraints on models of ocean circulation and on efforts to improve model estimates through data assimilation. In data assimilation we use observations as a constraint on the evolving fields of an ocean model to provide an improved estimate of the true state of the ocean. Altimetry provides a particularly useful constraint because in many regions sea-level changes are dominated by steric changes. In the tropical Pacific, for example, changes in the depth of the thermocline have a correlation of greater than 80% with changes in sea level. In other regions, such as the recirculation region of the North Atlantic, however, nonsteric variations are large and poorly correlated with sea level. By combining altimetry with gravity data, we can estimate the steric variations more precisely and, thus, provide a tighter constraint on the ocean thermal field in regions with large nonsteric variations. The use of bottom pressure has received little attention so far because the existing data coverage is far too sparse to be useful for this purpose.

Accuracy

The accuracy estimates described in Chapter 2 and in Appendix B, and the degree amplitude comparison shown in Figures 4.5 and 4.6 describe the sensitivity of the generic satellite missions to surface-mass changes. They do not address the problem of separating the gravitational effects of different geophysical processes, however, which can be critical in determining how well a satellite gravity mission could constrain a specific process.

The problem for oceanographic applications is best understood by noting that the most effective way to use the gravity data for oceanography will probably be to sum together the spherical harmonic geoid coefficients to construct mass anomalies (equivalent to bottom pressure anomalies) averaged over discs of some chosen radius. A method for estimating the errors in the disc averages is described in the appendixes and in Chapter 2. Briefly, discs of larger radius are less affected by satellite errors, because they are less dependent on the high-angular-order (and more poorly known) geoid coefficients. The precision with which a disc mass can be determined from the satellite data is shown in Figures B. 1-B.4 as a function of spatial scale.

For determining the time-varying oceanographic gravity signal, the most serious source of contamina

tion is likely to come from changes in the distribution of continental water (including snow and ice). This will probably be a negligible source of error in the open ocean, but could be potentially serious for determining changes in oceanic mass close to shore. For example, suppose the objective is to obtain bottom pressure estimates averaged over discs of radius 500 km covering the world's oceans. It is reasonable to expect that those estimates might be contaminated by the effects of continental water/snow/ice when the disc is centered within ~300 km of the shore (which would place about 15% of the disc's area over the continent); though the contamination could be more serious near continental areas that have considerable hydrological activity.

Contamination by atmospheric pressure fluctuations is not likely to cause problems for most oceanographic applications. The ocean's response to pressure is likely to be nearly that of the "inverted barometer," which means that for every millibar of pressure increase the ocean surface is depressed by 10 mm, so there is no net change in pressure below the surface of the ocean. The gravitational effects of atmospheric pressure are thus balanced by the effects of the ocean's response to that pressure, so that there is no net effect on the gravitational field. The ocean, in effect, removes that signal itself. The ocean's response will, of course, not exactly accord with the inverted barometer solution (see, for example, Wunsch and Stammer, 1997). Thus, there will be a residual effect on sea-floor pressure due to the combination of atmospheric pressure and oceanic response. But that is a real bottom pressure variation, contributing to bottom currents, and so is probably best left in the data for most applications. Thus, it would probably be best in most cases if atmospheric pressure data were not used to remove the geoid signal caused by atmospheric pressure over the ocean. In contrast, altimetry will still need to be corrected for atmospheric pressure variations. As a result, errors in atmospheric pressure will still enter the estimates of steric height obtained from combining altimetry and gravity.

CONCLUSIONS

1. SGG, SST, and SSI missions at 400-km altitude offer dramatic improvements in our knowledge of absolute dynamic topography and surface circulation from satellite altimetry. The most significant improvement will come at basin scales (~300-3000 km), effectively eliminating the geoid as an error source on these spatial scales. For phenomena with scales less than ~100 km, such as western boundary currents, gravity uncertainties (the error) will be on the same order as ocean dynamic height slopes (the signal). For features with intermediate length scales of 100-300 km, missions with the lowest orbits will offer the best improvement.
2. Interesting and detectable signals are expected for climate-related phenomena with seasonal to interannual time scales. For these phenomena a multi-year mission lifetime is required. This requirement gives priority to SST or SSI over an SGG-type mission.
3. Satellite measurements of time-dependent gravity provide global estimates of changes in sea-floor pressure averaged over spatial scales of a few hundred kilometers and larger. Results are likely to have reduced accuracy within a few hundred kilometers of shore, due to the gravitational effects of changes in water and snow on the continents. Contamination from other geophysical processes is apt to be minimal.
4. Studies suggest that gravity data will reduce the uncertainty in our knowledge of deep circulation, heat, and mass transport by a factor of two or more. Part of this reduction in uncertainty comes from an improvement in estimates of surface current. For example, the geostrophic advective terms in the mixed-layer heat budget would be resolvable to less than 10 Wm^{-2} uncertainty.
5. Studies in ocean regions with strong nonsteric fluctuations of sea level will benefit from knowledge gained from the static geoid. These include the recirculation cells in the western subtropical gyres of the western Atlantic, the Kuroshio Current in the North Pacific, the Agulhas Current in the southwest Atlantic, and the Antarctic Circumpolar Current.
6. In regions of strong nonsteric fluctuations in sea level, the combination of gravity and altimetry data will provide a much more powerful constraint on the ocean circulation than altimetry alone. Combining altimetry and gravity will allow separation of the time-dependent steric and nonsteric components of sea level. This separation will substantially increase the usefulness of sea level in testing ocean models and constraining ocean circulation through data assimilation.

5

Solid Earth Processes

Accurate determination of the Earth's gravity field over a wide range of spatial scales is of fundamental importance for understanding the structure and dynamics of the solid Earth. Gravity is used in combination with topography at commensurate resolution to resolve the compositional, thermal, and mechanical structure of the deep crust and upper mantle, and to elucidate fundamental aspects of the plate tectonic process (shown schematically in Figure 5.1), such as the nature of ridges and trenches, the dynamics of mountain building, and the planform of mantle convection. Results of such analyses bear directly on attempts to understand the dramatic surface manifestation of tectonic forces, i.e., earthquakes and volcanism.

The requirements for measuring the static gravity field as it relates to understanding the solid Earth were summarized schematically in Figure 1.1 (bottom panel). Those requirements have been well established in numerous previous reports (NRC, 1979, 1982; NASA, 1987, 1991) and the literature (e.g., Nerem et al., 1995). Here we present a synopsis of those results, with updates as appropriate, especially with regard to the utility of various mission approaches in achieving objectives. In addition, in Chapter 3 we discussed the importance of using satellite gravity measurements to "tie down" observations from surface gravimetry that are poorly referenced, but of high resolution, and that have application in many studies of continental and seafloor tectonics.

In this chapter, we discuss applications that reflect fundamental processes that are consequences of the dynamic nature of the Earth; namely, mantle convection and plumes, post-glacial rebound, tectonic activity, and earthquakes. Note that gravity measurements used in applications to the fluid Earth are commonly expressed in terms of the geoid, whereas many solid-Earth applications traditionally use gravity anomalies. We follow this convention. Figure 5.2 shows an overlay of the expected gravity-anomaly recovery accuracy from the generic GPS, SGG, SST, and SSI missions on a schematic of measurement requirements. Three of the four missions (SGG, SSI, and SST) are significantly more accurate than the best current gravity model (EGM96) (Lemoine et al., 1996), permitting new insights on a number of phenomena at finer resolution. The GPS mission only yields marginal improvement and only at the longest wavelengths (resolution >1,000 km). From 500 to 10,000 km, the SSI mission would give the greatest sensitivity, followed by SST and then by SGG. This new measurement regime will enable a better understanding of mantle convection in the 200 to 1,000 km range and permit improved insights into the structure of continental roots and mountain building.

MANTLE CONVECTION AND PLUMES: UNDERSTANDING THE EARTH'S HEAT ENGINE

Most of the heat loss from the Earth occurs via mantle convection—the process by which the Earth loses the bulk of its internal heat and which drives the plate-tectonic cycle. The primary manifestations of plate tectonics—volcanism and faulting—occur along plate boundaries. Understanding plate tectonics and its physical consequences requires knowledge of the driving mechanism. Satellite gravity measurements

achieve sufficient accuracy at long to intermediate wavelengths to constrain the nature of mantle convection. Relevant length scales span the range from the sizes of plates to the thickness of the Earth's convecting layer (Figure 5.2). Given the range of plate size and the possibility of convection at various scales—from small scale to whole mantle—spatial resolutions needed range approximately from 200 to 3,000 km.

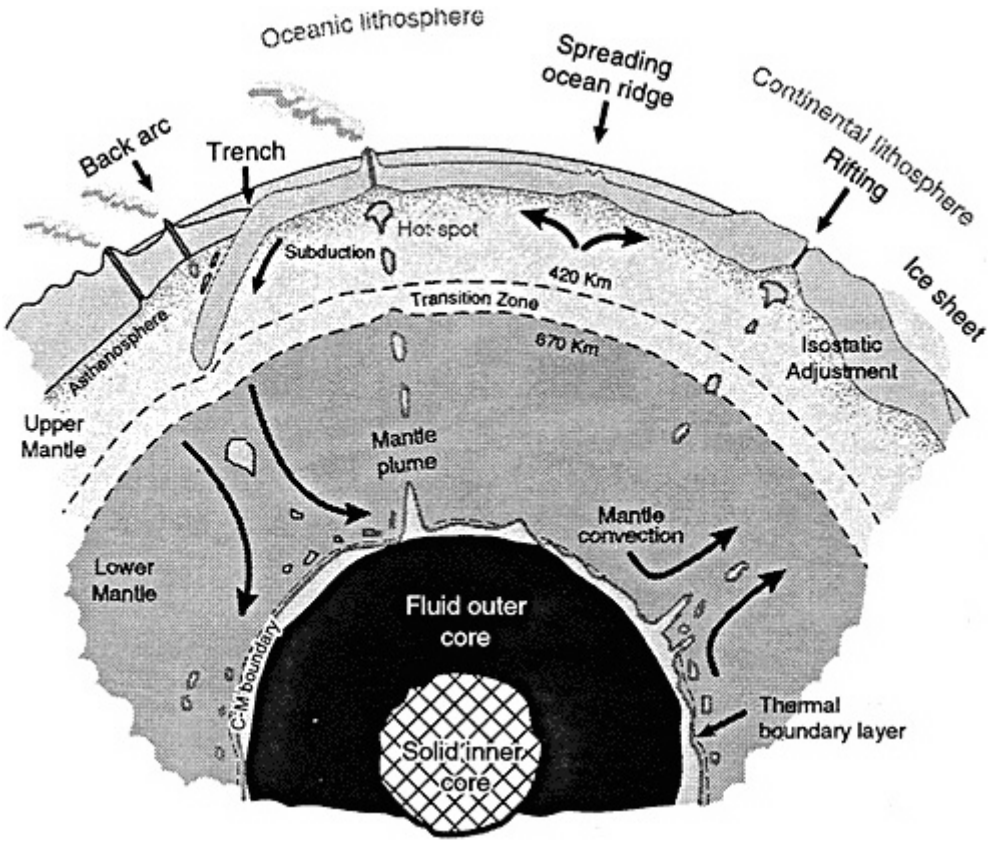

FIGURE 5.1
Schematic illustration showing internal structure and major dynamical processes associated with the solid Earth. Heat loss from the deep interior results in motion of mantle material via convection and mantle plumes. The manifestation of the Earth's internal dynamics is the interaction of surface plates at trenches and mid-ocean ridges in oceanic seafloor and rift zones and mountain belts in the continents. Isostatic adjustment of continental lithosphere associated with melting of major ice sheets results in slow vertical rebound indicative of mantle viscosity structure. Figure from ESA (1996).

Significant progress has been made in recent years in relating spatial variations in the gravity field to mantle convection (e.g., Hager and Richards, 1989; King and Masters, 1992; Forte et al., 1993; Phipps Morgan and Shearer, 1993; Ricard et al., 1993). While there is general agreement on the existence of an appreciable increase of viscosity with depth from the upper to the lower mantle, there is less agreement on the details of either the inferred viscosity structure or the predicted gravity field. The differences among models are largely the result of differences in assumptions of how to relate seismic velocity heterogeneity to density heterogeneity in the upper mantle. The question is whether the velocity variations result only from temperature variations, and can be directly interpreted as density variations, or whether there are compensating differences in composition, particularly under cratons, so that the seismic velocities could even have an inverse correlation with density.

Combined investigation of the changes in gravity and seismic velocity associated with continent-ocean and craton boundaries would provide a way to resolve this issue. Figure 5.3 shows a representative global model of seismic velocity heterogeneity at 200-km depth, expanded through degree and order 16 (Masters et al., 1996) and the global gravity field, expanded through degree and order 150 (Lemoine et al., 1996). The largest contrasts in seismic velocity are between shields and oceans (e.g., West African continental margin) or between shields and tectonically active

areas, such as the Canadian Shield and Western Cordillera. At this depth, in cold regions such as continental roots, the coupling between density heterogeneities and surface deformation is essentially isostatic, so that knowledge of density structure and gravity variations, rather than non-uniqueness in mantle flow models, are the limiting factors. Neither this seismic model nor the existing gravity field are sharp enough (~200 km resolution) to define precisely the geophysical transitions between geologic provinces. Seismologists are rapidly improving the spatial resolution of their models; if the improvement in the accuracy of the gravity field can keep pace, this type of investigation should be a frontier area of geodynamics in the next decade.

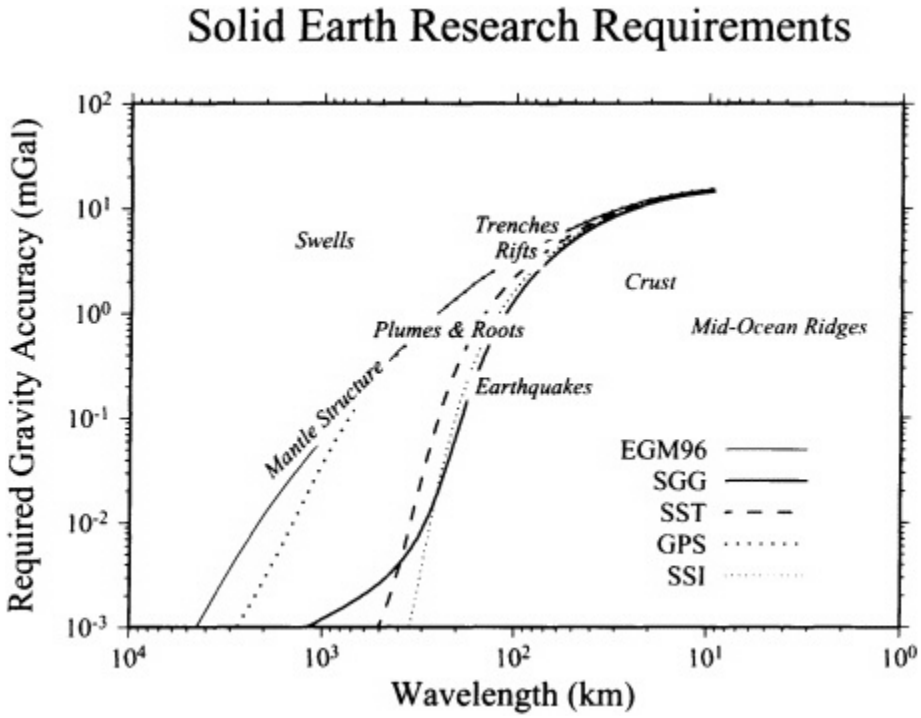

FIGURE 5.2
Measurement requirements for the Earth's static gravity field. Adapted from NASA (1991).

Other key questions in mantle dynamics concern the nature of mantle plumes, which are a major source of intraplate volcanism and enhanced heat flow. Gravity changes within plates that could be associated with mantle plumes can be as large as 10 mGal, but resolutions of approximately 1 mGal at the shorter wavelength limit down to ~10^{-2} mGal at the longer wavelength limit need to be obtained to characterize smaller, though important, variations in thermal structure and to distinguish between various models of mantle structure. For a mission flown at 400 km, the ~10^{-2} mGal accuracy level is met by SGG and SST for resolutions of 400 km and larger, and by SSI for resolutions of 300 km and larger. Separation of the longer-wavelength mantle structure effects from those caused by other phenomena will clearly be a challenge with current technology. However, the situation is more favorable for questions that require shorter wavelength measurements, such as the depths of origin of mantle plumes. To constrain plume depths it will be necessary to isolate the effects of dynamic upwelling from signals associated with lithospheric processes, which will require gravity resolution of approximately 1 mGal over length scales of order 100 km. As shown in Figure 2.13, three of the generic missions (SGG, SST, and SSI) at 400 km would provide 1-mGal-level measurements down to the necessary resolution levels of 100-200 km.

POST-GLACIAL REBOUND

During the last ice age, the extensive ice loads over Canada and Scandinavia caused deep depressions in the Earth's surface. Although this ice had mostly

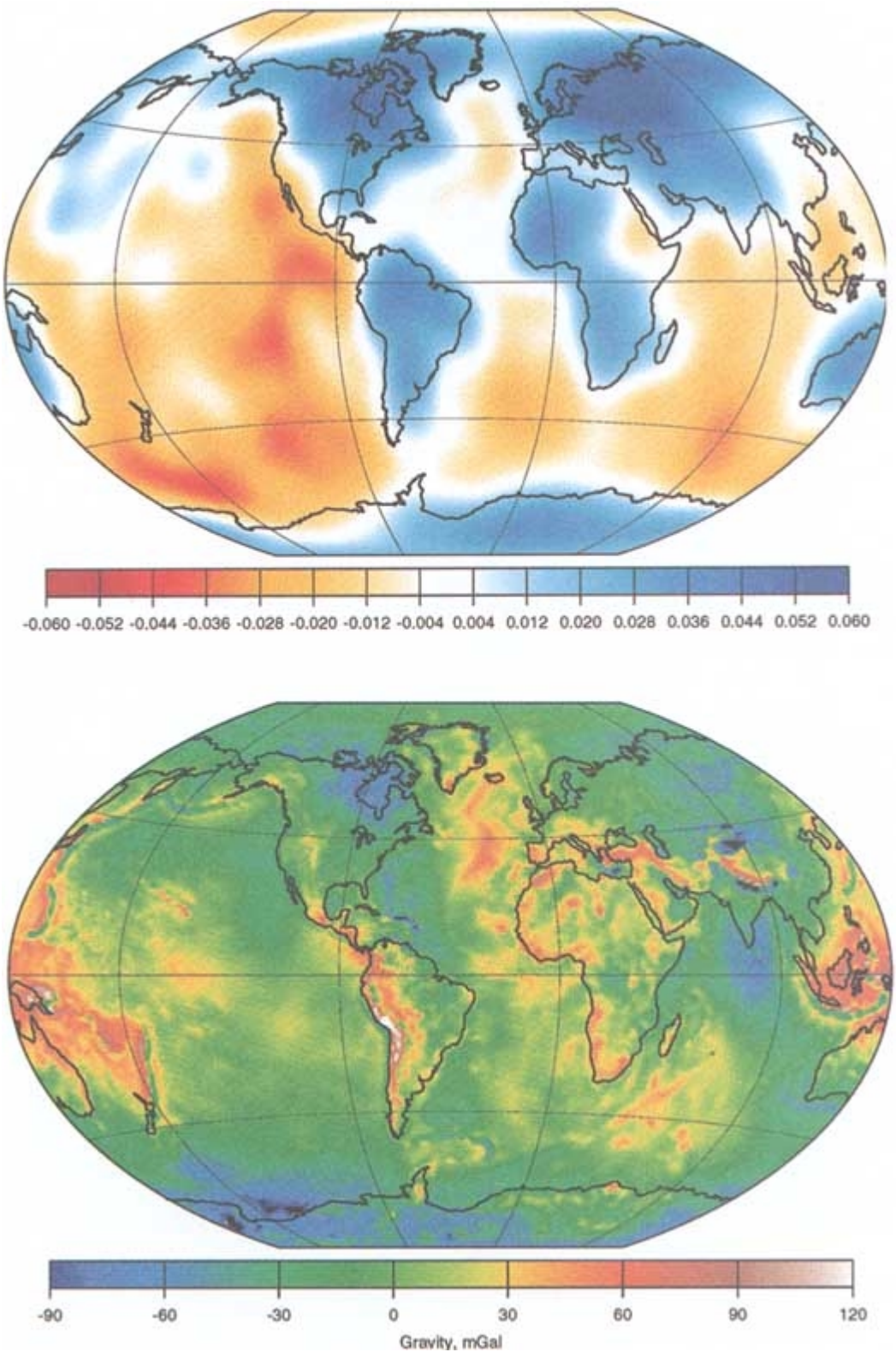

FIGURE 5.3
Top: shear wave velocity heterogeneity ($\delta V_s/V_s$) at a depth of 200 km for global tomograhic model S16B30 (Masters et al., 1996). Fast areas are blue and slow areas are red. Bottom: free air gravity anomalies relative to the hydrostatic reference figure for the gravity model of Lemoine et al. (1996). Courtesy of B. Hager, MIT.

vanished by about 9,000 years ago, the depressions have not yet completely disappeared; they are partially filled by Hudson Bay and the Baltic Sea. The Earth's surface continues to rise as a result of horizontal inflow of mass from the surrounding regions, because over long periods of time, the Earth behaves more as a viscous fluid than as an elastic solid. This process of readjustment is referred to as post-glacial rebound. (The elastic response of the Earth to present-day changes in polar ice is not considered in this chapter, but is included in Chapter 7.)

A primary goal of post-glacial-rebound studies is to provide constraints on the viscosity profile of the mantle. The community that models post-glacial rebound, however, has yet to reach a consensus on the results, particularly on how much the viscosity of the lower mantle (i.e., at depths below 670 km) increases. Progress has been hampered by the difficulty of finding observational constraints that are both sensitive to lower-mantle viscosity and unaffected by other geophysical processes. For example, the 40-50 mGal depression in the Earth's static gravity field over northern Canada has sometimes been interpreted as a measure of incomplete post-glacial rebound, but it has also been argued to reflect mass anomalies related to large-scale convection in the mantle (see, for example, Cathles, 1975; Peltier et al., 1992; Forte and Mitrovica, 1996). Similarly, a secular drift in the position of the Earth's rotation axis, a non-tidal acceleration of the Earth's rotation rate, and secular changes in the lowest-order zonal spherical harmonic components of the Earth's gravity field (e.g., C_{20}) have all been observed and could all be partly due to post-glacial rebound (Yoder et al., 1983; Rubincam, 1984; Yuen et al., 1982; Peltier and Jiang, 1996; Peltier, 1985). But there could also be important effects from other geophysical processes, including changes in polar ice mass (e.g., Sabadini et al., 1988; Mitrovica and Peltier, 1993; Trupin, 1993; James and Ivins, 1995) and the steady mass-redistribution caused by convective flow in the mantle (which could contribute to the secular drift of the rotation axis; see for example, Sabadini and Spada, 1995; Richards et al., 1995). (The effects of mantle convective flow on the secular terms in the gravity field are probably about two orders of magnitude smaller than the effects of post-glacial rebound [M. Richards, personal communication]. They are unlikely to be a significant source of error when using satellite gravity results to learn about the rebound process.) Crustal-uplift rates, as determined mainly from geological dating of raised beaches, are probably the least ambiguous data type in terms of their relative insensitivity to other processes and form the basic observational foundation of post-glacial-rebound studies. Still, it is difficult to unravel the competing effects of lower-mantle viscosity, upper-mantle viscosity, lithospheric thickness, and uncertainties in the time history and spatial distribution of the ice sheets, using this data set alone (see, for example, Lambeck et al., 1990; Mitrovica and Peltier, 1992; Han and Wahr, 1995).

There are other methods of inferring the Earth's viscosity profile from observational data. Most useful are attempts to explain the observed long wavelength geoid by modeling the Earth's response to internal mass loads (e.g., Richards and Hager, 1984; Ricard et al., 1993). The loads are estimated from seismic tomographic maps or tectonic models of the Earth, and the Earth's response to those loads depends on the viscosity contrast from one region of the Earth to another. These studies have their own characteristic set of difficulties and can only provide ratios of viscosities between regions, rather than absolute viscosity values. Nevertheless, they provide a useful complement to the post-glacial-rebound estimates. In fact, there has been recent progress in using both tomography and modeling techniques in a joint inversion (Forte and Mitrovica, 1996).

It is clear that post-glacial-rebound studies could benefit greatly from more unambiguous observational constraints. Measurements of the secular change in the gravity field using a dedicated gravity satellite could provide such constraints. The portion of the gravity signal relatable to the secular changes in the low-degree zonal components observed with satellite laser ranging to LAGEOS, for example are not, by themselves, sufficient to distinguish post-glacial rebound from other geophysical effects. More spherical harmonic coefficients, including a significant number of nonzonal terms, are needed and can only be obtained from a dedicated gravity mission.

The top and middle panels of Figure 5.4 show map views of the secular change in the geoid over North America as predicted by two versions of the model described in Appendix B. Both versions assume an upper-mantle viscosity of 1.0E21 Pa-sec and a lithospheric thickness of 120 km and use model ICE-3G of Tushingham and Peltier (1991) to represent the melting of the ice during the Pleistocene. The difference is that the lower-mantle viscosity is taken to be 10.E21 Pa-sec in the top panel and 50.E21 Pa-sec in the middle panel. The pattern of the geoid fluctuation depends largely on the ice-sheet model. Because the same model (ICE-3G) has been used in both cases, the patterns are similar, although the amplitudes are different The top panel predicts a rate of change as large as 2.3 mm/yr over the center of Hudson Bay, whereas the corresponding

amplitudes in the middle panel are about two-thirds that size (i.e., 1.5 mm/yr).

For satellite gravity measurements to be useful, they must be accurate and complete enough to be able to resolve differences between competing viscosity models and to allow separation of the post-glacial-rebound signal from the effects of other processes. In Figure 5.5, the degree amplitudes of the secular change in the geoid caused by the rebound beneath Canada (the effects of ICE-3G from Antarctica, Greenland, and Scandinavia are not included in these results) are compared with uncertainties for the SST, SSI, and SGGE generic missions described in Chapter 2. For these comparisons we have assumed that each mission length is 5 years. The short (<1 year) length of an SGG mission makes it impractical for studying post-glacial rebound or other secular processes, and the GPS mission has not been included, because its relatively poor performance at all but the very lowest degrees make it far less useful than the other missions for this application. All three missions shown in Figure 5.5 are assumed to orbit the Earth at 400-km altitude, which is likely to be the minimum altitude compatible with any long-lifetime mission.

The results for a lower-mantle viscosity of 10.E21 Pa-sec (Figure 5.5, plus symbols) are at or above the SST satellite errors for degrees below 28 (corresponding to half-wavelengths of 740 km and longer) and above the SSI errors at degrees below 40 (half-wavelengths longer than 500 km). This suggests that the post-glacial-rebound signal could readily be seen with the SST or SSI missions. The SGGE mission, however, has uncertainties much higher than the rebound effects for all but the very largest wavelengths (i.e., smallest degrees) and so would be far less useful for post-glacial rebound studies.

An SST or SSI mission could also provide data needed to resolve differences between models of lower-mantle viscosity and to separate the effects of post-glacial rebound from the effects of other processes, such as changes in ice sheets and in ground and surface water. Figure 5.5 shows the predicted degree amplitudes of the difference between results for 10.E21 and 50.E21 Pa-sec lower-mantle viscosities (triangle symbols). The degree amplitudes of the difference between the two lower-mantle-viscosity models lie above the SST uncertainty levels up to about degree 12 (half-wavelengths greater than about 1700 km) and above the SSI uncertainties up to degree 18 (half-wavelengths in excess of 1100 km). At higher degrees, the results for the two lower-mantle-viscosity values converge because the Earth's response at those shorter wavelengths does not penetrate into the lower mantle.

Satellite gravity measurements would be less effective for inferring the trade-off between upper-mantle viscosity and lithospheric thickness. Those parameters tend to have significant effects only at the higher degrees, where even the SST and SSI uncertainties begin to rise above the predicted signal. On the other hand, this means that uncertainties in those parameters would probably have little impact on estimates of lower-mantle viscosity derived from the satellite data.

It is possible that errors in the Pleistocene ice model could map into errors in the inferred lower-mantle viscosity. It is not clear how large these ice-load errors might be. Fortunately, only the large-scale components of the ice model are important for lower-mantle studies. Thus, the problem of separating ice-sheet and viscosity parameters is less of an issue for the interpretation of gravity data than it is for the interpretation of geological crustal uplift data, where short-wavelength terms in the load are more important.

The other issue is whether a satellite mission could differentiate between the effects of Canadian post-glacial rebound and the effects of other processes. A 5-year SST or SSI mission would be able easily to separate the Canadian rebound from the effects of any ongoing secular change in the volume of Greenland ice. This requires only that the effects of the rebound rise above the satellite uncertainties for values of l up to about $l = 4$ or 5 (the half-wavelength of an $l = 4$ spherical harmonic is 45°, which is about equal to the angular separation between Greenland and Hudson Bay). This criterion is satisfied by both SST and SSI (see Figure 5.5).

It is harder to assess the possible contamination from changes in surface water and groundwater over this region of Canada and from changes in the total water content of Hudson Bay. Seasonal effects would presumably average out over a 5-year mission. Longer-period effects could be partially absorbed into a viscosity estimate, if their spatial patterns are similar to the rebound pattern.

To estimate the hydrologic effects, we used five years (1987-1991) of monthly output from the global soil moisture/surface water model described in Chapter 6 and Appendix B. The geoid was computed for each month of output. Although the results are dominated by seasonal terms, there is also interannual variability that could leak into the secular solution, particularly since the solution is based on only five years of data.

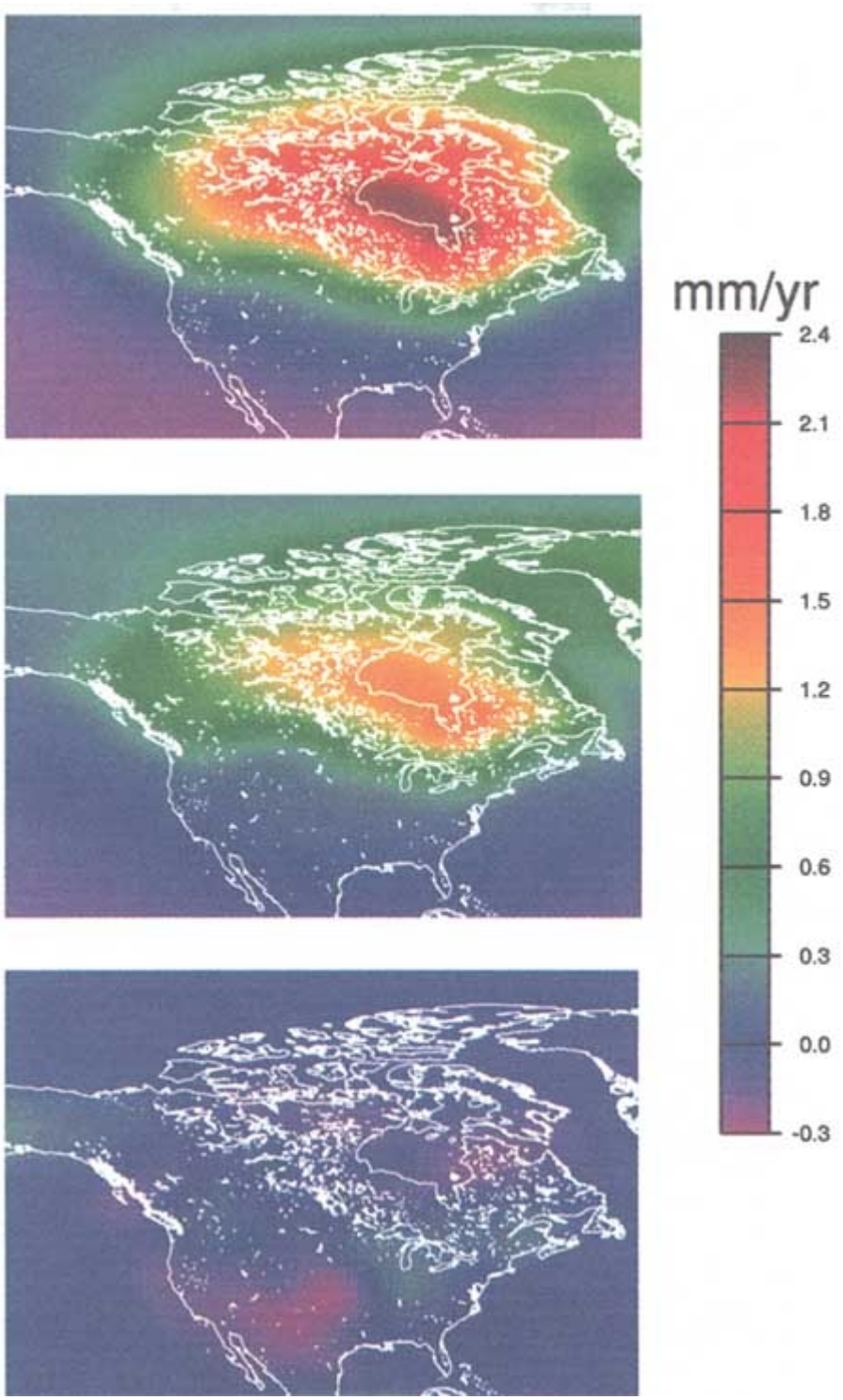

FIGURE 5.4
The secular geoid signal over North America due to post-glacial-rebound for two lower-mantle viscosity values: v_{lm} = 10.E21 Pa-sec in the top panel, and = 50.E21 Pa-sec in the middle panel. In both cases the upper-mantle viscosity is l.E21 Pa-sec, the lithospheric thickness is 120 km, and ICE-3G is used as the Pleistocene ice load. The bottom panel shows the secular signal in the geoid due to changes in continental water storage during 1987-1991, as inferred from the soil moisture data described in the text. The amplitude of this hydrological signal can be as large as 0.2 mm/yr, which is about 10% of the rebound signal. But the spatial patterns are quite different, suggesting that the hydrology is not apt to have much of an impact on the solution for the rebound.

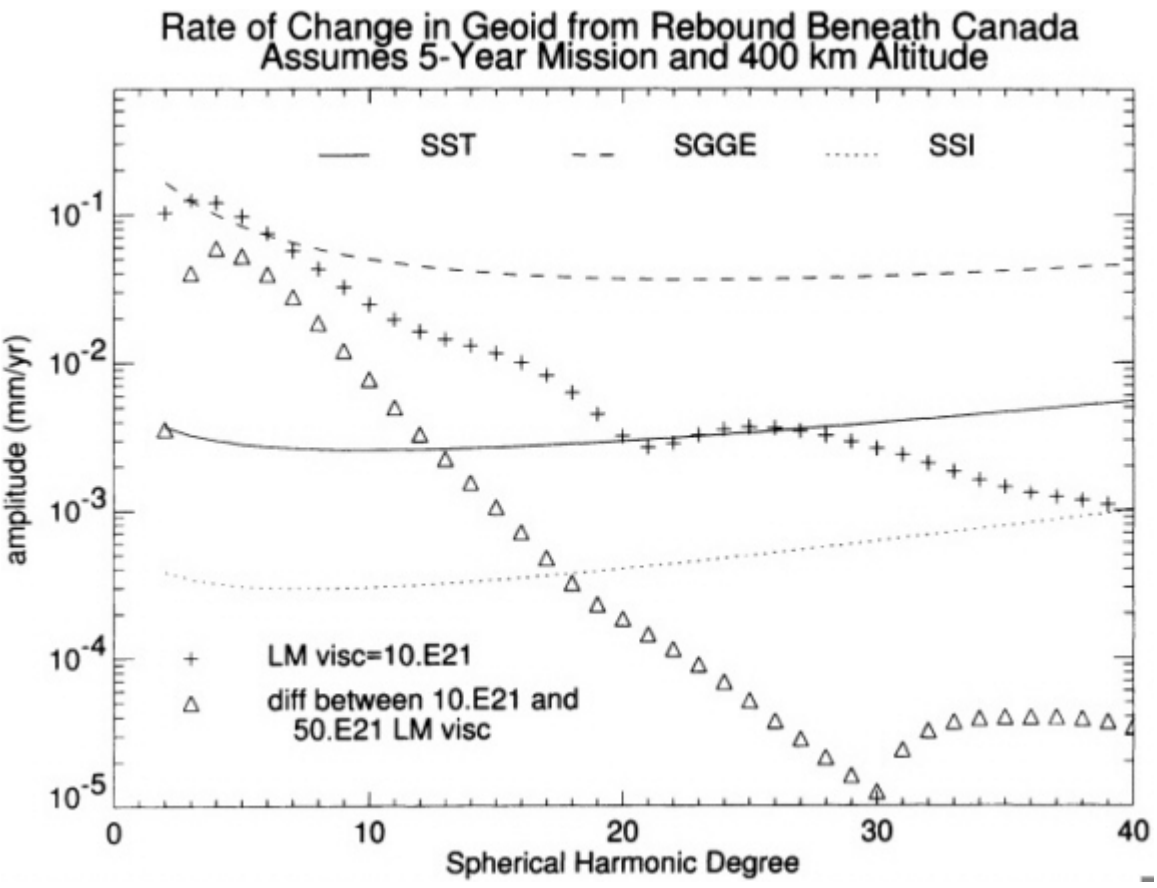

FIGURE 5.5
The degree amplitudes for post-glacial rebound in North America for a lower-mantle viscosity of 10.E21 Pa-sec and for the difference between results for viscosities of 10.E21 and 50.E21 Pa-sec, compared with degree variances from 3 generic missions.

To estimate that leakage, the geoid was fit with a linear function of time. The bottom panel of Figure 5.4 shows the portion of the hydrological signal over North America that would have affected post-glacial-rebound estimates from a 1987-1991 satellite gravity mission. The amplitude of the geoid perturbation from the hydrology in this region is about 0.2 mm/yr, only about 10% of the post-glacial-rebound amplitudes shown in the other panels of Figure 5.4. Because the hydrological and post-glacial-rebound contributions have different spatial patterns, the hydrological effects on the inferred rebound signal would be further reduced. For example, fitting the post-glacial-rebound geoid patterns from the top two panels in Figure 5.4 to the hydrological pattern shown on the bottom panel, we find that the hydrology perturbs the regression coefficient by 1% or less, which is far smaller than the 30-40% difference between the 10.E21 and 50.E21 Pa-sec lower-mantle-viscosity models.

The effect of a linear increase in the water mass of Hudson Bay is also likely to be small. Suppose, as a worst-case scenario, that Hudson Bay is rising, due to water inflow, at a rate of 3 mm/yr, which is probably a little more than twice the global estimate inferred from

tide-gauge data, after removing the estimated effects of thermal expansion (see Chapter 7). This would produce a secular geoid perturbation with an amplitude of about 0.07 mm/yr, centered over Hudson Bay. This is about 3% of the rebound signal shown in the top panels of Figure 5.4. The spatial pattern of the Hudson Bay geoid is similar to that of the rebound, but is of somewhat smaller scale. When the rebound signal is fit to this Hudson Bay geoid, the regression coefficient is slightly less than 0.01. This implies that an unmodeled 3 mm/yr increase in Hudson Bay would have about a 1% effect on the rebound signal inferred from satellite gravity, which in turn is far smaller than the effects of different viscosity models.

The implicit basis of this discussion has been largely a uniform linear rheology. The more accurate data from a gravity mission should be an important step toward inferring lateral heterogeneities and, possibly, non-linear effects in the rheology.

REGIONAL DEFORMATION AND STRUCTURE: THE SURFACE MANIFESTATION OF PLATE TECTONICS

Post-glacial rebound is mainly a transitory perturbation on a mantle with irregularities that are much larger, but less inferable because their causes are much more obscure in their spatial and temporal distribution than the geologically recent glaciation. The convection causing the irregularities is thus much more complex, entailing non-linear rheology, differentiation, and interaction with the thermal (lithosphere) and compositional (crust) boundary layers. Hence, the subsequent discussion is more qualitative and dependent on indications from other data types.

Despite decades of observations of the Earth's interior, the fundamental question of the thickness of the continents is still debated. Resolving the discrepancies between estimates of the depths of continental roots at length scales of 500-1,000 km requires gravity measurements at the mGal level (Figure 5.2), which would be feasible from all four generic mission types. On the regional scale, variations in the thermal and mechanical properties of the crust preserve the record of the history of tectonics. Gravity data, in conjunction with topography, have been applied in increasing detail and refinement to infer the tradeoffs between elastic and buoyant support of topography and the extent of buried loads. The thermal and mechanical structure of continental lithosphere is commonly studied by flexural analysis of a thin elastic plate that may contain surface and subsurface loads. The pertinent parameter is the effective elastic thickness, which is a measure of the mechanical competence of the lithospheric plate and can be directly related to its thermal structure (McNutt, 1984). In analyses of this genre, gravity and topography measurements provide the observational basis for the load estimation. The observed power spectral ratio of gravity to topography as a function of wave number (or wavelength) is compared to that predicted for an elastic plate with the observed loads. Figure 5.6a plots the correlation coefficient of Bouguer gravity and topography, termed the coherence, as a function of wavenumber for a model of an elastic plate of various effective elastic thicknesses assuming equal amounts of surface and subsurface loading. The basis of the estimation of elastic thickness using the coherence (Forsyth, 1985) is that at short wavelengths the lithosphere supports loads by its elastic strength and so gravity and topography are uncorrelated. In contrast, at long wavelengths a load deflects the lithosphere and produces a gravity anomaly indicative of the compensation of the load, so gravity and topography are correlated. The wavelength of the transition between coherent or correlated and incoherent or uncorrelated loads provides a measure of the effective elastic thickness.

The coherence approach to characterizing the thermomechanical structure of the continents is illustrated for the Australian lithosphere in Figure 5.6b, where the large (130-km) thickness estimate is consistent with that continent consisting largely of old, thermally cool craton (Zuber et al., 1989). However, smaller tectonic subregions of the continents display varying ages and thermal states and so in a regional sense thickness variations occur. In regions of dense gravimetry, such as Australia and North America (Bechtel et al., 1990), there has been a fairly complete mapping of lithospheric thicknesses on the regional scale. However, note in Figure 5.6a that for thick lithospheres the transition from high to low coherence occurs at long wavelengths so gravity and topography data with high geodetic integrity are required. In contrast, for thin lithospheres the transition occurs at short wavelengths so data with high spatial resolution is required. Also note that in addition to high quality gravity, topography at commensurate resolution is required. While some local areas have high enough quality topography and gravity data to have been studied in a systematic sense (e.g., McNutt et al., 1988; Bechtel et al., 1987; Lowry and Smith, 1994), there remains a need for detailed analysis of interesting tectonic regions, such as orogenic provinces, conti

nental rift zones, and sedimentary basins. Mechanisms of support of surface and subsurface loads provided by the gravity and topography constrain models of continental evolution. To contribute further, properly referenced gravity should have a resolution that is at least comparable to the thicknesses of the structural layers, which may be as thin as 10-30 km; the latter range would not be obtainable with satellite gravity alone and are appropriate applications for high-resolution airborne gravimetry (Brozena, 1991; NRC, 1995).

Topography must be at the same resolution as gravity to be useful in geophysical studies. Current data resolution varies considerably. In well sampled areas such as North America, Europe, and Australia, the spatial resolution is higher than the resolution that can be expected from a new satellite gravity mission. But in parts of Asia, South America, and Africa, topographic coverage is poor. NASA's Shuttle Radar Topography Mission, which is scheduled to be launched on the space shuttle in 1999, will map land topography south of about 60° latitude at 30-m spatial resolution. Topography obtained from that mission will have a higher spatial resolution than that expected from an SST mission.

There are appreciable regions of interest where even moderate resolution is lacking, such as the Andes-Altiplano region, where recent studies have attempted to isolate the effects of plate subduction, magmatism, and erosion in controlling the style of mountain building (Isacks, 1988; Kono et al., 1989; Masek et al., 1994). On the regional scale, data gaps would best be filled in using measurements of the gravity field provided by airborne platforms (e.g., NRC, 1995). Detailed corrections to such gravity measurements to assure geodetic integrity will require accurate knowledge of spacecraft position provided by GPS, as well as a precise record of aircraft velocity. The recent availability of gravity data from former communist nations will help elucidate some interesting structures, such as the Himalayas and the Tibetan Plateau, particularly as related to the dynamics of the India-Eurasia collision zone and the mechanism of strain accumulation (Jin et al., 1994; Willet and Beaumont, 1994). Here, satellite data may help to put both the gravity and topographic observations on a unified datum through the calibration and rescue discussed in Chapter 3. The continuity of gravity data from continents into the oceans is also a matter of great need in addressing the structure of continental margins (e.g., Karner and Watts, 1982), and a satellite gravity mission would be helpful in tying land and marine surveys to a common datum. Passive margins are of great importance because they represent the transition of continental to oceanic lithosphere and they also contain sedimentary basins that hold the record of macroscale continental erosion. In addition, they are often the source of petroleum reserves of economic interest.

The seafloor produced at mid-ocean ridges has a thermal structure that reflects both the mechanical structure of the lithosphere and the coupling of the lithosphere to the convecting mantle below. Heat-flow measurements are often corrupted by local processes such as hydrothermal circulation (Sclater et al., 1980), so gravity measurements with regional-scale integrity can make a significant contribution to understanding the lithosphere structure from a thermal point of view as well as a compositional one. The basic characterization of mid-plate swells in the oceanic lithosphere on length scales of ~1,000 km has been accomplished from the altimetric geoid. At shorter wavelengths gravitational data have contributed greatly to understanding the evolution of the oceanic lithosphere in the seafloor spreading process. The recent release of Geosat Geodetic-Mission and European Remote Sensing Satellite (ERS-1) altimetry has helped greatly to provide high-quality, short-wavelength marine gravity (Sandwell and McAdoo, 1990; Sandwell, 1992; Smith and Sandwell, 1995a), so that now the limiting factor for detailed studies of oceanic structure in many areas is accurate, high resolution bathymetry. In these studies, attention is focused on processes such as rifting, subduction, and volcanism. One particular question to which globally referenced satellite gravity may contribute significantly is in resolving whether there exists a straightforward relationship between lithospheric age and plate thickness (Watts et al., 1980), as has been suggested by flexural analysis of trench and seamount loads (Calmant and Cazenave, 1987; Smith et al., 1989; Wessel, 1992; Smith and Sandwell, 1994) or whether there has been significant reheating of oceanic lithosphere to reset thermal age (McNutt, 1984) in areas affected by hot spots. A complete gravity data set from a satellite mission could be used to investigate the nature of the flexural strength of the lithosphere, the isostatic compensation of seamounts, and the role of thermal anomalies in the lithosphere associated with the south Pacific and other areas. Wavelength resolution of ~100 km and gravity measurement accuracy to ~3-4 mGals (for rifts) and 10 mGals (for subduction zones) are required; these requirements can be met by the SGG, SSI, and SST missions.

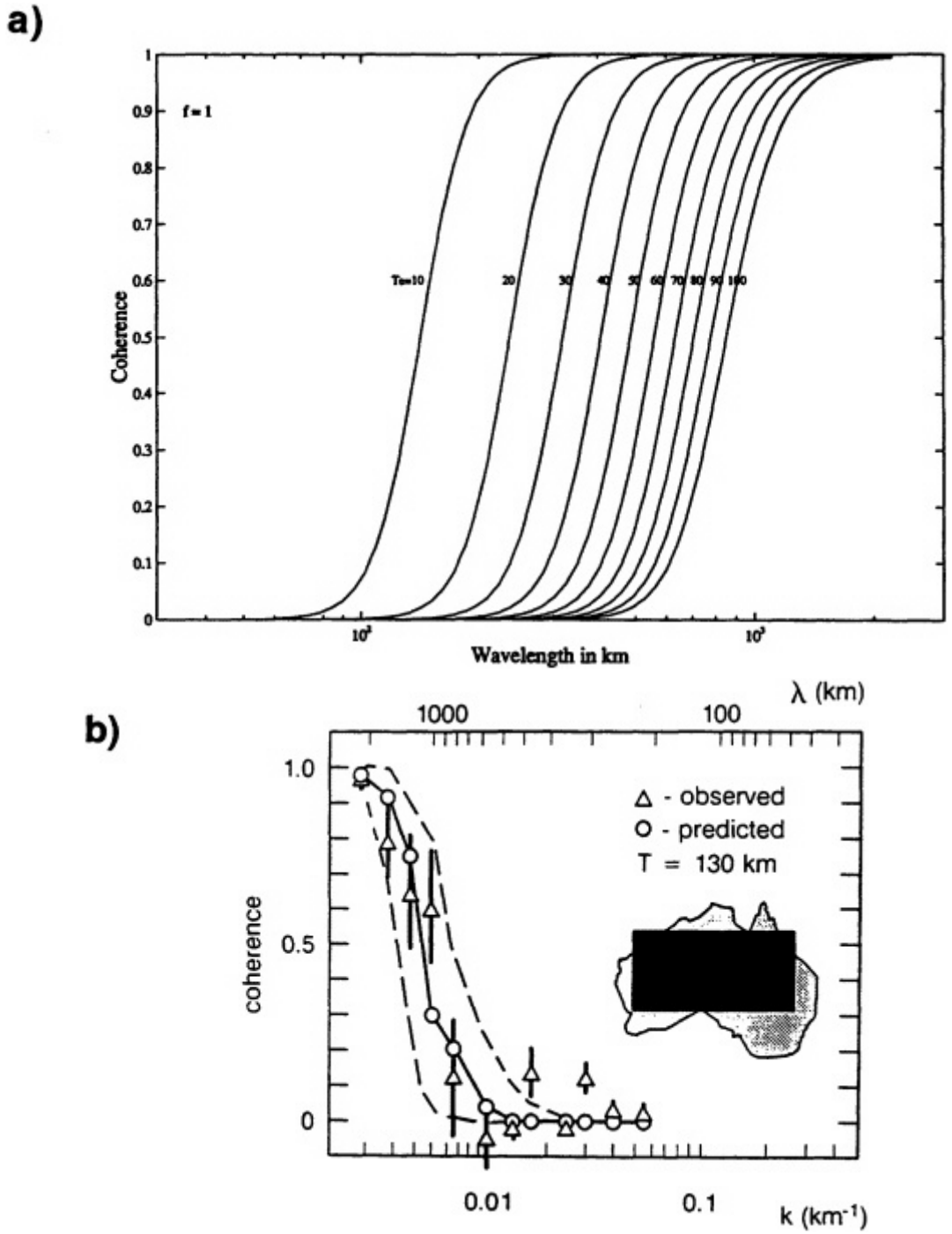

FIGURE 5.6
(a) Theoretical coherence, the correlation coefficient between Bouguer gravity and topography, for an elastic plate equally loaded from at the surface and bottom. The transition wavelength or wave number from high coherence to low coherence provides a measure of the elastic thickness of the lithospheric plate that can be related to the thermomechanical state of the lithosphere. Courtesy of Y. Jin.
(b) Observed coherence pattern for Australia indicating a thick elastic lithosphere. The black box on the Australia figure shows the region from which data for the coherence calculation was gathered. Figure from Zuber et al. (1989).

EARTHQUAKES

Earthquakes release in a few seconds the elastic strain energy accumulated over decades, centuries, or millennia. Most of the world's earthquakes occur near plate boundaries and result from strain associated with motions of a few centimeters per year. Earthquakes, occasionally quite large, occur much less often in plate interiors. The study of earthquakes and associated precursory and post-seismic phenomena is of great societal importance.

Seismology furnishes a means of locating earthquakes, imaging rupture surfaces, estimating energy release, and so on. GPS, along with tilt meters and strain meters, can monitor surface displacements and strains at instrumented points. SAR interferometry can furnish areal images of surface displacements. Such approaches represent the methods of choice for characterizing short-term Earth deformation. The contribution of a satellite gravity mission to these existing techniques would probably be limited to a volume-integrated measure of displacements of mass.

Mass displacements associated with earthquakes arise from surface deformation (Freund and Barnett, 1976; Savage, 1983) and internal densification (Singh, 1970; Jovanovitch et al., 1974). Models of these phenomena can be used to estimate the changes in the Earth's gravity field associated with an earthquake (Walsh and Rice, 1979; Savage, 1984). The details of the expected signal depend on the width and dip of the rupture surface and the slip on it. Since a satellite gravity mission would be largely insensitive to structures with wavelengths shorter than the orbital altitude, only those earthquakes with rupture surfaces extending over a few hundred kilometers will generate detectable signals. For the largest known earthquakes, such as the 1960 Chile and 1964 Alaska events, the expected signals are of order 0.3 mGal of gravity change or 3 cm of geoid change with wavelengths of a few hundred kilometers. Such signals would be near the limit of resolvability for even the most sensitive mission scenarios studied here. We thus conclude that the deformation accompanying interseismic and coseismic processes is more readily monitored from near the fault zone using measurements of surface gravity, strain, and displacement. The scales and rates of earthquake processes, and more so those of volcanic eruptions, is evidently too small for a significant increase in our understanding to be developed from the gravity field observed from orbiting satellites.

CONCLUSIONS

1. Satellite gravity measurements from four generic missions (SGG, SGGE, SSI, and SST) would constrain the nature of mantle convection on spatial scales of 200-1,000 km. An accuracy of ~10^{-2} mGal at resolutions larger than 300-400 km would suffice to characterize the variations in thermal structure that distinguish between various models of mantle structure. Observations with 1 mGal accuracy at length scales of 500-1,000 km would resolve discrepancies between estimates of the depths of continental roots and would distinguish between models of mantle flow. Gravity resolution of approximately 1 mGal over length scales of order ~120 km would help constrain the depths of origin of hotspot mantle plumes, which are a major source of intraplate volcanism and enhanced heat flow.
2. The medium- to long-wavelength effects of post-glacial rebound could be resolved at the 1% level by a 5-year SST or SSI mission at 400-km altitude. Measuring these effects is important for providing increased understanding of the Earth's interior, particularly the viscosity of the lower mantle. The SGGE mission is less useful because of its lower accuracy at long wavelengths. A multi-year mission is highly desirable for post-glacial rebound studies.
3. Recent availability of gravity data from former communist nations will help elucidate interesting structures in areas of active continental deformation, such as the Himalayas-Tibetan Plateau. Satellite data from any of the generic missions would permit these data to be put on a unified datum, which will be essential for understanding the subsurface structure and dynamics of these regions.
4. The best satellite missions for regional studies of ocean tectonics are SGG, SSI, and SST. For a 300-km mission, the SGG mission provides marginally better resolution over the SST mission for resolutions finer than 300 km. GPS-guided airborne gravimetry is ideal for obtaining regional high-resolution measurements.
5. Continuity of gravity measurements across the continent-ocean boundary is badly needed to address the structure of passive margins. All the generic gravity missions would provide information that would assist significantly in tying together oceanic and continental observations.

6

Water Cycling

The exchange of water among the oceans, atmosphere, and upper crust of the Earth constitutes the hydrologic cycle. Whereas most of the storage and exchange of water occurs within and above the oceans (Figure 6.1), understanding temporal and spatial variations in water exchange on land is of critical and world wide environmental and economic importance. Measurements of changes in land-based water exchange are of use in long-term weather prediction, global climate modeling, assessment of the health of agricultural lands, and major groundwater supplies. Space-based measurements of the temporal variations in gravity have the ability to quantify variations in storage of continental components of the hydrologic cycle that are not currently known with sufficient accuracy. Satellite gravity measurements cannot, by themselves, discriminate between changes in water on the surface, in the soil, or in the water table. Instead, they provide constraints on changes of the total water in vertical columns, integrated from the Earth's surface down through the base of the water table. In areas undergoing large scale aquifer depletion, this quantity will be dominated by the groundwater signal. In other areas, auxiliary land-based measurements of seasonal changes in groundwater levels offer the potential to separate the groundwater component from the soil water component.

WATER TRANSFER TO THE ATMOSPHERE

The transfer of water to the atmosphere from the land surface is a complex process that is not only a part of the hydrologic cycle but also a key control of energy cycling on the Earth. An SST mission could provide seasonal values of changes in water mass with 10-mm uncertainty over about 550,000 km^2 (Figure B.4), and the annually-varying amplitude could be determined at an accuracy of 10 mm over about 250,000 km^2 (Figure B.2; see Appendix B for a description of how these errors are estimated). For an SSI mission, the results improve to give a 10-mm monthly value over 150,000 km^2 and a 10-mm annually-varying amplitude over 100,000 km^2. Measurements of mass and energy exchange at this spatial resolution would be useful for long-term weather forecasting on continental and whole-Earth scales, since this exchange has a significant influence on weather processes. For both missions, conversion of water mass changes to estimates of land/atmosphere mass transfer will require auxiliary land-based measurements. They would also be of significant use to global-climate modelers.

Water transfer to the atmosphere can occur through a number of processes. Evaporation occurs from moist soils, plant surfaces, snow bodies, and lakes and rivers. Sublimation (the direct transfer of water from solid to

gas form without melting) occurs from snow bodies. Transpiration (the transfer of water from plant matter to the atmosphere primarily through the leaves of plants) is critically important in forested and agricultural lands.

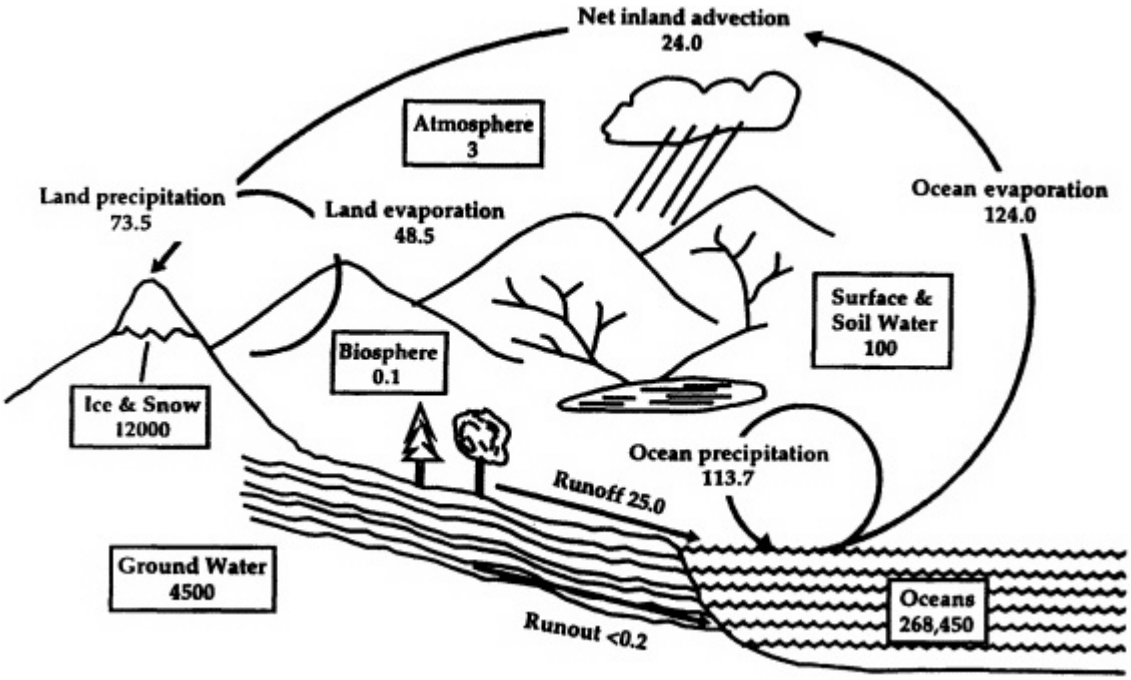

FIGURE 6.1
The global hydrologic cycle, illustrating storages in 10^6 cubic kilometers (boxed) and fluxes in 10^6 cubic kilometers per year. Figure from NRC (1986); Berner and Berner (1987).

Some of these processes are influenced by human activity. Deforestation and agricultural development affect the distribution and amount of biomass on Earth and alter both the storage of water in soils and rivers and the transfer of water to the atmosphere by evaporation and transpiration (evaporation and transpiration are often lumped as evapotranspiration). Irrigation of agricultural lands redistributes surface water, transfers groundwater to the land surface, and accelerates evapotranspiration.

While continental-scale averages of this transfer are somewhat well known (Figure 6.1), spatial and temporal changes in these processes are imprecisely known owing to the difficulty of direct measurement. Also, measurements made directly on the land surface are point measurements and, in general, are so widely spaced that it is not possible to derive meaningful estimates of spatial variations. Over spatial scales of several hundred thousand square kilometers, measurements of seasonal changes in water mass with a resolution of 10-30 mm in thickness would be useful for weather forecasting, climate modeling, and soil moisture and aquifer assessments. Measurements of water mass changes at this resolution and spatial scale should be possible with either an SST or SSI mission.

The amount of water mass transferred from the land surface to the atmosphere depends strongly upon such factors as soil moisture, biomass, air temperature, and air humidity. The global average annual amount of water transfer from the land surface to the atmosphere is about the equivalent of a column of water of 0.5 m. Because gravity depends directly on mass, variations in this transfer should have a direct impact on gravity. Currently, spatial and temporal variations in this transfer are typically inferred from empirically derived water-balance formulas (such as the Thornthwaite formula, [Dunne and Leopold, 1978]) whose accuracy is questionable. However, these empirical formulas suggest that annual and spatial variations are large.

For example, in estimates of the fluctuations in global soil-water mass (Figure 6.2) the seasonal (annual) variations dominate up to degree 10; at higher degrees the contributions from the seasonal and non

seasonal terms are approximately equal. Spatial and temporal variations are as large as 0.3 m. This would produce a geoid signal that would vary annually by as much as 6 mm (Figure 6.3). The amplitude of these signals is well above the uncertainties of measurement error for a 5-year SST mission at values of *l* below 30, and a 5-year SSI mission at values of *l* below 40 (Figures 4.5 and 4.6).

In theory, a five-year SST mission at an altitude of 400 km should allow us to resolve annual changes in water mass in the subsurface equivalent to a 1-mm column of water for an area of 1,500,000 km and annual changes equivalent to a 10-mm column of water for an area of 250,000 km^2 (Figure B.2). For the nominal SSI mission, the 1-mm error could be achieved over about 125,000 km^2, and a 10-mm error for an area of about 80,000 km^2.

As discussed in Chapter 4, these accuracy estimates do not consider the problem of separating the hydrological gravity effects from the effects of other geophysical processes. The effect of changes in oceanic mass could cause problems for hydrological estimates at locations near the shore. Atmospheric pressure could cause problems anywhere, although the gravitational effects of atmospheric pressure could be largely removed using global, gridded pressure data available from meteorological centers. Nevertheless, any error in the pressure data would map directly into an error in the hydrologic estimates for that region. For example, a 0.3-mbar pressure error would correspond to a 3-mm error in the inferred water storage. The accuracy of future pressure data over continental regions is difficult to predict; it could range upward from a few tenths of a mbar, depending on the location (see Chapter 8). Consequently, detection of changes in water mass of less than a few millimeters must be accompanied by accurate atmospheric pressure measurements.

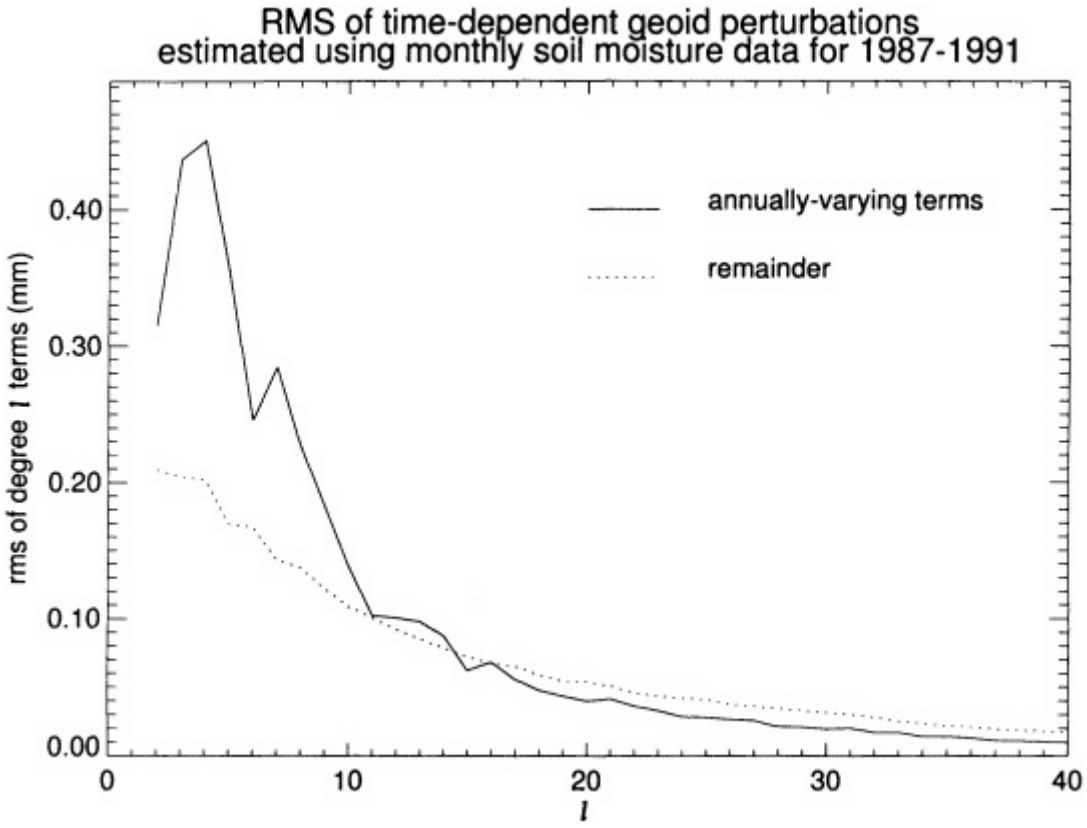

FIGURE 6.2
The rms of the degree variances found from the monthly soil moisture data from 1987-1991, showing the annually-varying and the non-annual contributions. Note that the non-annual contributions are about one-half to two-thirds the size of the annually-varying effects for $l<10$; but that they are of equal importance at higher degrees (i.e., shorter wavelengths). See Appendix B for a detailed discussion of the accuracy of the generic missions.

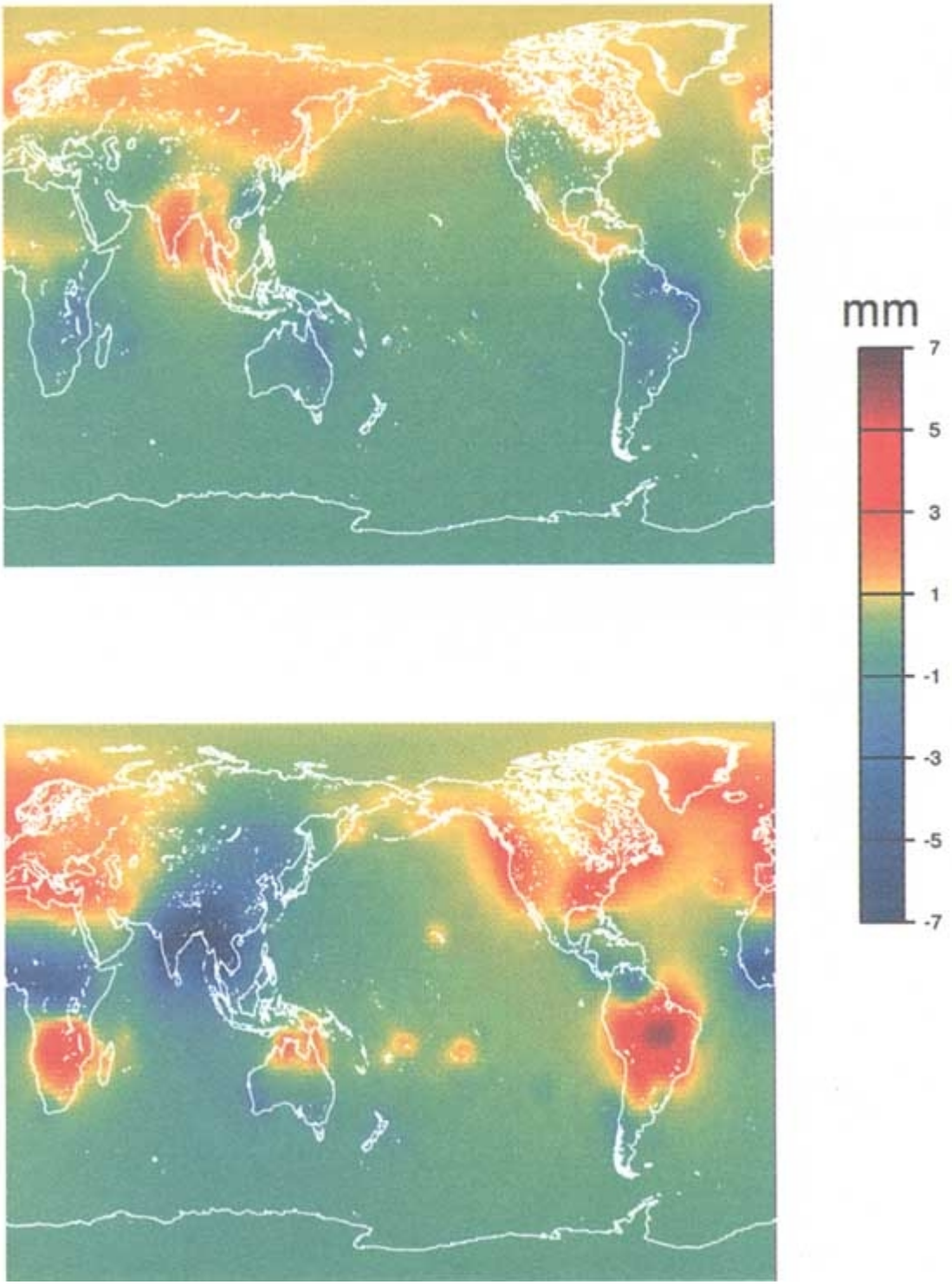

FIGURE 6.3
The annually-varying contributions to the geoid from changes in continental water storage, as estimated from the soil moisture data set for 1987-1991. Top panel: the amplitude of cosine(ωt), where ω = 1 cycle/yr and t = 0 on January 1. Bottom panel: the amplitude of sine(ωt).

While detection of water-mass changes with a resolution of 10 mm would be extremely valuable for estimating sub-continental energy and water-mass exchange between the Earth's surface and the atmosphere, it should be noted that this signal does not strictly represent land-atmosphere mass and energy exchange. The detected water-mass changes largely reflect the combined changes in water mass in groundwater and soil moisture. Water mass changes in groundwater are generally not directly linked with atmospheric exchange and are strongly influenced by direct transfer and exchange with surface water. Estimates of mass exchange between the land surface and the atmosphere will require the use of existing land-based measurements of soil moisture and groundwater levels. Monitoring groundwater levels over large regional areas would enable separation of the groundwater influence on water mass changes. Since land/ atmosphere mass exchanges are dominated by soil moisture changes, point measurement of soil moisture will provide a partial control on the mass changes inferred from gravity measurements.

SOIL MOISTURE INVENTORY

Crop abundance in agricultural regions depends on proper levels of soil moisture. About 15 million square kilometers, or 10% of the world's land surface, is used for growing crops (World Resources Institute, 1990). More than four-fifths of these lands and more than nine-tenths of lands outside Asia are not irrigated and depend wholly upon precipitation.

Agricultural production is thus highly dependent upon annual and seasonal variations in precipitation. Yearly projections of agricultural production would be greatly improved by measurements of soil moisture on a semi-annual basis. Such information would be highly valuable to commodity futures markets and to those world wide agencies that assess food availability, particularly if we can provide seasonal measurements with a resolution of 10-30 mm over an area of a few hundred thousand square kilometers (Figures 4.5 and 4.6).

The seasonal variability in soil moisture ranges widely, depending on the plant cover, soil type, and precipitation. Typical seasonal variations in water thickness are on the order of 150 mm (Dunne and Leopold, 1978). Seasonal variations in soil moisture of one tenth this magnitude should be detectable from a SST mission at 400-km altitude at a spatial resolution of roughly 300,000 km^2 (Figure B.2). For a nominal SSI mission, the area that can be resolved is 90,000 $km^{2.}$ The potential exists for space-based gravity measurements to provide a world wide inventory of the ability of agricultural lands to produce high yields in a given year. As in the case of inferring land-atmosphere water exchange from gravity, the use of spaced-based gravity to infer changes in soil moisture levels has an inherent ambiguity due to other water-related influences. Inferences of seasonal changes in soil moisture from gravity would be abetted by land-based measurements of groundwater levels and point measurements of soil moisture.

GRAVITY AND THE GEWEX CONTINENTAL-SCALE INTERNATIONAL PROJECT

Estimates of evapotranspiration rates and soil moisture levels would be of direct use to the GEWEX (Global Energy and Water Cycle Experiment) Continental-Scale International Project (GCIP). Satellite-based estimates of hydrologic properties at the large scales (such as the Mississippi River basin scale), which can be inferred from a satellite gravity mission, are considered an essential part of GCIP. The overall goal of GCIP, which was formed in 1990, is to improve climate models by bridging the gap between small scales appropriate for modeling discrete processes over land and large scales practical for modeling the global climate system. The primary objectives of GCIP are to determine the variability of the Earth's hydrological cycle and energy-exchange budget over a continental scale; to develop and validate techniques for coupling atmospheric and surficial hydrological processes in climate models; and to provide a basis for translating the effects of future climate change to impacts on regional water resources. The initial focus area of GCIP is the Mississippi River basin, which was selected because of its extensive hydrological and meteorological observation network. Both the SST and SSI missions would be able to provide estimates of changes in water mass at a resolution of 10-30 mm over the spatial scale of the initial GCIP focus area (Figure 4.5). Part of the initial phase of GCIP is to build up the science base and technical expertise on regional and continental-scale processes. The surface-based, model-derived, and satellite-based data will be used to develop models that couple complex atmospheric and surficial hydrological processes on a wide range of spatial scales. A second phase of GCIP will focus on extending this capability to the global scale, using observations that will be forthcoming near the turn

of the century from the next generation of Earth-observing satellites.

SNOWLOAD AND ASSOCIATED RUNOFF

Estimates of snowload in mountainous regions are important in assessing the level of potential flood hazard associated with snow melt. Prediction of flood magnitude associated with spring snow melt is highly dependent upon the water content of the snowpack. Currently, the annual snow load in mountainous regions can be monitored to about 300-mm accuracy (approximately 60 mm water equivalent) using passive-microwave remote sensing. The data are validated using point measurements from surface stations located at wide spatial intervals. These point measurements typically overestimate snow cover because they are often biased to regions of larger-than-mean snow accumulation. Snow hydrologists would find useful a gravity mission that could estimate integrated water equivalent, thus providing an independent validation of the radiometer data. This is desirable in the Rocky Mountains (500 km × 1,000 km) but is especially needed in the Tien Shan and Pamirs (1,000 km × 2,000 km) of central Asia where validation points are currently very sparse. For the SST case, the accuracies for the Colorado Rockies and the Tien Shan are about 10-20 mm and 2-3 mm, every 90 days, respectively. For SSI, they become about 0.35 mm and 0.25 mm, respectively. Practical flood hazard assessment using space-based gravity would likely require 30 day or more frequent sampling.

AQUIFERS

In many regions of the world, groundwater is the primary source for irrigation. Groundwater reserves are commonly being used faster than they can be replenished in these regions. In the United States alone, groundwater reserves are being depleted in vast regions of the western U.S. and throughout Georgia and Florida. The most publicized U.S. example of groundwater depletion is the High Plains aquifer (formerly called the Ogallala aquifer) in the Great Plains region (Figure 6.4). In the late 1970s this aquifer supplied over a quarter of the groundwater used for irrigation in the United States (Gleick, 1993). The estimated average area-weighted water-level decline from about 1940 to 1980 was 3.0 m, which represents an average water mass decline in the vertical of 11 mm/yr (Dugan and Cox, 1994). Since 1980, water levels have continued to decline, but at a slower rate. The estimated average area-weighted water-level decline from 1980 to 1993 was 0.6 m, representing an average rate of mass decline of 7 mm/yr. The lower rate of decline since 1980 is associated with above normal precipitation and reductions in irrigation use. By the early 1990s, severe depletion of the aquifer was a significant factor in driving much of the region out of agricultural production.

Saudi Arabia, an exporter of wheat, depends upon groundwater reserves that are being depleted. During the latter half of the 1980s, groundwater pumping exceeded estimated recharge in the country by a factor of five. Groundwater overdrafting is also widespread in many regions of India, China, Mexico, northern Africa, and the former Soviet Union. Groundwater levels are falling up to one meter per year in parts of northern China. Heavy pumping in portions of southern India dropped water levels by as much as 25-30 m in the previous decade.

Future growth in the agricultural use of arid and semi-arid lands partly fueled by population growth and partly influenced by a desire for self-sufficiency of agriculture and economic diversification will further increase the overdrafting of aquifers world wide. For example, in the near future Libya plans to irrigate some 200,000 hectares with water drawn from aquifers that receive little recharge.

Annual space-based gravity surveys offer the potential to measure long-term declines in the world's large aquifers. These declines, the equivalent of tens to hundreds of millimeters of water mass per year, are large enough to be detectable; indeed, in regions of large-scale groundwater withdrawal, the associated gravity change should be the dominant signal in a space-based measurement. Given an SST mission at an altitude of 400 km, secular changes in water mass on the order of 10 mm per year should be readily detectable in a region the size of the High Plains aquifer (Figure 4.5; Figure B.). An SSI mission could do more than an order of magnitude better than this, although the interpretation of the data would probably be limited by contamination from the effects of other geophysical processes.

CONCLUSIONS

1. Gravity missions can provide centimeter and better accuracies for the changes in the thickness of water stored on continents at spatial scales of several

tens of thousands of kilometers and larger. The amplitude of these signals is well above the uncertainties of measurement error for a 5-year SST mission at values of *l* below 30, and a 5-year SSI mission at values of *l* below 40. Estimates would be of direct use to GEWEXGCIP.

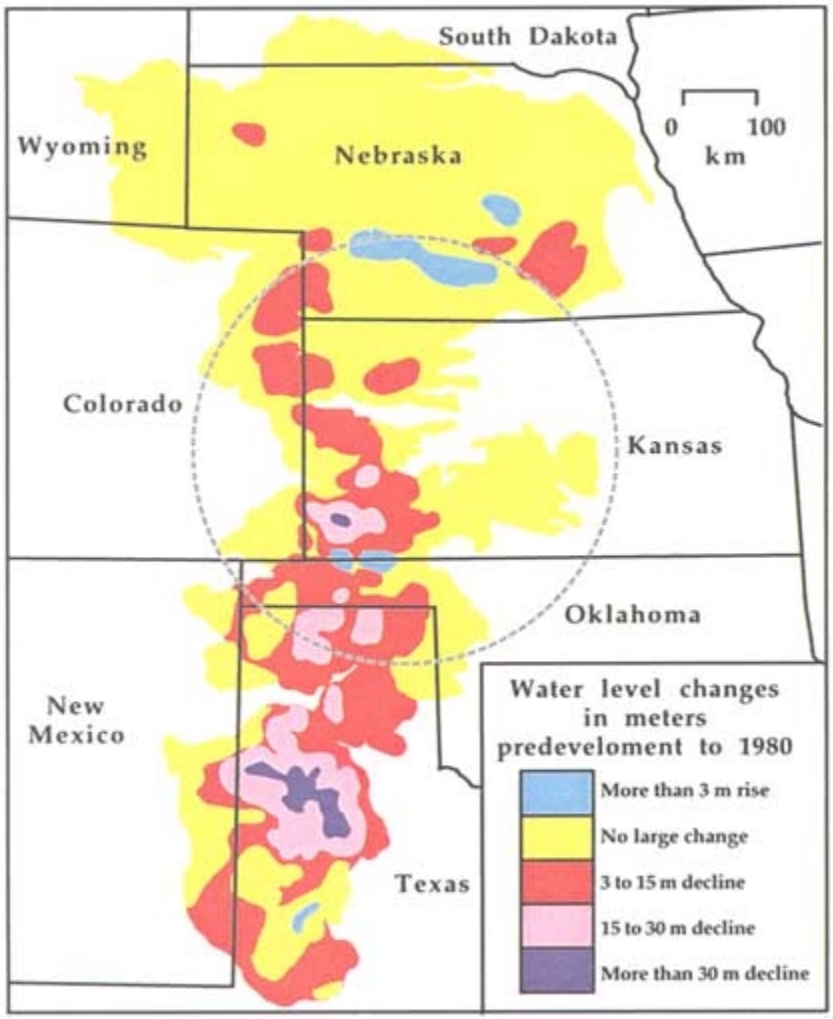

FIGURE 6.4
Groundwater overdraft in the High Plains aquifer, predevelopment (approximately 1940) to 1980 (modified from Dugan and Cox, 1994). Center circle represents an area of 250,000 km^2 for reference.

2. Gravity measurements of changes in water storage are important to hydrologists for making the connection between hydrological processes at traditional hydrological length scales (tens of kilometers and less) and those of longer scales useful for estimating global water and energy balances.
3. Gravity measurements of changes in water storage are important to meteorologists because of the impact of soil moisture on evapotranspiration. Seasonal variations in soil moisture of 10-30 mm should be detectable from an SST mission at 400-km altitude at a spatial resolution of roughly 300,000 km^2. For an SSI mission, the area that can be resolved is 90,000 km^2.
4. Both monitoring and prediction are technologically feasible and hold promise for the mitigation of natural hazards and ongoing evaluation of the state of one of the world's most important renewable resources, its fresh water. Measurements of gravity variations can help monitor aquifer depletion. Gravity results can aid in monitoring snow pack, predicting floods and the runoff available for irrigation, and assessing agricultural productivity on large scales.

7

Sea-Level Change

Climate models used to study the effects of atmospheric greenhouse gases predict an overall increase in the global temperature during the next century of 1 to 3.5° C (Warrick et al., 1996). An increase of this magnitude could have numerous catastrophic effects, not the least of which would be caused by a substantial rise in global sea level due to a combination of melting glaciers and polar ice sheets and thermal expansion of sea water (Box 7.1).

Tide-gauge data show that sea level is already rising at a rate of between 1.0 and 2.5 mm/yr averaged over the past century (Warrick et al., 1996). The sources of this sea-level rise are not well understood, however. Estimates of various effects are included in Table 7.1. Most of the likely mechanisms involve the transfer of mass from the continents to the ocean basins. This mass redistribution would cause a secular perturbation in the geoid. The thermal expansion effect, however, involves no horizontal transfer of mass and so has no associated geoidal signal.

Satellite observations of time-dependent gravity could constrain changes in global sea-level in two ways. First, they could help identify the continental sources of water transferring into the ocean, through monitoring of the mass of ice sheets, continental glaciers, and groundwater aquifers. Second, they could be used to help identify the thermal-expansion component of sea-level rise by using the observations to solve directly for the mass increase in the ocean. These applications are discussed below.

THERMAL EXPANSION OF THE OCEANS

By comparing satellite gravity observations with tide-gauge or altimeter results over the time-span of the mission, it should be possible to discriminate between a mass influx, which affects both sea level and gravity, and thermal expansion, which affects only sea level. The contribution of thermal expansion to global sea-level rise is estimated to be between 0.2 and 0.7 mm/yr averaged over this century (Table 7.1). To improve the determination of this component, a gravity satellite would need the capability to detect a sea-level rise with an accuracy on the order of a few tenths of a mm/yr. This would constrain the total mass influx more closely for each year that the gravity data are available. Separating the relative contributions among the four sources listed in Table 7.1 will also require a gravity mission of some years.

Figure 7.2 shows the predicted secular geoid perturbation caused by a 1 mm/yr rise in sea level, assuming that the rise is due entirely to an increase in water mass (the geoid in Figure 7.2 changes over the continents because a spatial constant has been removed from the output at each time step: i.e., the mass of the Earth, as a whole, is assumed to be conserved). Note that the geoid amplitudes are small, no more than a few hundredths of a mm/yr. The signal caused by a rise of a few tenths of a mm/yr would be smaller still. This will be a difficult signal to detect.

BOX 7.1 IMPACT OF GLOBAL SEA-LEVEL RISE

A large fraction of the Earth's total population resides close to sea level, and few societies would remain unscathed by the global agricultural and industrial effects of a rise of sea level by I m or more. Half of the world's megacities (population >8 million) are located near sea level with a total yea 2000 population exceeding 150 million, and these constitute but a small fraction of the ports and communities that thrive globally on coastal commerce, agriculture, and industry. An estimated 46 million people per year are at risk of flooding due to storm surges, and a l-m rise in sea level would raise that number to 118 million people per year (IPCC, 1996).

A rise in sea level has its greatest effects on low-lying regions that slope gently inland (e.g., Florida and Indonesia with 15% of the world's coastlines) or are on the flood plains of large river systems (eg., Rhine, Ganges, Nile, Mekong). In these areas, a rise in sea level triggers landward transgression of the coastline and subsurface incursion into fresh water reservoirs, resulting in a loss of arable land. By the year 2100, a 1-m rise in sea level could lead to land loss ranging from 0.05% in Uruguay, 1.0% in Egypt, 6% in The Netherlands, and 17.5% in Bangladesh to 80% in the Marshall Islands (IPCC, 1996). In the United States, it has been estimated that a rise in sea level by 1 m would drown 20-85% of coastal wetlands and would result in coastal encroachment of up to 7,000 square miles, an area the size of Massachusetts (Titus et al., 1991).

The loss of coastal ecosystems would also have negative effects on tourism, infrastructure, freshwater supplies, biodiversity, and fisheries. In Blackwater National Wildlife Refuge of the Chesapeake Bay, for example, sea-level rise has resulted in the inundation of a significant fraction of marshland (Figure 7.1), altering the ecological balance of the area With regard to infrastructure, more than 90% of all power stations in the United States are located close to the coasts; so also are many industrial complexes, to he within easy reach of harbors and raw materials. For many nations, economic losses caused by sea-level rise could exceed 10% of their Gross Domestic Product (IPCC, 1996). The social impact of large communities migrating inland and the economic costs of increased sea-level defenses are likely to have adverse effects throughout coastal societies.

The current global sea-level trend is a rise of approximately 0.2 m/century, but it is possible that this could be accelerated by a factor of *3-5* by global warming trends, although smaller rates of acceleration are more likely. Current rates, if they remain constant, are slow enough to permit appropriate societal responses to sea-level rise. However, an acceleration by a factor of 5 would affect low-lying areas at rates that would require more immediate remedial action by coastal societies, so early detection of an acceleration is an important planning requirement.

TABLE 7.1 Estimated Ranges of Likely Contributions to Sea-Level Rise, Averaged over the Past 100 Years (from Warrick et al., 1996)

Contribution	Rate of Increase or Decrease (mm/yr)
Thermal expansion	0.2 to 0.7
Antarctica	-1.4 to 1.4
Greenland	-0.4 to 0.4
Glaciers and small ice caps	0.2 to 0.5
Surface and groundwater	-0.5 to 0.7

The degree amplitudes from a 1 mm/yr rise in sea level do exceed (slightly) the 5-year, 400-km SST-mission uncertainties for $l < 6$ (see Figure 7.3). Because the pattern of the geoid signal is well known in this case (shown in Figure 7.2), it might be possible to obtain a useful estimate for the amplitude of this effect by fitting that pattern to the satellite data. Using the uncertainties described in Chapter 2, we find that data from the 5-year SST mission would provide a 1-sigma error on the mass contribution to sea level of about 0.1 mm/yr. The results obtainable with an SSI mission would have even smaller formal errors—the effects of a 1 mm/year change in sea-level rise above the SSI errors at degrees all the way up to $l = 20$

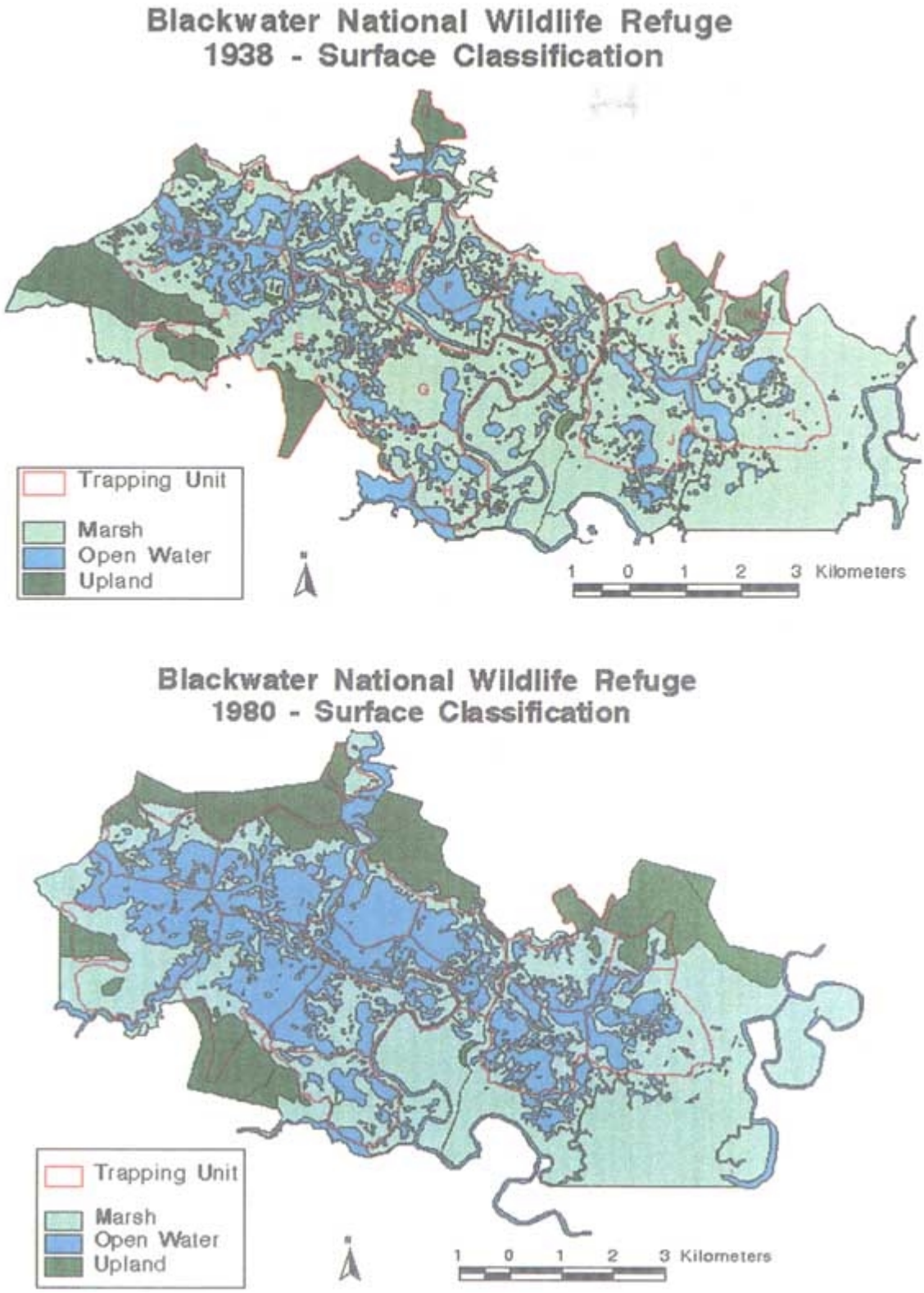

FIGURE 7.1
Changes in marsh and upland (higher ground) land types in Blackwater National Wildlife Refuge, Chesapeake Bay, Maryland due, in part, to sea-level rise. From 1938 to 1980,an average of 17.3 hectares/yr of marsh was inundated. Figure based on aerial photography and prepared under the auspices of NOAA's Coastal Change Analysis Program. Courtesy of C. Stevenson, University of Maryland Center for Environmental and Estuarine Studies.

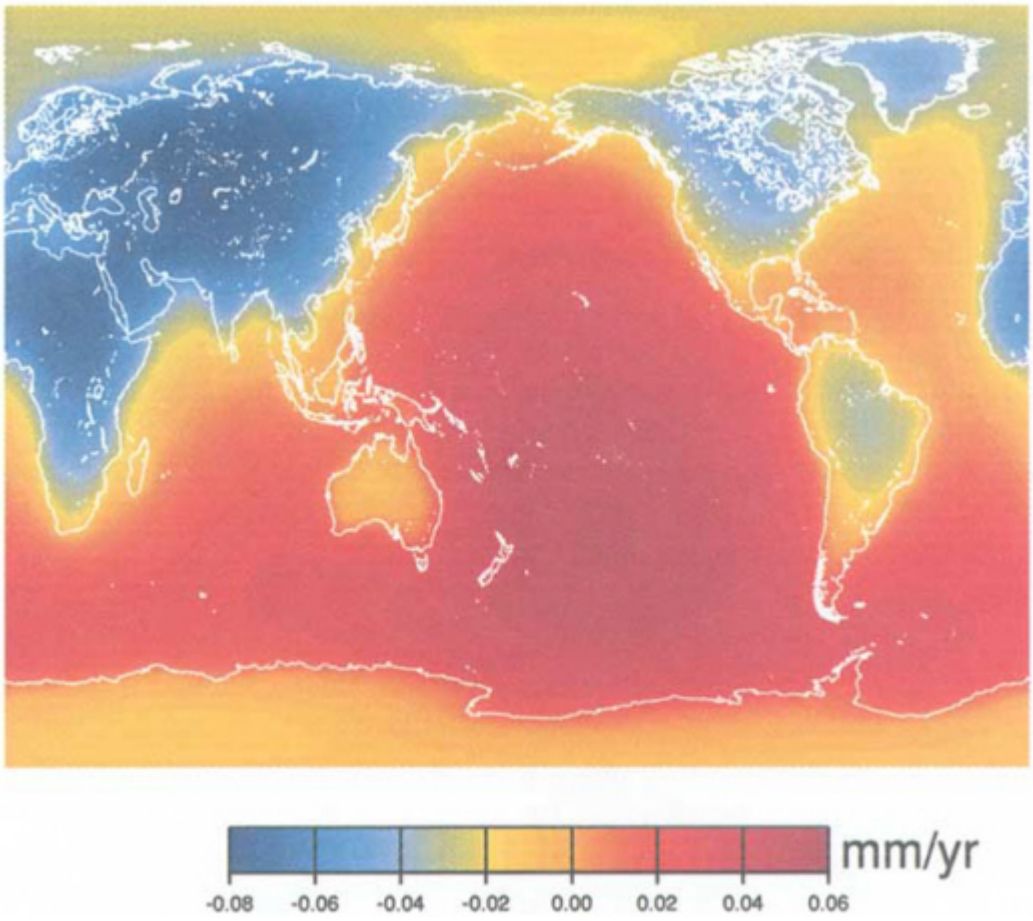

FIGURE 7.2
The secular change in the geoid caused by a 1 mm/yr rise in global sea level, assuming that sea-level rise is due entirely to an increase in water mass. The spatial mean is set to zero, consistent with the assumption that the Earth as a whole conserves mass.

(Figure 7.3, bottom panel). But problems of separating the global sea-level signal from the effects of other secular geophysical signals are likely to limit the sea-level accuracies to about 0.1 mm/yr in any case. (An SGG mission, even the extended-duration SGGE mission, is not sufficiently accurate at low degrees to be useful for this application.) An accuracy of 0.1 mm/yr could, indeed, be useful in separating the thermal expansion effects from the effects of an increase in mass, provided that the total global sea-level rise has been measured to this same high accuracy using some other technique (satellite altimetry, for example), during the same time period. Note that any conclusions obtained from this study would be based on data from the limited time-span of a satellite mission (nominally assumed throughout this report to be about five years) and might not reflect true long-term trends. A long-term monitoring capability would be desirable.

In addition to providing information on global and regional sea-level rise, satellite gravity data could be used to study changes on basin scales. For example, sea level in the North Atlantic is believed to have risen by 3 cm between 1994 and 1995, with much of the increase occurring over a few months (Figure 7.4)

(Carton and Miller, 1997). This increase, which should be readily detectable by an SST or SSI mission (cf. Figure B.3 in Appendix B), was associated with an anomalous warming of surface temperatures and changes in the structure of the thermocline. For identifying the causes of such basin-scale anomalies, a vitally needed piece of information is the relative contribution of thermal expansion compared with an overall increase in mass. Thus again, satellite measurements of the increase in mass would be invaluable in sorting out the causes of sea-level rise.

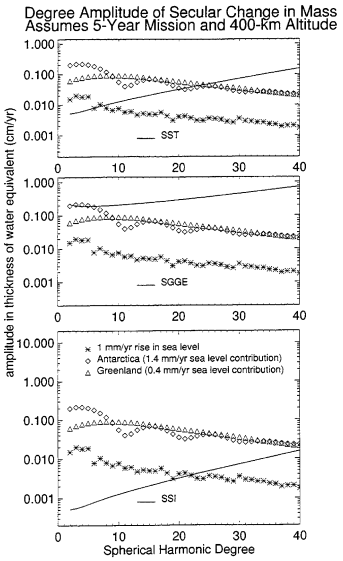

FIGURE 7.3
The degree amplitudes for secular fluctuations in geoid, compared with the expected uncertainties for 5-year SST, SGGE, and SSI missions at 400-km altitude. The geophysical processes considered here include post-glacial-rebound (for the entire globe: North America, Scandinavia, Greenland, and Antarctica; and assuming a lower-mantle viscosity of 10.E21 Pa-sec); present-day changes in Antarctic and Greenland ice, at a level to cause a global sea-level change of 1.4 mm/yr for Antarctica and 0.4 mm/yr for Greenland, which are the upper bounds from Warrick et al. (1996); and a 1 mm/yr change in global sea level, assuming that this is entirely due to the transport of mass between the oceans and continents.

ICE MASS BALANCE

The masses of glaciers, ice caps, and ice sheets (the term "ice sheet" is reserved for the vast ice covers of Antarctica and Greenland) vary temporally through the exchange of water with the oceans. These ice bodies on land can shrink in two ways—by excess melting and liquid water runoff and by breaking off as icebergs. In either case the mass lost soon reaches the ocean. Conversely, ice bodies can gain mass only by an excess of snowfall on their surfaces; the moisture source is evaporation from the oceans. Thus, the measurement of the total mass balance (deviation from constant mass through time) of the ice on land is a direct, though partial, measure of the changes of water mass in the oceans.

There are two important advantages of gravity measurements for large-scale mass-balance studies. The first is that, since gravity depends simply on mass, changes in gravity provide a direct measure of ice-mass balance that is independent of changes in the mean density of the ice bodies, which can change with time. Secondly, gravity serves as an automatic integrating tool, thus obviating the huge difficulty that glaciologists face in extrapolating results from field studies in a few areas to much larger regions, especially to the entirety of the vast ice sheets. For both these reasons, glaciologists eagerly await future satellite-gravity missions.

Contributions from the Greenland and Antarctic Ice Sheets

Currently, the large-scale mass balances of Greenland and Antarctica are poorly known. Estimates of their contributions to the global sea-level rise during this century are in the range of ± 1.4 mm/yr for Antarctica and ± 0.4 mm/yr for Greenland (Table 7.1)—not even the sign is known. Both upper bounds correspond to geoid amplitudes of 2.0 to 2.5 mm/yr, spread over the respective ice sheets.

Figure 7.3 shows the degree amplitudes of a uniform change in mass of each sheet, assuming the

mass changes are equal to the upper bounds cited by Warrick et al. (1996). These results include the effects of the Earth's elastic response to the changes in ice load, as described in Appendix B. Note that the results rise well above the uncertainties for a 5-year SST mission at values of *l* below 25 (corresponding to half-wavelengths greater than 800 km), and for a 5-year SSI mission at values of *l*below 40 (half-wavelengths greater than 500 km). Approximating Antarctica and Greenland as squares about 3500 km and 1300 km on a side, respectively, we estimate from Figure B.1 that a 5-year, 400-km altitude SST mission would be sensitive to changes in the overall mass of Greenland and Antarctica to an accuracy corresponding to better than 0.01 mm/yr of sea-level rise for each ice sheet. (The water thickness results from Figure B.1 can be converted to sea level by multiplying by the ratio of the ice sheet area to the area of the world's oceans.) A 5-year SSI mission would be about an order of magnitude more sensitive.

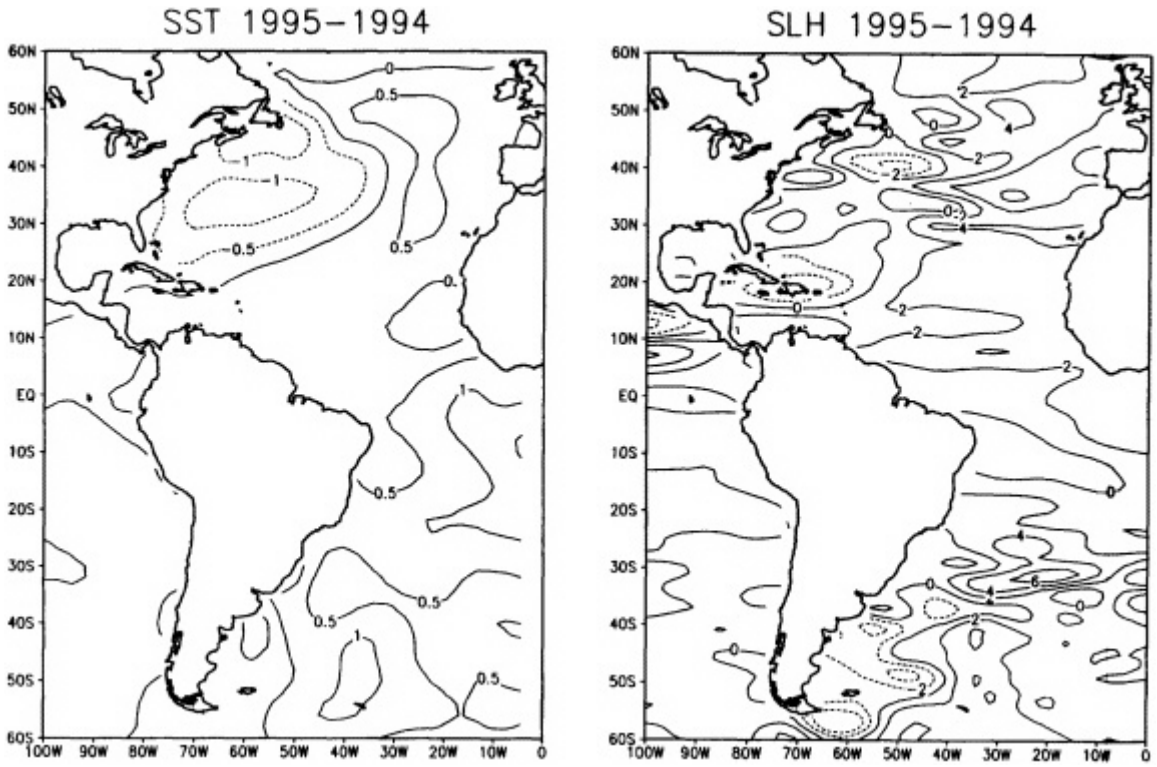

FIGURE 7.4
Observed change in annual averaged sea level in cm (right-hand panel) and sea-surface temperature in degrees C (left-hand panel) for 1995 relative to 1994. The warm El Niño conditions of the tropical Pacific have receded, causing sea level to drop. In the eastern North Atlantic, a warming of sea-surface temperature is reflected in a rise of sea level.

It is important to note, however, that there are ambiguities in interpreting gravity signals over ice sheets because of problems in separating the effects of ice-sheet changes from the effects of isostatic rebound, interannual variations in snow accumulation rates, and atmospheric pressure. These problems are discussed in turn below.

Isostatic Rebound

It is difficult to distinguish between effects of present-day changes in ice-sheet mass and effects of the Earth's visco-elastic response to changes in ice mass over the past few hundred to several thousand years, particularly in Antarctica. In principle, one could correct for the isostatic uplift by measuring it on exposed rock. Although most of Antarctica is ice-covered, there are many exposures in the extensive Transantarctic Mountains, which cut through the continent from the Atlantic to the Pacific (Figure 7.5). Hence a campaign of GPS measurements along the Transantarctic Mountains (and some nuna

taks elsewhere) to determine uplift rates would be a valuable undertaking. Accuracies on the order of 1-2 mm/yr (taking into account the poorer geometry and increased ionosphere delays in polar regions) should be attainable with five years of continuous GPS measurements. (Tectonic uplift rates in the Transantarctic Mountains could be as large as 1 mm/yr [Behrendt et al., 1991], but are more likely no more than a few tenths of a millimeter per year [Fitzgerald, 1994].) This corresponds to an uncertainty in the secular gravity signal that is equivalent to about 4 mm/yr of ice, or about 0.15 mm/yr of global sea-level rise. The problem is, however, that crustal uplift rates measured for the Transantarctic Mountains, which occupy only a small fraction of the total area of Antarctica, would likely not be representative of the average uplift rates for the entire continent. It is thus probable that the best use of such GPS measurements would be to help assess independent models of the rebound, which would then be used to remove the effects at all locations.

Rebound models in their current state of development would not suffice to solve the problem. Uncertainties in the Earth's viscosity profile and the time evolution of the Antarctic ice sheet correspond to uncertainties on the order of 30 mm/yr in present-day thickness changes of the Antarctic ice sheet, which is equivalent to about 1.2 mm/yr of global sea-level change. At first glance, this result suggests that a gravity mission would not improve the global sea-level change estimates of Warrick et al. (1996). However, it is likely that a dedicated gravity mission would lead to a solution for secular changes in the gravity field over northern Canada that would greatly improve our knowledge of the Earth's viscosity profile (see Chapter 5). In that case, the main source of uncertainty in the Antarctic visco-elastic change would be the detailed time evolution of the Antarctic ice sheet itself. The level of that uncertainty would depend on the Earth's viscosity profile. If the lower-mantle viscosity is 4.5×10^{21} Pa-sec or smaller, the uncertainty in the Antarctic contribution to present-day sea-level rise would probably be on the order of 0.6 mm/yr, with about equal contributions from uncertainties in the Pleistocene ice history and estimates of what the mass balance might have been over the past several hundred to several thousand years. At larger values of lower-mantle viscosity (e.g., 20×10^{21} Pa-sec or greater), the Earth would respond more slowly to past changes in ice, and the total uncertainty might be reduced to 0.3 mm/yr or smaller. Uncertainty estimates this small would indeed lead to improved estimates of the Antarctic contributions to sea-level change, though any such result would be representative of the ice sheet for only the relatively brief duration of the satellite mission.

Snow-Accumulation Rates

Another interpretation difficulty arises from the consideration of interannual variations in the rate of snow accumulation on the ice-sheet surfaces (Figure 7.5). Here the problem is not in determining the change in mass of the ice sheets, but in distinguishing between changes in the mass of the solid ice, which can occur only by ice-dynamic processes with time scales of decades to millennia and which, consequently, are of the greatest interest in terms of secular changes in sea level, and ephemeral changes associated with a few years of higher-than-normal or lower-than-normal snowfall rates. It is not well known how large the average variability in snowfall might be over an entire ice sheet, but on a more local scale an average interannual variability of 25% has been estimated for Antarctica (Giovinetto, 1964); a similar figure is likely for Greenland. (The interannual variability in outflow is much less than this because outflow is principally by solid ice discharge into the ocean.) Even if interannual variations were uncorrelated from year to year, which is climatologically unlikely, this would yield an error in estimating the secular change in ice mass from a 5-year mission that would be on the order of 10% of the annual mass input, or approximately 18 mm of ice, equivalent to 0.6 mm/yr of sea-level change, for Antarctica, and 70 mm of ice (0.3 mm/yr sea-level equivalent) for Greenland. An error of this magnitude would be a serious hindrance in determining the true, long-term contribution of the ice sheet to sea-level change.

Fortunately, this error can be reduced in two ways. The first is by the calculation of broadly averaged snowfall rates from the atmospheric-moisture-flux divergences over the ice sheets determined from atmospheric numerical analyses that incorporate satellite-based soundings of water vapor and winds over the surrounding oceans, as well as regular rawinsonde observations from a small number of surface stations. Meteorologists expect that by the year 2000 the total input can be known to ± 10% for Antarctica and a few percent for Greenland (D.H. Bromwich, personal communication). Furthermore, a substantial portion of the uncertainties would be systematic, i.e., not varying from year to year. Thus the error in the interannual differences from a long-term mean could be less than 10% of the total input; if it were half that, the combined error for Antarctica and

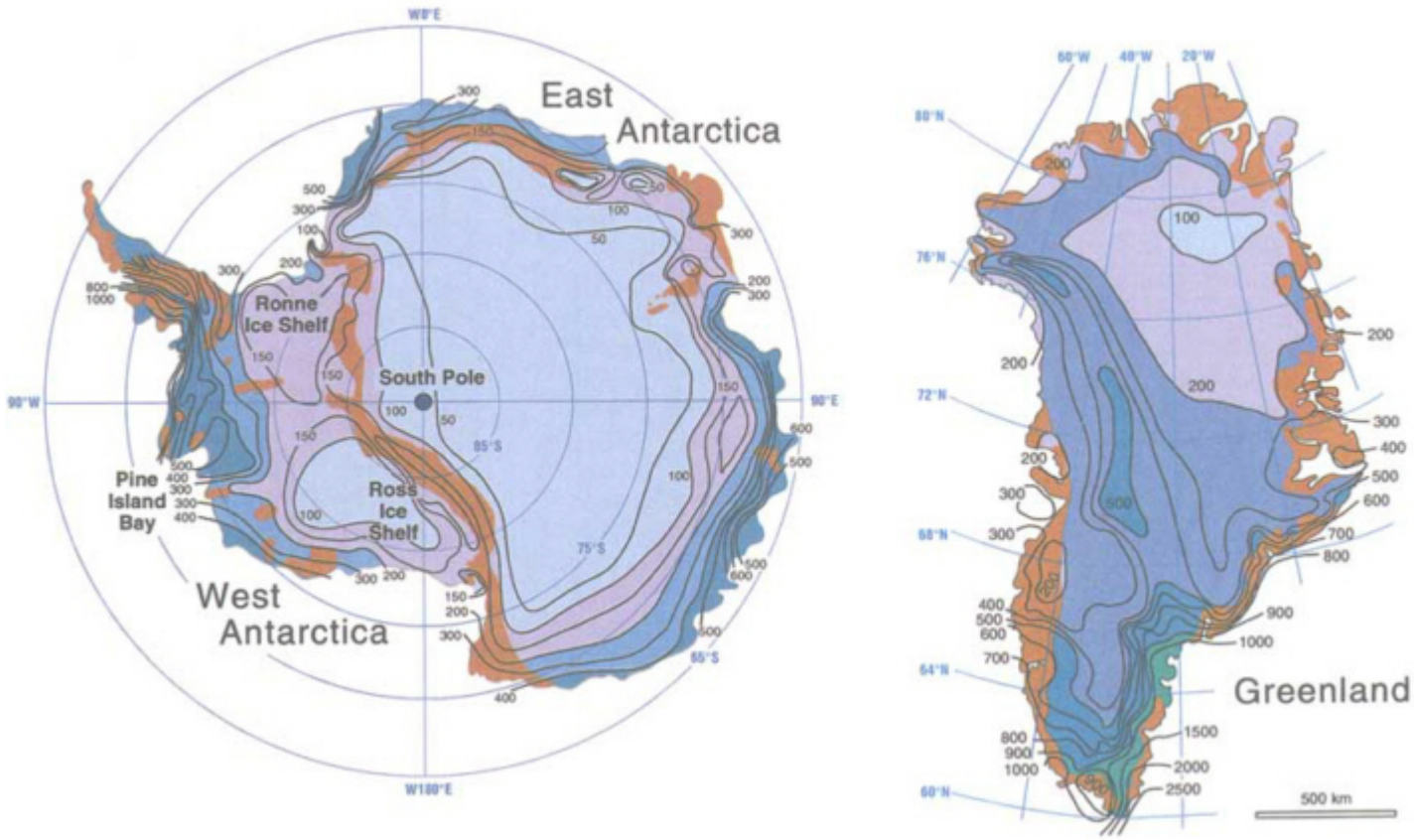

FIGURE 7.5
Map of the ice sheets, showing mean annual accumulation rates in kg/m^2 yr. The contourinterval is 100 kg/m^2 yr, with additional contours at 50 kg/n 150 kg/m^2 yr in Antarctica (left). Colors change at accumulation rates of 100, 200, and 400 kg/m^2 yr in Antarctica and 100, 200, 500, and 9900 kg/m^2 Greenland Brown zones are mountainous regions with extensive exposed rock. The Transantarctic Mountains cut across Antarctica between the South Pole and the two great ice and divide the continent into East Antarctica and West Antarctica. The latitude lines provide the scale for Antarctica—10° of latitude equals 1100 km. Note that the s Antarctica and Greenland differ by about a factor of two; Greenland is comparable in size to East Antarctica.

Greenland could be reduced to 10 mm/yr of ice (0.3 mm/yr in sea level).

Secondly, the gravity measurements themselves can help determine the interannual variations, at least for the period of the mission. According to our calculation, geoid amplitudes could well vary by 1 mm or more over both Antarctica and Greenland (Figure 1.2), if average interannual thickness changes, in water equivalent, were about 18 mm for Antarctica and 70 mm for Greenland. We conclude from Figure B.2 that an SST mission at an altitude of 400 km could in principle resolve these thickness variations to an accuracy of about 0.3 mm and 1.0 mm for Antarctica and Greenland, respectively. For a nominal SSI mission, those numbers are 0.08 mm for Antarctica and 0.1 mm for Greenland, but in actuality the accuracy will be less, because the gravity signal of the ice sheet is contaminated by the signal from the surrounding ocean and by the atmospheric pressure over the ice sheet itself. We estimate, using the annually-varying geoid predicted from the ocean general circulation data described in Chapter 4, that the oceanic effects could limit the accuracy in determining interannual changes in snowfall to about 2 mm (0.07 mm of sea level) for Antarctica and about 10 mm (0.04 mm of sea level) for Greenland. This still would represent a great improvement over current methods of determining changes in snowfall over time. We consider the effect of atmospheric pressure next.

Atmospheric Pressure

Yet another problem arises, particularly in Antarctica, from the fact that the gravity satellite will sense the mass of the atmosphere as well as the masses of the ice sheet and the solid Earth. The mean atmospheric pressure over the ice sheet (which reflects the overlying mass) must be determined from a very small number of measuring points; consequently there may be an error as large as 1 mbar (about equal to 10 mm of ice or 0.3 mm of sea-level equivalent) in evaluating annual averages. This could be a relatively static error, however, so it would not notably affect a calculation of secular change rates. There still remains a random-error component, which is on the order of a millibar on annual averages (Chen et al., 1997; D.H. Bromwich, personal communication), hence presumably is less than 0.5 mbar (5 mm of ice; 0.2 mm of sea level) with respect to secular change rates. The uncertainties in mean pressures can best be reduced by extending the number of automatic weather stations over the Antarctic surface and assuring that data from them are available and used in mean-pressure calculations. The situation is less serious in Greenland because Greenland is smaller and contains a better distribution of weather stations.

Complementarity with Satellite Laser Altimetry

Estimates of mass balance could be further improved if the present-day changes in the heights of the ice sheets could be determined separately using laser altimeter measurements from an orbiting satellite—specifically, NASA's planned Laser Altimetry Mission. For a given mass increase, the surface height changes would be in the ratio of 1:3.5:10 for isostatic uplift, changes in solid ice, and changes in snow accumulation at the surface, respectively, because the source of mass change in each of those cases is characterized by a different mean density. If the cause were atmospheric pressure changes there would be no change in height at all (the response of the ice to pressure fluctuations is negligible). It follows that measurements of both change in height and change in gravity should, in principle, make it possible to distinguish between uplift and changes in mass of the ice sheet. NASA's planned Laser Altimetry Mission, carrying a laser altimeter in a 94° orbit with a nominal lifetime of 4 years, is designed to detect mean surface-height changes to better than 10 mm/yr; an accuracy of a few mm/yr in mean height change over large areas probably will be attained. An accuracy of 3 mm/yr, combined with the satellite gravity measurements, would make it possible to calculate the contribution of the ice sheet to sea-level change at the 0.1 mm/yr level. Neither satellite gravity nor satellite laser altimetry has that capability alone—the two types of measurement are strongly complementary. (The laser altimeter measurements are subject to most of the same uncertainties about causes as the gravity measurements, but with different sensitivities. Without better knowledge of the isostatic-rebound and snowfall-variation effects, such as could be obtained using satellite gravity, estimates from laser altimetry of the ice sheet contributions to sea level would probably be on the order of 0.2 mm/yr.)

Drainage Systems Within Ice Sheets

Ice sheets are complex composites of individual drainage systems or basins, some of which are characterized by fast-moving, low-gradient ice streams bordered by slowly flowing ice, some by huge outlet glaciers through peripheral mountain ranges, and some by broad expanses of open sheet flow with only small, local glaciers. Although from a direct societal standpoint the total mass balance of the ice on land is the most relevant quantity to measure, from a glaciological standpoint it is equally important to measure the mass

changes in individual drainage systems within the ice sheets, because they are the basic dynamic units; glaciologists can only learn how to predict future changes in ice-sheet mass balance by understanding the dynamics of these basic units. A complicating factor is that the dynamic behavior of a particular drainage system may be nearly independent of the dynamic behavior of even its nearest neighbors.

The ice sheets are so large that satellite gravity can provide a valuable approach to the study of subdivisions like individual drainage systems as well as entire ice sheets. For example, the mass of ice in the large drainage system that empties into the east side of the Ross Ice Shelf is suspected to have fluctuated dramatically in the past because of unstable dynamic behavior, including a rapid retreat at the end of the last ice age that may even be continuing at present, albeit at a reduced rate. Our gravity model indicates that secular changes in the thickness of this drainage system, which could be as large as 50 mm/yr of water equivalent, could cause a geoid change of up to 0.7 mm/yr over an approximate square of 600 km on a side. Using the method described in Appendix B for determining the resolving power of the different generic missions, we conclude that a 5-year SST mission flying at an altitude of 400 km could determine the secular change in ice thickness in this region to an accuracy of about 4 mm/yr. The determination of secular changes in the masses of this and other large drainage systems would allow models of ice-sheet dynamics to be tested.

Unfortunately, the same problems arise with the interpretation of gravity changes over a drainage system as with the interpretation of changes over the encompassing ice sheet as a whole, and the same approaches to alleviating those problems mostly apply. There is a special situation to note with respect to isostatic rebound, however. Isostatic rebound models, such as those based on the ICE4G model of Peltier (1994), that incorporate the results of analyses of ice-sheet dynamics, show an isostatic rebound rate on the east side of the Ross Ice Shelf in West Antarctica that is much greater than the Antarctic average because of the major modeled ice-sheet retreat there at the end of the last ice age. Modeled rebound rates greater than 10 mm/yr extend widely and the maximum rate is over 15 mm/yr. It is no coincidence that the highest modeled uplift rates are focused on the regions where the greatest likelihood of rapid change from a glaciological perspective exists today—it is the same high glaciological sensitivity of concern today that presumably led to large changes in ice mass in these areas in the past. As a 15 mm/yr rebound rate is gravitationally equivalent to an ice-thickness change of about 60 mm/yr, even a large glaciological imbalance could be obscured by ongoing isostatic uplift.

Fortunately, the Transantarctic Mountains cut through the regions showing large modeled uplift rates, so GPS surveys in those mountains of the type recommended above would provide an excellent check on the models. Furthermore, because the rates of change that might be attributed to either changing ice mass or isostatic rebound are so large, this region is particularly well suited to testing by comparing results from a gravity satellite with those from a satellite-borne laser altimeter.

Contributions from Glaciers

Satellite gravity could also be used to study secular, interannual, and seasonal changes in the mass balance of ice and snow in regions characterized by a concentration of a large number of glaciers and ice caps. These systems are important for inferring sea-level change because, even though their masses are much smaller than those of the ice sheets, they are capable of much more rapid response to climate change. Consequently, they may at present be contributing at least as much to sea-level change as the ice sheets (cf. Table 7.1).

An example of a large glacial system that could change sufficiently in mass to be detected by a gravity satellite is the system of glaciers that runs from the Kenai Peninsula in southern Alaska down along the Coastal Ranges of the Yukon and British Columbia. This region is characterized by unusually heavy snowfall, particularly in the winter; field observations suggest that the thickness of the glaciers varies annually with an amplitude of about 2.5 m water equivalent (Meier, 1984). This would produce a geoid signal that varies annually by as much as 20 mm over the region (an area equivalent to a square about 300 km on a side) (Figure 1.2). For comparison, we estimate from Figure B.2 that a 5-year SST mission at 400-km altitude could resolve such a system to an accuracy of about 0.5 m of water (about 1/5 of the total effect). For the nominal SSI mission, the accuracy is much better—about 5 mm (see Appendix B for a description of how these accuracies were estimated). The secular trend in this system could total about 0.4 m/yr of water equivalent (Meier, 1984), causing a geoid perturbation with an amplitude of 2-3 mm/yr over the same 300-km spatial scale. This could be resolvable with a 5-year, 400-km altitude SST mission to an accuracy of about 20 cm/yr water equiv

alent, which is good enough to be useful for constraining the secular trend. For the SSI mission, the accuracy becomes 2 mm/yr. Although this glacier system is likely to have the largest annually-varying signal of any system around the world, there are other large glacier systems that could have comparable secular effects.

These estimates for the detection of the seasonal changes in glaciers are somewhat misleading, because there is also a large wintertime snowfall on the surrounding non-glaciated region and there is no good way of knowing what proportion of the seasonal signal to attribute to snow on the glaciers. A gravity mission would provide the total seasonal signal over the entire glaciated and non-glaciated region, which would help constrain estimates of the seasonal snowfall in the region. (Seasonal snow is not a problem on ice sheets because the area of exposed land is so small compared with the area of the ice sheet.)

CONCLUSIONS

1. The sources of global sea-level rise (measured by tide gauges to be between 1.0 and 2.5 mm/yr over the last century) are not well understood. Most of the likely mechanisms involve mass redistribution from the continents to the oceans; gravity measurements can give unique insights through the continual monitoring of geoid changes, not only on global scales, but also on regional and basin scales. From an SST type mission (5-yr mission assumed), accuracy of perhaps a tenth of a mm/yr is attainable.
2. The measurement and interpretation of changes in Greenland and Antarctica is a complex issue, given the complex nature of the phenomena involved: secular changes in ice-sheet mass, post-glacial rebound, interannual variability in snowfall, and the effect of atmospheric pressure trends.

(a) Post-glacial rebound could be partly separated from ice changes using a network of GPS receivers on the land surface, numerical models of rebound that use improved determinations of mantle viscosity provided by the gravity mission, and comparisons with satellite laser altimetry.
(b) Separation of interannual mass changes from true secular changes will be aided greatly by the continually improving calculations of mass input to the ice-sheet surfaces from measurements of moisture-flux divergence around the perimeters of the ice sheets.
(c) The removal of pressure effects over Antarctica will become more effective as the number of automatic weather stations in the interior of the continent increases.
(d) Gravity measurements would be most effective in combination with the observations planned for NASA's Laser Altimeter Mission. Together, an accuracy of 0.1 mm/yr in the determination of the contribution of the ice sheets to sea-level change should be attainable.

3. Satellite gravity measurements are capable of yielding valuable information about the mass balance of individual drainage systems within the Antarctic ice sheet, as well as of the ice sheet as a whole. Glaciologists could use such information to test models of ice dynamics, which are essential to the prediction of future sea-level change.
4. Satellite gravity could be used to study secular, interannual, and seasonal changes in the mass balance of ice and snow in regions characterized by a concentration of a large number of glaciers and ice caps. A prime example is the glacier system that runs from the Kenai Peninsula in southern Alaska down to the coastal ranges of the Yukon and British Columbia.
5. The need for long time series strongly favors SST- or SSI-type missions. SGG missions do not have enough accuracy at low degrees, nor do they have sufficient mission length.

8

The Dynamic Atmosphere: Unraveling the Contributions of the Earth's Subsystems

The mass of the atmosphere is only about 10^{-6} that of the Earth, so the atmosphere's contributions to the Earth's static gravity field, although observable, are much smaller than those from the solid Earth. The atmosphere, though, is highly mobile. Cyclones and atmospheric tides cause the mass of the atmospheric column to vary by 1 to 10%. Consequently, gravity measurements at an accuracy 10^{-8} or better will contain an atmospheric signal. Indeed, the atmosphere contributes a significant fraction of the Earth's total time-dependent gravity field and is one of the largest sources of time-dependent signal at periods of about 1 year and less.

The importance of the atmospheric signal at a period of one year can be seen from the degree amplitude results shown in Figure 8.1. These have been estimated from ECMWF analyses and are shown superimposed on the satellite errors for a 5-year solution. The atmospheric signal is one of the larger annually-varying signals we have considered (cf. Figure 4.5)—it rises above the SST and SSI errors up to degrees of 28 and >40, respectively. In fact, the annually-varying atmospheric gravity signal has already been identified in the lowest-degree zonal gravity coefficients using satellite laser ranging to LAGEOS (Figure 8.2) (e.g., Yoder et al., 1983; Chao and Au, 1991; Nerem et al., 1993a, b; Gegout and Cazenave, 1993; Chao and Eanes, 1995; Dong et al., 1996).

Because the atmospheric signal is so large, it is a potential source of error when using satellite gravity to learn about other processes. This has been discussed in general in Chapter 1 and has been further addressed for each relevant geophysical application in later chapters. In summary, uncertainties in atmospheric pressure data used to remove the atmospheric signal from the gravity estimates are large enough that they could sometimes be the dominant error source for hydrological or glaciological estimates. They are usually not apt, however, to limit seriously the scientific value of those estimates.

Because the uncorrected atmospheric effects are a large time-dependent signal in the gravity data, it is of interest to understand the origin of the atmospheric signal in its own right. Accordingly, in the remainder of the chapter we describe the general characteristics of the atmospheric pressure field.

The global mean surface pressure is close to 984.5 mbar (Trenberth and Guillemot, 1994) and has an annual cycle of about 0.45 mbar (Trenberth 1981; Van den Dool et al., 1995), with a maximum in July that is caused by variable atmospheric water loading (Chen et al., 1996). By differencing the July and January climatologies, one can derive the peak-to-peak magnitude of the annual cycle (Figure 8.3). At least three redistributions of atmospheric mass can be identified: (1) between land and ocean, (2) between the

Southern and Northern Hemispheres, and (3) between high elevations, such as the Tibetan Plateau, and lower elevations. These mass variations are caused by differential heating of the Northern and Southern Hemispheres and the land and the ocean (Van den Dool and Saha, 1993; Saha et al., 1994) and, as such, they are the mass counterparts of the monsoons. The mass redistributions are sufficiently large, both in terms of the pressure difference (20 mbar = ~200 mm of water) and the spatial scale, and they move sufficiently slowly to be detectable from space.

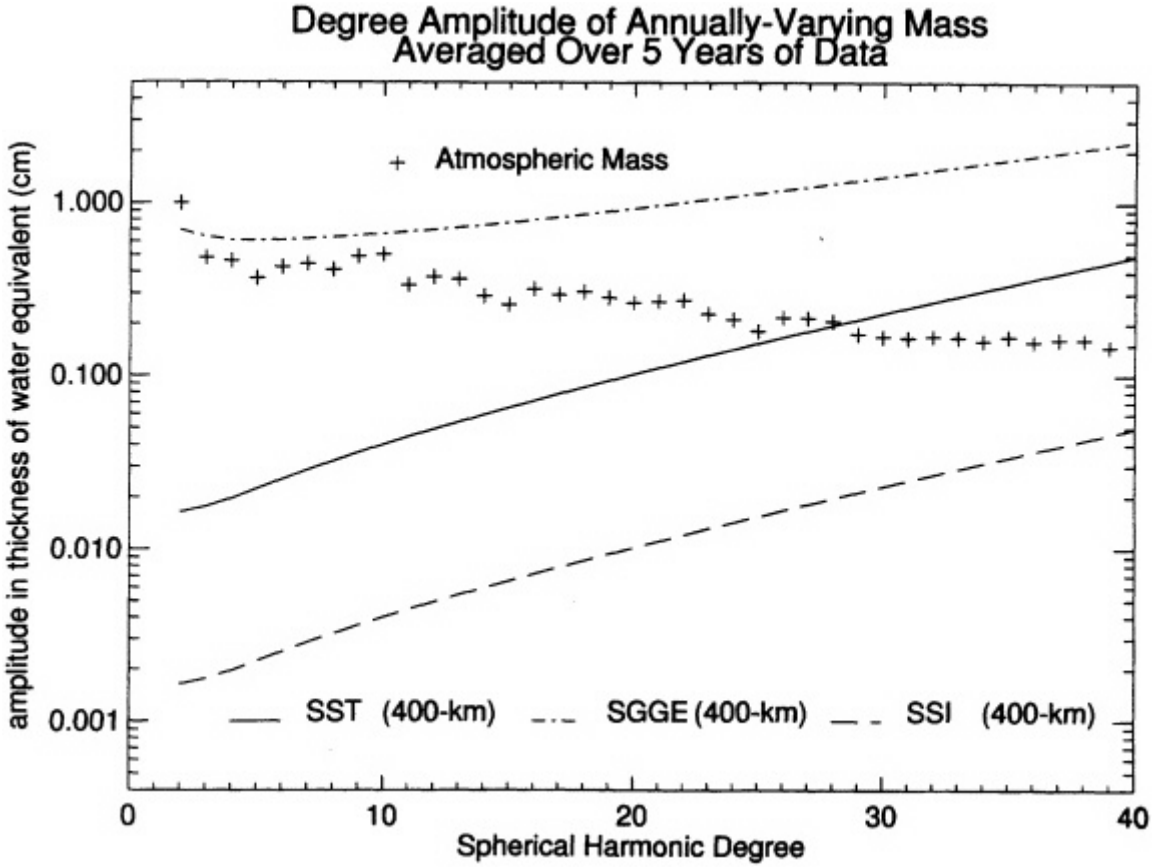

FIGURE 8.1
The degree amplitudes in mass, expressed as the thickness of a water layer, for the annually-varying terms in the atmosphere. The atmospheric results are inferred from ECMWF pressure data from 1992-1993. The results for the satellite errors assume a 5-year satellite mission. The units on the y-axis are approximately equivalent to mbar of pressure.

Other prominent regular features in the atmosphere are the diurnal and semi-diurnal solar tides. The departure of the surface pressure from the daily mean at a specific universal time is an expression of propagating tides (Figure 8.4). The tides are up to 2.5 mbar but exhibit both regular changes (April and October appear to have the strongest tides) and irregular changes. Although the tides move too quickly to be observed directly by gravity measurements, they are an important source of noise and, through their near-resonances with some orbits, can produce long-period (observable) perturbations to orbital elements. In Sun-synchronous measurement systems like the proposed gravity missions, it is important to know how the tides alias into lower frequencies.

Figures 8.3 and 8.4 display "climatology" or normal variations. Departures from normal variations can be large (up to about 50 mbar) and can occur over a wide spectrum of temporal and spatial scales, particularly at high and mid-latitudes (Figure 8.5). These anomalies drift around, decay, develop, and merge, usually with a slight net eastward phase speed at mid-latitudes, and a net westward phase speed at low lati

tudes. This is a reflection of the chaotic nature of weather. Some anomalies are quasi-persistent, existing for weeks or months. Surface pressure anomalies in the tropics are small (a few mbar)—exceptions include hurricanes, which cause pressure anomalies of up to 100 mbar for a short time.

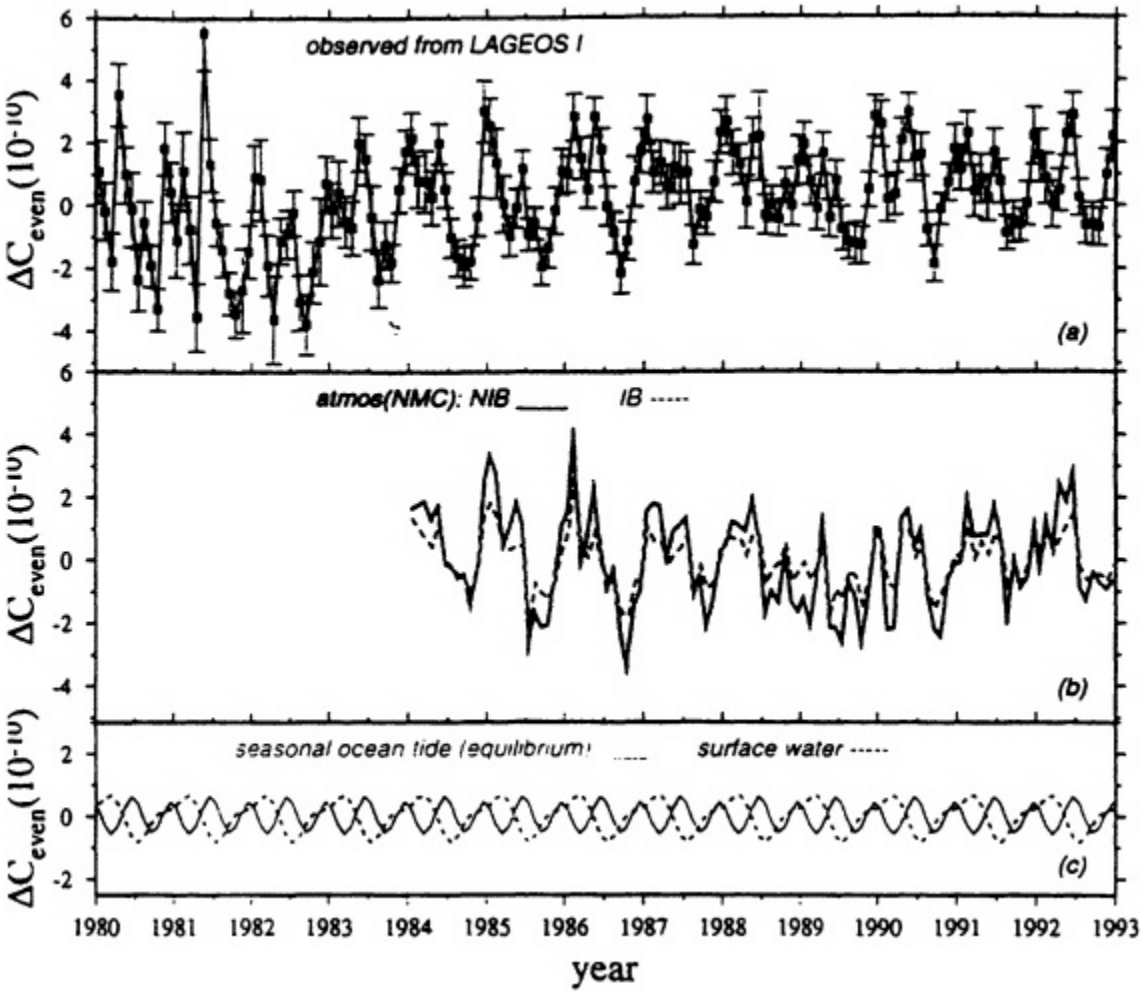

FIGURE 8.2
(a) Monthly Ceven (even zonal harmonics of the Earth's gravity field) series spanning 1980-1992 recovered from LAGEOS I satellite laser ranging data (the mean value has been removed). The error bars represent a I sigma uncertainty.
(b) Monthly Ceven calculated from NMC (1984-1992) atmospheric surface pressure data using the same linear combination of the spherical harmonic coefficients to which the observations are sensitive. Solid line: NIB model; dashed line: IB model.
(c) Monthly Ceven calculated from an equilibrium seasonal ocean tide model (solid line) and the surface water (dashed line) results of Chao and O'Connor (1988). Figure from Dong et al. (1996).

There are many atmospheric phenomena that cause variations in pressure—Table 8.1 lists those that will likely be sensed by a gravity satellite. The list is not exhaustive and does not include phenomena that are unlikely to significantly influence gravity. For purposes of modeling, each phenomenon is presented in terms of a spatially-isolated mass anomaly, with its characteristic diameter on the Earth's surface, magnitude (in mbars of surface pressure), and typical lifetime and speed. These specifications were used to generate the atmospheric curves in Figure 1.2.

The geographic structure of, and dynamical mechanisms responsible for much of the atmospheric contribution to time-dependent gravitational anomalies have not yet been fully explored. A possible source for these effects on seasonal time scales, for example, might be the Indian monsoon system, which involves large mass transfers between the Asian continent and

surrounding ocean areas, capable of inducing significant local gravity anomalies. While concomitant atmospheric pressure perturbations over the oceans would be redistributed more or less uniformly by the inverted barometer effect (see Chapter 4), the large land-ocean mass flux involved in this and other seasonal phenomena may be capable of inducing an average pressure change over the surface of the world oceans that could have a significant impact on the global gravitational field.

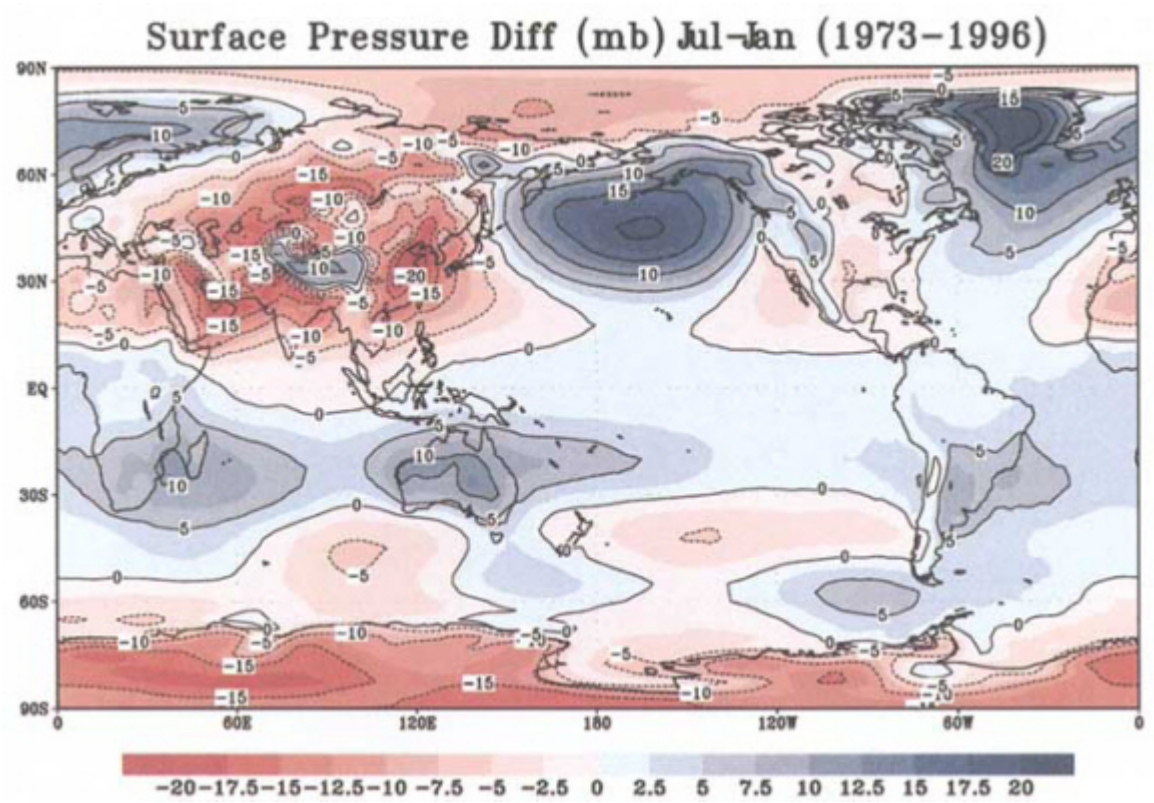

FIGURE 8.3
The difference between the surface pressure climatologies for July and January, showing the peak-to-peak variation due to the atmospheric annual cycle in mass. Contour interval is 5 mbar. Blue values are positive, red values are negative. The climatology is a multi-year average for the month in question, based on recent reanalysis at NCEP (Kalnay et al., 1996).

On short time scales, intraseasonal variability includes the important effects of cold (blocking) outbreaks over mid-latitude continents (cf. Figure 1.2), and the effects of the eastward-propagating surface pressure waves associated with the tropical Madden-Julian Oscillation. At interannual time scales the El Niño-Southern Oscillation (ENSO) phenomenon dominates global-scale atmospheric variability, with concomitant meridional redistribution of atmospheric wind and mass fields (e.g., Dickey et al., 1992; Mo et al., 1997).

The detection of atmospheric gravitational effects is not likely to be an important goal of time-dependent gravity studies because of the continued generation of high-quality pressure fields by meteorological forecast centers. Although it is possible that satellite gravity constraints on atmospheric pressure over data sparse regions (e.g., parts of the Southern Hemisphere such as Antarctica) could provide results that are more accurate than those available from meteorological analyses and that such results could be used as a proxy data type in reanalysis efforts (e.g., Kalnay et al., 1996), extending barometric networks on the surface would most likely provide the best return on available resources (see Chapter 7).

The better recovery of certain non-atmospheric signals could also greatly enhance atmospheric modeling capabilities. Particularly promising are the hydro

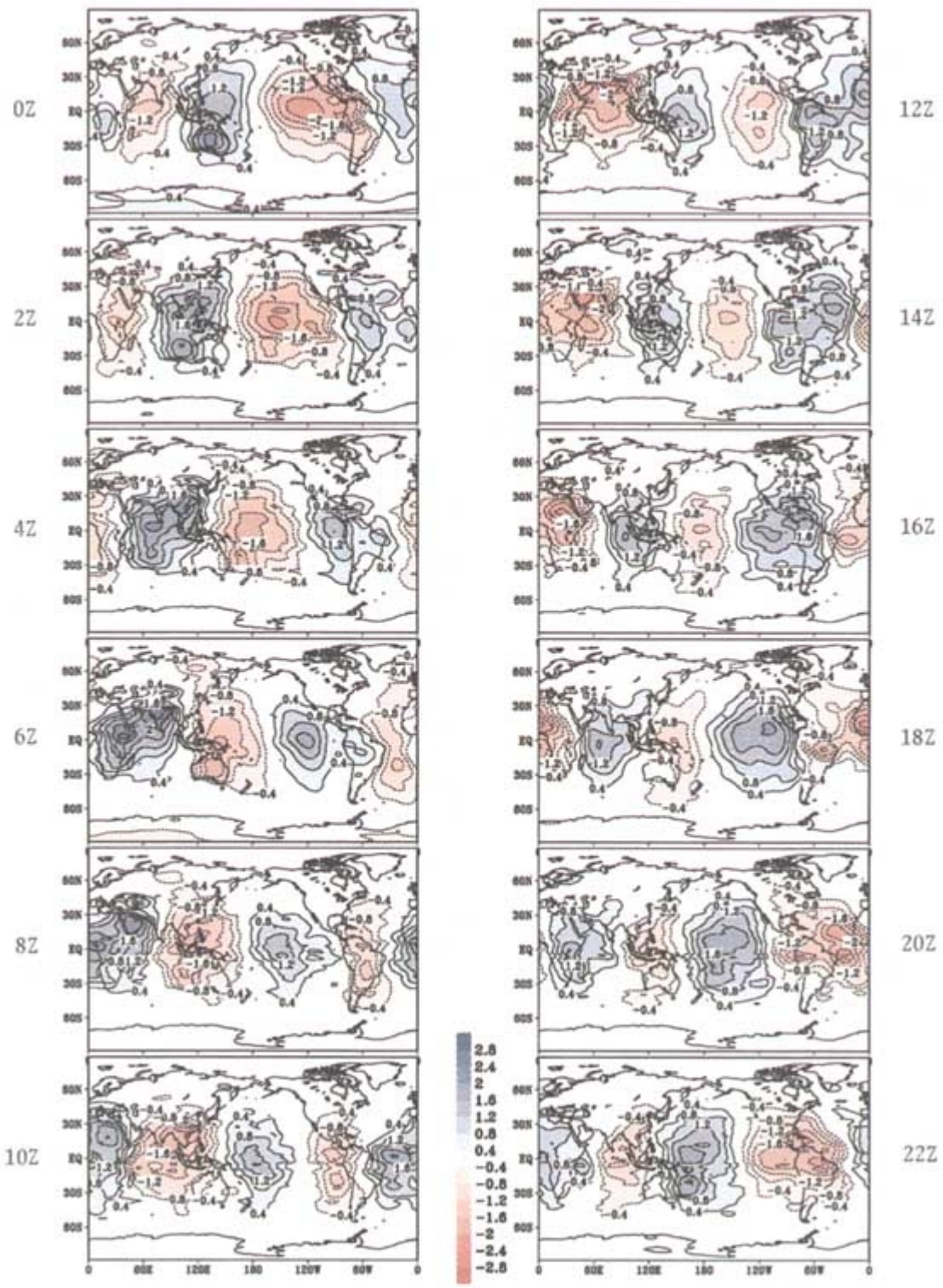

FIGURE 8.4
The climatological daily cycle in surface pressure for the month of January, showing the westward motion of atmospheric tides. Contour interval is 0.4 mbar (no zero line). Red is negative and blue is positive. Each panel shows the surface pressure at a given time of day minus the daily mean. Based on recent reanalysis at NCEP (Kalnay et al., 1996). The reanalysis output at 0, 6, 12 and 18Z has been interpolated as in Van den Dool et al. (1996).

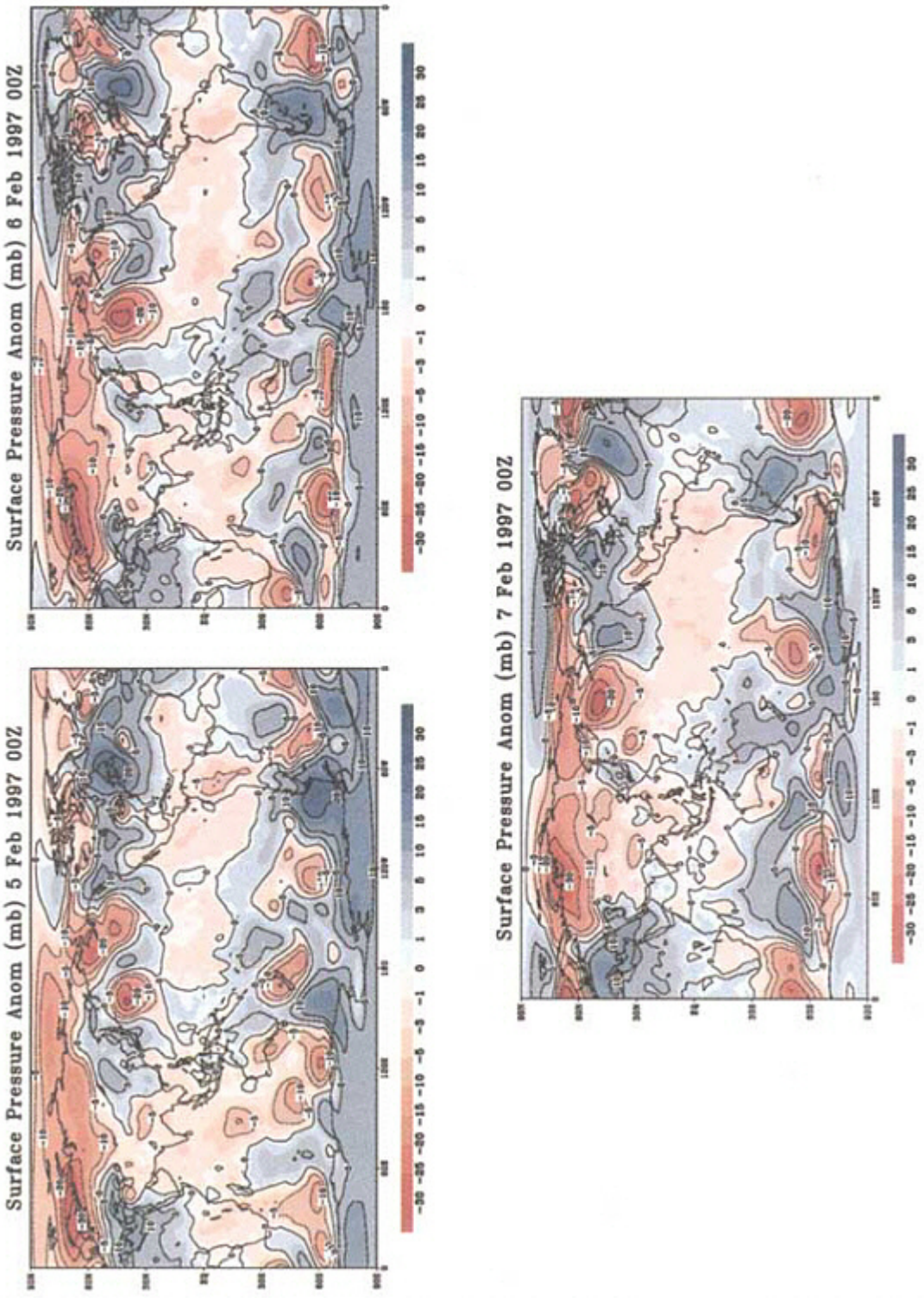

FIGURE 8.5
The surface pressure minus the February climatology on three successive days (OZ only) in February 1997, showing the irregular weather con atmospheric mass variations. Figure calculated according to real-time NCEP analyses. Contour interval is 5 mbar. Red is negative and blue is positive.

TABLE 8.1 Weather and Climate Phenomena, Expressed as Anomaly Mass Discs, that Likely have a Bearing on Temporal Gravity Variations.

Feature	Diameter (km)	Magnitude	Time scale	Motion
Mid-latitude cyclone	500-2,000	10-50 mbar	≤10 days	≤20 m/s irregular
Mid-latitude anticyclone	1,000-3,000	10-40 mbar	≤15 days	≤10 m/s
Atmospheric blocks	2,000-3,000	20-30 mbar	10-50 days	little at high mid-latitude, often a cutoff low on equatorward side
30-60 waves or Madden-Julian tropical oscillation	5,000-10,000	<10 mbar		5-10 m/s
Precipitation events[1]	100-500	0.1-10 cm per event	hours if runoff, weeks if slow evaporation, melting	after deposition: virtually no motion
Atmospheric tides	10,000	≤2 mbar	daily, regular	one revolution around the Earth in a day
Annual cycle 1 (air shuttle between land and sea, monsoon)	10,000	10 mbar	365 days	none, standing-type oscillation
Annual cycle 2 (air shuttle from Northern to Southern Hemisphere)	40,000	2 mbar	365 days	none, standing oscillation
Annual cycle 3 (air shuttle from high to low terrain and back a half year later)	3,500	few to 10 mbar	365 days	none
Southern Oscillation	5,000-10,000	a few mbar	months to years	none, seesaw of mass between tropical Indian Ocean and Pacific
North Atlantic Oscillation	3,000-8,000	≥10 mbar	days to years	none, seesaw of mass between Iceland low and Azores high.
Pacific North American pattern	3,000-6,000	≥10 mbar	days to months (weaker power out to years)	none[2]

[1] The accumulated effect of several events may have larger diameters (approximately 1/4 of United States) and longer time scales (months).
[2] Chain of mass anomaly centers over the Pacific and North America; adjacent centers are opposite in sign.

logical applications described in Chapter 6. Reliable, extended-range forecasting and simulation is possible only through interactive coupling to water conditions in soils and the ocean. To the extent that a gravity mission improves models for the hydrosphere, therefore, meteorology will benefit in turn.

CONCLUSIONS

1. Knowledge of atmospheric variations is vital to unraveling the effects of the other subsystems (such as the hydrological cycle) involved in gravity variations. With increasing accuracy in gravity measurement, precise knowledge of the uncertainty in atmospheric surface pressure at seasonal, annual, and secular time scales becomes increasingly important
2. Reliable, extended-range forecasting, which would require interactive coupling between the atmosphere and the water in soils and the ocean, would benefit from the hydrological constraints discussed in Chapter 6.
3. Satellite gravity measurements with high temporal and spatial resolution may improve the atmospheric databases and models both as a proxy data type and for verification in areas where atmospheric measurements are lacking and water levels are constant It would be more effective, however, to have a global network of barometers, sufficient to remove the atmospheric signals from the gravity data.

9

Conclusions

The Earth's gravity field provides a record of the mass distribution within the system and can be used to understand the evolution and dynamics needed to maintain that distribution. For the fluid portions of the Earth, gravity measurements can be used to sense directly the motions of mass within the system. The inversion of the gravity signals to obtain the mass distribution and the dynamics that cause them is not a straightforward problem, but through a combination of spatial and temporal analyses, knowledge of the gravity field and its temporal variations can provide insights into the processes that control these dynamics. The reliability of these inferences depends on the accuracy, spatial resolution, temporal resolution, and duration of the gravity measurements. Within this report, we have summarized the expected performance for a series of generic, space-spaced, gravity-measurement missions and the expected signals that are likely to exist in the Earth's gravity field.

The generic missions fall into two basic classes: spaceborne gravity gradiometry (SGG) and satellite-to-satellite tracking (SST and SSI). The SGG class missions accentuate the high-spatial-frequency variations in the Earth's gravity field by making measurements of gradients in gravitational acceleration over very short distances (typically a few centimeters). To achieve the accuracy needed, current gradiometer technology requires cooling to very low temperatures to minimize thermal noise, so an SGG satellite will need to be equipped with a helium dewar. The loss of helium from the dewar limits the duration of this class of missions to less than one year, although improved miniaturization and cryogenic techniques may permit extended missions in the future (SGGE). The SST and SSI missions, which measure the differential accelerations between satellites separated by several hundred kilometers, are more sensitive to longer-wavelength features in the gravity field and do not need to be super-cooled. To meet accuracy requirements at shorter wavelength, both satellites need to be flown at a low altitude. A feature common to all these systems is that tracking Global Positioning Satellites (GPS) from the orbiting vehicle is feasible and inexpensive. The technology exists currently to fly the SGG and SST missions. Future technology using laser interferometry offers the potential for the development of the SSI mission, with its order-of-magnitude improvement in performance over the microwave differential tracking of the SST. In the remainder of this chapter, however, we will limit our attention to the two currently available technologies.

Both the SGG and SST missions would significantly improve our knowledge of the Earth's gravity for wavelengths longer than 200-300 km, depending on the altitude of the mission; the lowest-altitude missions (300 km) provide the shortest-wavelength resolution. Almost independent of altitude (within the 300500 km range), the SGG mission provides better results than SST for wavelengths shorter than 300 km. For long-wavelength signals (2,000 km), SST is expected to improve our knowledge of the gravity field by approximately 3 orders of magnitude, whereas the

SGG mission provides improvement by a factor of about 30 over current knowledge.

A long-duration mission (5 years) would enable temporal variations in the Earth's gravity field to be measured during a single mission. For example, at wavelengths of 2,000 km, the SST mission could provide measurements of changes in the gravity field of 10^{-4}-10^{-5} mGal every 90 days. Successive snap shots of the Earth's gravity field could also be measured with a series of SGG class missions.

The gravity missions provide a means of studying a series of geophysical problems ranging from deep Earth structure to tracking mass redistribution on and near the surface of the Earth. Fields of study that would be significantly advanced by a dedicated gravity mission include oceanic dynamic topography and seafloor pressure variations, sea-level rise (separation of steric and nonsteric contributions), ice-sheet mass change (glacial waxing and waning of Antarctica and Greenland), continental water storage, and post-glacial rebound. Knowledge of the static portion of the field also provides a reference frame that can be used to provide absolute dynamic topography of the oceans and to re-calibrate terrestrial, marine, and airborne gravity surveys, thus providing higher spatial resolution in selected locations than obtainable purely from space-based gravity measurements. With any of the generic missions, it is expected that oceanographic currents on basin scales (>1,000 km) and on the scale of the Antarctic Circumpolar Current (500-1,000 km) can be resolved accurately, whereas the measurement of processes on the scale of the western boundary currents (50-100 km) will not be significantly improved. However, knowledge of the latter could be improved by accurate registration of ship gravity data in these regions.

Tracking mass redistribution on or near the surface of the Earth should be possible with the SST class missions. The sensitivity of the measurements should be such that changes in mass equivalent to 10 mm of water over an area of 500,000 km^2 could be measured monthly. Annual signals of this size could be measured in areas about half this size. Some specific applications of these measurements would be: monitoring the secular change in the High Plains aquifer, global monitoring of soil moisture, which could provide a world wide inventory of the yield potential of agricultural lands; and studying evapotranspiration on large spatial scales. These measurements would also provide a means for monitoring the total mass of the world's continental ice sheets and the effects of their changes on global sea level. In a 5-year mission, SST should be able to resolve whether the masses of the Greenland and Antarctic ice sheets are increasing or decreasing—even that basic fact is not currently known. In general, SST will have sufficient spatial resolution to isolate the regions where change is occurring, but the exact process causing the change will not be identifiable from gravity alone. Ancillary data and synthesis of the gravity data into models of processes will be needed to exploit fully the information contained in the gravity field.

Satellite gravity measurements can provide unprecedented views of the Earth's gravity field and, given sufficient duration, its changes with time. Not only can they provide a truly global integrated view of the Earth, they have, at the same time, sufficient spatial resolution to aid in the study of individual regions of the Earth. In many cases, the gravity data will be exploited best by assimilating them, together with other geophysical data, into geophysical models of known processes. Examples of processes that require ancillary data to better interpret the gravity data are structure and evolution of the mantle and plumes, structure and evolution of the crust and lithosphere (including regional deformation of the seafloor and continents, structure of passive margins, and the continent-ocean transition), and ice-sheet mass balance.

Afterword

As this report was entering review, NASA announced plans to fly the Gravity Recovery and Climate Experiment (GRACE), a three- to five-year gravity mission that is very similar to the generic SST mission described in this report. The satellites are scheduled to be launched in 2001.

Appendix A

Spherical Harmonics: Degree Variances, Wavelengths, Upward Continuation, Anomalous Potentials, Signal and Error Spectra, and Gaussian Averages

A.1 SPHERICAL HARMONIC EXPANSIONS OF GRAVITATIONAL POTENTIALS

In geodesy, the Earth's gravitational field is commonly expressed as an expansion in spherical harmonic functions. These functions arise when Laplace's equation (the fundamental differential equation of gravity) is solved in spherical coordinates. Gravitational potentials satisfy Laplace's equation in regions of free space, that is, where densities are zero; thus the spherical harmonic expansion of the Earth's gravity field is a useful device for describing the field outside the Earth, such as is felt by orbiting satellites. (One assumes that the entire mass of the atmosphere lies below the satellite for this purpose.)

The derivation of the spherical harmonics can be found in many books (e.g., Heiskanen and Moritz, 1967; MacRobert, 1967; Jackson, 1975; Sansone, 1991), so we merely sketch the pertinent results here. Choose a polar coordinate system with r the radial distance from the origin, θ the angular distance from the ("north") pole (the colatitude), and ϕ the longitude. Let $V(r, \theta, \phi)$ be a gravitational potential satisfying Laplace's equation

$$\frac{1}{r^2}\frac{\partial}{\partial r}\left(r^2\frac{\partial V}{\partial r}\right)+\frac{1}{r^2\sin\theta}\frac{\partial}{\partial\theta}\left(\sin\theta\frac{\partial V}{\partial\theta}\right)+\frac{1}{r^2\sin^2\theta}\frac{\partial^2 V}{\partial\phi^2}=0, \tag{A1}$$

with the boundary conditions that it be finite and single valued for $0 \le \theta \le \pi$, $0 \le \phi \le 2\pi$, and that $V \to 0$ as $r \to \infty$. Define

$$\begin{aligned} F_{m,1}(\phi) &= \cos m\phi \\ F_{m,2}(\phi) &= \sin m\phi \end{aligned} \tag{A2}$$

for non-negative integers m. Define the associated Legendre functions $P_{l,m}(x)$ for integer $l \ge 0$, integer m with $0 \le m \le l$, and x in $-1 \le x \le 1$ by

$$P_{l,m}(x)=\frac{(1-x^2)^{m/2}}{2^l l!}\frac{d^{l+m}}{dx^{l+m}}(x^2-1)^l. \tag{A3}$$

This definition is that of MacRobert (1967); some authors (e.g., Jackson, 1975) include a factor of $(-1)^m$. Define normalization constants $A_{l,m}$ as

$$A_{l,0} = \frac{1}{2l+1}$$

$$A_{l,m} = \frac{1}{2(2l+1)} \frac{(l+m)!}{(l-m)!}, \tag{A4}$$

then the "geodetically normalized surface spherical harmonics" (hereafter, "spherical harmonics") of degree I and order m may be defined as

$$H_{l,m,n}(\theta,\phi) = (A_{l,m})^{-1/2} P_{l,m}(\cos\theta) F_{l,m,n}(\phi), \tag{A5}$$

with n= 1,2 and the understanding that when m = 0, $H_{l,0,1}(\theta, \phi) = (A_{l,o})^{-1/2} P_l(\cos\theta)$ and $H_{l,0,2}$ is not used; thus, for a given l there are $2l + 1$ spherical harmonics. The spherical harmonics so defined form an orthonormal set over the surface of a sphere, which means that

$$\frac{1}{4\pi} \int_0^{2\pi} d\phi \int_0^{\pi} \sin\theta \, d\theta H_{l,m,n} H_{l',m',n'} = \delta_{ll'} \delta_{mm'} \delta_{nn'}. \tag{A6}$$

The set is complete under the inner product norm, so that any function $f(\theta, \phi)$ whose square is integrable over the surface of the unit sphere can be approximated by an expansion in spherical harmonics in such a way that the mean squared error of the infinite series expansion vanishes.

The solid spherical harmonic

$$V_{l,m,n}(r,\theta,\phi) = r^{-(l+1)} H_{l,m,n}(\theta,\phi) \tag{A7}$$

satisfies Laplace's equation (A1) and the boundary conditions, and therefore so also will the sum

$$V(r,\theta,\phi) = \sum_{l=0}^{\infty} \sum_{m=0}^{l} a_{l,m} V_{l,m,1}(r,\theta,\phi) + b_{l,m} V_{l,m,2}(r,\theta,\phi), \tag{A8}$$

where $a_{l,m}, b_{l,m}$ are constant coefficients, provided that the infinite sum converges uniformly and sufficiently rapidly to permit term-by-term differentiation in (A1). For the twice differentiable functions such as V, such convergence has been established. Proofs can be found in Sansone (1991). In writing (A8) $b_{l,o}$ appears, although $H_{l,o,2}$ is not used; this is for convenience of notation. In what follows, such a coefficient should be taken to be zero.

If a gravitational potential is expanded in the form (A8), then the coefficients $a_{l,m}$, $b_{l,m}$ have the rather awkward dimensions of potential per unit length$^{(l+1)}$. In order to avoid this, geodesy uses a scaled version of (A8) which makes the constants dimensionless:

$$V(r,\theta,\phi) = \frac{GM}{r} \left\{ 1 + \sum_{l=2}^{\infty} \left(\frac{a}{r} \right)^l \sum_{m=0}^{l} c_{l,m} H_{l,m,1}(\theta,\phi) + s_{l,m} H_{l,m,2}(\theta,\phi) \right\}. \tag{A9}$$

Here, G is the Newtonian gravitational constant, M is the total mass of the Earth, and a is the equatorial semi-axis of the ellipsoid chosen as the reference shape of the Earth. The sum starts at l = 2 because the degree-one terms are made to vanish by taking the origin at the center of mass of the Earth. The degree

zero term, *GM/r,* is explicitly factored out of the sum; it represents the potential of a spherically symmetric mass distribution. The remaining terms in the sum have coefficients $c_{l,m}, s_{l,m}$ which are dimensionless fractions of the spherically symmetric potential on the surface $r = a$.

A.2 DEGREE VARIANCES

From the above it can be shown that the spherical harmonics $H_{l,m,n}(\theta, \phi)$ have m zeros on meridians in π radians of longitude and l — m zeros on parallels in π radians of colatitude; thus the degree $l \geq 0$ counts the total number of zero crossings in any hemisphere bounded by a meridian plane, while the order $0 \leq m \leq l$ counts how many of those zero crossings are along meridians. The (θ, ϕ) coordinates of a point on the sphere depend on what point has been chosen as the pole ($\theta = 0$) and what half-plane has been chosen as the prime meridian ($\phi = 0$). Therefore, the coefficients in a spherical harmonic expansion of a function depend on the choice of coordinates. However, there is a quantity, σ_l^2, called the "degree variance" and defined by

$$\sigma_l^2 = \sum_{m=0}^{l} (c_{l,m}^2 + s_{l,m}^2), \tag{A10}$$

which is constant for all choices of the coordinate system.

A.3 WAVELENGTH RELATED TO HARMONIC DEGREE

Physical properties that depend on distance but not on direction turn out to depend on 1 but not *m,* for the same reasons that the degree variances depend on 1 but not m. Although the spherical harmonics are functions on a two-dimensional surface, in discussions of isotropic phenomena it is convenient to characterize them by a one-dimensional "wavelength" λ_l. Since $H_{l,m,n}(\theta, \phi)$ has l zeros in π radians, λ_l is taken to be $2\pi a/l$, where a is the semi-major axis of the Earth's reference ellipsoid or an average value for the radius of the Earth. This works out to $\lambda_l \cong (40{,}000 \text{ km})/l$.

A.4 ATTENUATION WITH ALTITUDE

According to Newton's inverse-square law for the gravitational force, gravity fields decay with distance away from their sources. It turns out that this decay is dependent on wavelength, so that for any given distance away from the source, short-wavelength anomalies are attenuated more strongly than long-wavelength anomalies. The amount of attenuation depends on both the wavelength of the anomaly and the distance from the source. If $V^{(a)}(\theta, \phi)$ is the gravitational potential on the surface $r = a$ with coefficients $c_{l,m}$, $s_{l,m}$

$$V^{(a)}(\theta,\phi) = \frac{GM}{a}\left\{1 + \sum_{l=2}^{\infty}\sum_{m=0}^{\infty} c_{l,m} H_{l,m,1}(\theta,\phi) + s_{l,m} H_{l,m,2}(\theta,\phi)\right\}, \tag{A11}$$

then the gravitational potential on the surface $r = a + h$ is

$$V^{(a+h)}(\theta,\phi)=\frac{GM}{a+h}\left\{1+\sum_{l=2}^{\infty}\left(\frac{a}{a+h}\right)^{l}\sum_{m=0}^{\infty}c_{l,m}H_{l,m,1}(\theta,\phi)+s_{l,m}H_{l,m,2}(\theta,\phi)\right\}. \quad \text{(A12)}$$

Thus a satellite orbiting the Earth at an altitude h above the Earth's surface is affected by a constituent of the potential with harmonic degree l less strongly than it would be at the surface, the amplitude being reduced by a factor $[a/(a+h)]^{(l+1)}$. These factors are shown in Figure 2.1. Because of the form of the r dependence in (A9) and the fact that differentiating (A9) introduces a factor 1 /r, the attenuation factor for first derivatives of the potential, such as gravity anomalies, is $[a/(a+h)]^{(l+2)}$, and for second derivatives, such as gravity gradients, it is $[a / (a +h)]^{(l+3)}$. These factors may be approximated by a simpler formula for large harmonic degree l, corresponding to wavelengths $\lambda << a$ (that is, less than a few hundred kilometers): the attenuation factor then is approximately $e^{-2ph/l}$ for both potentials and their derivatives.

The attenuation with altitude has important consequences for satellite gravity missions. A satellite orbiting the Earth at some altitude h above the surface experiences an attenuated version of the gravity field on the surface of the Earth. The measurements made by that satellite must be downward continued (amplified by the reciprocals of the attenuation factors) to produce a gravity field on the surface, and in so doing, measurement errors are amplified. Thus there is a critical wavelength, usually approximately equal to h, such that wavelengths much longer than the critical can be resolved while wavelengths much shorter than the critical cannot.

A.5 ANOMALOUS POTENTIALS AND "KAULA'S RULE"

In this report we are interested in anomalies in the Earth's gravity field and their expansions in spherical harmonics. It is therefore convenient to distinguish several kinds of gravitational potentials. Let V be the potential of the Earth's gravitational attraction, and W be equal to V plus a term accounting for the effect of the Earth's rotation; W is the potential of the field felt by an observer on the surface of the rotating Earth, whereas V is the potential of the field felt by a satellite, that is, not rotating with the Earth. Define a reference ellipsoidal shape with a standard ellipsoidal potential, U, including the effects expected from the Earth's ellipticity and rotation. Then we define the anomalous potential $T= W-U$. This is the potential of the anomalous gravitational attractions, which are those parts of the gravity field not accounted for by the ellipsoidal shape of the Earth or its rotation. Some authors call T the "disturbing potential," rather than the "anomalous potential." We prefer the latter term, because in celestial mechanics the former term is used to denote all terms in V with the exception of GM/r; these terms cause satellite orbits to depart from Keplerian ellipses.

Because of the rotation of the Earth and its ellipsoidal rather than spherical shape, the $c_{2,0}$ coefficients in the spherical harmonic expansions of U, V, and W are of the order 10^{-3}. All the other coefficients are much smaller, of the order 10^{-5} or less. Because this large effect is accounted for in the definition of the reference potential U,the $c_{2,0}$ coefficient in the expansion of the anomalous potential T is as small as the other coefficients. If we form the degree variances σ_l^2 of the coefficients in the expansion of T for the Earth, then we find that σ_l, the square root of the degree variance, has a magnitude approximated by the formula:

$$\frac{\sigma_l}{\sqrt{2l+1}}\approx\frac{10^{-5}}{l^2}. \quad \text{(A13)}$$

This rule of thumb is known as "Kaula's rule" because it was deduced by Kaula (1966) from studies of the covariance of surface gravity anomalies (Kaula, 1959, 1963). It appears in this report as an example

of the expected degree variance spectrum of the static gravity anomaly field, and provides an upper bound on the uncertainties in spherical harmonic coefficients at high degrees. This upper bound is used to estimate the total uncertainty in a gravity or geoid anomaly.

A.6 DEGREE AMPLITUDE SPECTRA

A graph of σ_l^2, versus l is called a "degree variance spectrum," while a graph of σ_l, versus l is called a "degree amplitude spectrum." Several kinds of spectra are shown in this report. Signal spectra represent the amplitude of expected signals in the Earth's gravity field. The static field amplitudes are based on the degree variances of the anomalous potential σ_l^2, and are shown as the expected dimensionless amplitude, σ_l, the expected geoid height anomaly amplitude, $a\sigma_l$,and the expected gravity-anomaly amplitude, $(GM/a^2)(l-1)\,\sigma_l$. We also show error spectra that are analogous quantities derived from the estimated degree variances of the uncertainties in the anomalous potential coefficients expected for various missions or gravity field models.

A.7 ERRORS IN OBSERVABLES RELATED TO ERRORS IN THE GRAVITY FIELD

In Chapter 2 of this report we estimate the resolving power of various satellite gravity missions. Our estimates are obtained under the assumption that the power spectral density (PSD) of the errors in the observable is white and that the orbit distributes the errors isotropically over the surface of a sphere. Under these assumptions, equations given by Jekeli and Rapp (1980) and a chosen mission duration can be used to obtain the degree variances of the observable on a sphere at satellite altitude.

When a random variable is isotropically distributed over the surface of a sphere, the expected covariance between the error at a point P and the error at another point Q depends only on , the angular distance between P and Q, and does not depend on the location of P or the direction from P to Q. In such a case, the relationship between the degree variances of the errors σ_l^2 and the covariance function $C(\psi)$ is

$$C(\psi) = \sum_{l=0}^{\infty} \sigma_l^2 P_l(\cos\psi). \tag{A14}$$

Rummel and van Gelderen (1995) discuss further the properties of isotropic distributions as used in geodesy.

We approximate the SST and SSI missions by assuming the two spacecraft are in the same orbit but separated by an angle δ. The observable is $\dot{R}$,the "range rate," the time derivative of the line-of-sight distance between the two spacecraft. We obtain the degree variances of the σ_l^2 range rate, ($\dot{R}$), by the method of Jekeli and Rapp (1980), and then relate it to the degree spectrum of the gravity potential coefficient errors, σ_l^2, by

$$\sigma_l^2(\dot{R}) = \sigma_l^2\left\{\left(\frac{a}{r}\right)^{2l+1}\left(\frac{GM}{a}\right)[1 - P_l(\cos\delta)]\right\}. \tag{A15}$$

For the error estimates given here we assumed that δ would be two degrees.

An SGG mission will measure second derivatives of the gravity potential at the spacecraft altitude. We approximate the errors in the gravity field obtained in such a mission by assuming that the dominant source of gravity-field error is the error in the second radial derivative of the potential, V_{rr}. We obtain the degree

variances of the radial gravity gradients at satellite altitude, $\sigma_l^2(V_{rr})$, by the method of Jekeli and Rapp (1980), and then relate it to the degree variances of the gravity potential coefficient errors, σ_l^2 by

$$\sigma_l^2(V_{rr}) = \sigma_l^2\left\{\left[(l+1)(l+2)\left(\frac{a}{r}\right)^{l+3}\left(\frac{GM}{a^3}\right)\right]^2\right\}. \tag{A16}$$

A.8 ACCURACY VERSUS RESOLUTION IN GAUSSIAN-WEIGHTED AVERAGES OVER A SPHERICAL CAP

We follow Jekeli (1981) in using a spherical approximation to an isotropic Gaussian convolution filter (weighted average) as follows. Define the weight function

$$w(\psi) = \frac{2\alpha}{1-\exp[-2\alpha]}\exp[-\alpha(1-\cos\psi)], \tag{A17}$$

where again Ψ is the angular distance between two points on the sphere, and α is a positive constant. The leading constant in (A17) normalizes the weight function so that its integral over the surface of a sphere is one. The parameter α is analogous to the reciprocal of the variance in a Gaussian weight function, for when Ψ is small we have

$$\exp[-\alpha(1-\cos\psi)] \approx \exp\left[\frac{-\alpha}{2}\psi^2\right]. \tag{A18}$$

The angle at which the weight function has one half of its maximum amplitude, $\Psi_{1/2}$, is

$$\psi_{1/2} = \cos^{-1}\left[1-\frac{\log 2}{\alpha}\right], \tag{A19}$$

and the resolution length appearing on the horizontal axis of many figures in this report is $\sqrt{\pi}R\Psi_{1/2}$ where R is the mean radius of the Earth. This resolution length is the side of a square having the same area as a spherical cap of radius $\Psi_{1/2}$

In order to form Gaussian-weighted averages from degree variances, we need the Legendre expansion of the weight function. Define β_l by

$$\beta_l = \frac{1}{\sqrt{2l+1}}\int_{-1}^{1}\frac{2\alpha\exp[-\alpha(1-x)]}{1-\exp[-2\alpha]}P_l(x)dx \tag{A20}$$

so that

$$w(\psi) = \sum_{l=0}^{\infty}\beta_l P_l(\cos\psi). \tag{A21}$$

Now, to form the resolution accuracy estimate, let be the degree variances of the errors in the spherical harmonic coefficients of the gravity field. These are adjusted, as explained in Chapter 2, so that if the degree variance of the error from a satellite mission exceeds the degree variance of the signal in the

gravity field, the signal in the gravity field is used instead. The root-mean-square accuracy of the Gaussian-averaged geoid height, $\varepsilon_{\text{geoid}}$, is given by

$$\varepsilon_{geoid} = R\left[\sum_{l=0}^{L}\beta_l^2\sigma_l^2\right]^{1/2}, \tag{A22}$$

and the root-mean-square accuracy of the Gaussian-averaged gravity anomaly, $\varepsilon_{\text{gravity}}$, is given by

$$\varepsilon_{gravity} = \frac{GM}{R^2}\left[\sum_{l=2}^{L}(l-1)^2\beta_l^2\sigma_l^2\right]^{1/2}, \tag{A23}$$

where the sums can be safely truncated at a finite limit L that depends on α. We found that, for the range of resolution lengths considered here, $L = 1900$ was sufficient.

Appendix B

Modeling

RATIONALE

In Chapters 4-8, which describe time-dependent gravity, we discuss a number of geophysical processes and their effects on the geoid. We attempt to assess whether those effects would be detectable with the generic missions described in Chapter 2. In this Appendix we describe the methods and geophysical models used to address these questions.

To determine whether the effects of a geophysical process are large enough to be detected, we first estimate the geoidal perturbation caused by that process. Suppose the process perturbs the gravitational potential at co-latitude θ and longitude ϕ by the amount $\delta V(\theta, \phi)$.The resulting geoid anomaly is given by $N(\theta, \phi)=\delta V(\theta, \phi)/g$, where g is the gravitational acceleration at the Earth's surface and is approximately $g = GM/a^2$. With the notation shown in (Al 1), the geoid perturbation has the form

$$N(\theta,\phi) = a\sum_{l,m}(c_{lm}H_{l,m,1}(\theta,\phi)+s_{lm}H_{l,m,2}(\theta,\phi)), \qquad \text{(B1)}$$

where c_{lm} and s_{lm} are dimensionless coefficients and $H_{l,m,n}$ are defined in (A5).

Once we have computed the c_{lm} and s_{lm} for a specific geophysical process (see B2 below), we construct the degree amplitudes, $a\sqrt{(\sum_m[c_{lm}^2+s_{lm}^2])}$ and compare them against the expected degree amplitude uncertainties described in Chapter 2 above. For several processes (e.g., post-glacial rebound, oceanographic fluctuations, changes in ground and surface water/snow/ice), the degree amplitude of the signal stands well above the degree amplitude uncertainties of generic SST and SSI missions at low degrees, indicating that those processes are readily detectable with those missions.

A degree amplitude comparison, however, is not always the most meaningful way to assess the resolving power of a mission. For example, the effects of processes with well-known spatial patterns could be detected, even though the degree amplitude is smaller than the expected satellite uncertainties. In that case, we can fit the spatial pattern of the geoid to the data to obtain the amplitude. This approach involves expanding the geoid pattern as a sum of spherical harmonics, and then fitting an overall amplitude of that sum to the spherical harmonic coefficients determined from the satellite data. Since the satellite errors for the individual coefficients are likely to be uncorrelated, the formal error for the fitted amplitude tends to

decrease as $1/\sqrt{N}$, where N is the number of coefficients that make important contributions to the spatial pattern.

There are many processes where the spatial pattern can be approximated as a uniform mass change over a surface disc of known radius. In those cases, it is convenient to pose the issue in a somewhat different (though equivalent) form, and ask how well a satellite gravity mission can determine the change in surface mass averaged over the disc. As discussed in Chapter 2 and Appendix A, however, a gravity mission can provide a better result if the averaging kernel is a Gaussian weighting function over the entire Earth, with a full-width half maximum equal to the disc's diameter (rather than equal to 1 across the disc and 0 outside of it).

CALCULATIONS

It is straightforward to calculate the geoid perturbation caused by an arbitrary surface mass distribution with mass/area = $\sigma(\theta, \phi)$. The geoid perturbation is defined as the gravitational potential due to this mass, divided by g (= 9.8 m/s^2; the unperturbed gravitational acceleration at the Earth's surface). By expanding σ into spherical harmonics, finding the gravitational potential from each individual harmonic, and then arranging the result into the form (B1), we obtain

$$c_{lm} + is_{lm} = \frac{3}{4\pi} \frac{(1+k_l)}{(2l+1)a\rho_{ave}} \int_{surface} \sigma(\theta,\phi)(H_{l,m,1}(\theta,\phi) + iH_{l,m,2}(\theta,\phi)) \sin\theta d\theta d\phi, \quad \text{(B2)}$$

where k_l is the load Love number of degree l, ρ_{ave} is the average density of the Earth (5517 kg/m^3), and $i = \sqrt{(-1)}$. The Love number kl is included to represent the instantaneous elastic response of the solid Earth to the applied load. The Earth's non-elastic response, which is not included in (B2), depends on the time history of the load and is important only for loads that change at temporal scales of many centuries and longer. The only such loads considered in this report are large-scale continental ice sheets. The computation of the Earth's visco-elastic response to slow changes in the ice sheets is difficult, and must be done separately.

The result (B2) can be used to estimate degree amplitudes $a\sqrt{(\sum_m [c_{lm}^2 + s_{lm}^2])}$ from an assumed mass distribution, which can then be compared with the expected satellite degree amplitudes. B2 can also be used to construct accuracy-versus-resolution estimates for a surface mass disc. To accomplish this, we expand the surface mass distribution in a form equivalent to the geoid expansion (B1):

$$\sigma(\theta,\phi) = a\rho_w \sum_{l,m} (\hat{c}_{lm} H_{l,m,1}(\theta,\phi) + \hat{s}_{lm} H_{l,m,2}(\theta,\phi)), \quad \text{(B3)}$$

where ρ_w is the density of water (assumed to be 1000 kg/m^3), and is included in (B3) so $\hat{c}_{lm}$ and $\hat{s}_{lm}$ that are dimensionless coefficients describing the spherical harmonic expansion of the surface mass expressed in the thickness of an equivalent mass of water. This is a useful measure of surface mass, because most of the surface processes for which accuracy-versus-resolution results are useful involve changes in water, ice, or snow.

The orthogonality properties of the $H_{l,m,n}$ (see A6) can be used to infer from (B3) that

$$\hat{c}_{lm} + i\hat{s}_{lm} = \frac{1}{4\pi a\rho_w} \int_{surface} \sigma(\theta,\phi)(H_{l,m,1}(\theta,\phi) + iH_{l,m,2}(\theta,\phi)) \sin\theta d\theta d\phi. \quad \text{(B4)}$$

So, by comparing (B4) with (B2), we conclude that

$$\hat{c}_{lm} + i\hat{s}_{lm} = \frac{\rho_{ave}}{3\rho_w}\frac{2l+1}{1+k_l}[c_{lm} + is_{lm}]. \quad \text{(B5)}$$

Equation (B5) can be used to transform geoid expansion coefficients c_{lm} and s_{lm} to mass expansion coefficients, and to construct degree amplitudes of the mass distribution in equivalent water thickness Several figures in the text (e.g., Figures 4.5, 4.6, 7.3, and 8.1) compare the mass degree amplitudes estimated by using assumed mass distributions in (B4), with the expected mass degree amplitudes of the satellite errors, which were computed using (B5) and the estimates of the geoid degree amplitudes described in Chapter 2. These comparisons are fundamentally equivalent to comparisons of the geoid degree amplitudes, and are included above only because the mass anomaly is often of greater direct interest than the geoid when interpreting the observations.

The mass degree amplitudes of the satellite errors can be used to estimate the accuracy-versus-resolution of the generic satellite missions. We use the geoid degree amplitudes described in Chapter 2, transform them to mass degree amplitudes using (B5), and use the results to estimate accuracy-versus-resolution as described in Appendix A, except that here we do not apply the constraint that the degree amplitude error not exceed the EGM96 error, since the EGM96 model does not provide information on the time-dependent gravity field. We do, however, use the GPS degree errors in constructing the SGG and SGGE accuracy-versus-resolution estimates, whenever the GPS degree errors are smaller than the SGG degree errors (see Chapter 2). The results are shown in Figures B.1-B.4. These figures are similar to the results shown in Figures 2.7 and 2.10, except that Figures B.1-B.4 are for surface mass, in water-equivalent thickness.

The degree amplitude and accuracy-versus-resolution results described in Chapter 2 are pertinent to 90-day geoid averages. Many of the time-dependent processes considered in this report are dominated by components that vary on seasonal or longer time scales. We use the 90-day uncertainty estimates to infer uncertainties of annually-varying and secular terms in the geoid by assuming that those terms would be least-squares fitted to the 90-day values. Using our estimates for the co-variance matrix of 90-day values, we can infer the uncertainties we would obtain for each individual temporal term using standard statistical arguments (see, for example, section 15.6 of Press et al., 1992). For example, if we were simultaneously to fit cos (wt), sin(wt), t, and a constant term to N days of data (where w = 1 cycle per year), we would obtain uncertainties for both the cos (wt) and sin(wt) terms equal to $\sigma\sqrt{(2*90/N)}$, where s is the 90-day uncertainty. Our uncertainty for the secular term would be approximately $(\sigma/N)\sqrt{(12/N)}$, in units of σ/day. These transformations are used when estimating the annually-varying and secular components of the satellite degree amplitudes, both for the degree amplitude figures and for the accuracy-versus-resolution figures in the text.

SPECIFIC APPLICATIONS

These accuracy-versus-resolution results are particularly useful for estimating what changes in the thickness of disc-shaped mass anomalies can be resolved. Examples of disc-shaped anomalies considered in this report are the Antarctic drainage into the east side of the Ross Ice Shelf (estimated from Bentley and Giovinetto, 1991); seasonal, interannual, and secular changes in the Antarctic and Greenland ice masses (the non-secular variability was estimated from Bromwich et al., 1993, 1995, and the secular trend was estimated from the IPCC limits described by Warrick et al., 1996); continental glacier systems (ice-thickness changes from Meier, 1984); certain atmospheric processes, such as mid-latitude cyclones and large-scale precipitation events (with temporal and spatial scales taken from Holton, 1979); and individual aquifers and river drainage systems.

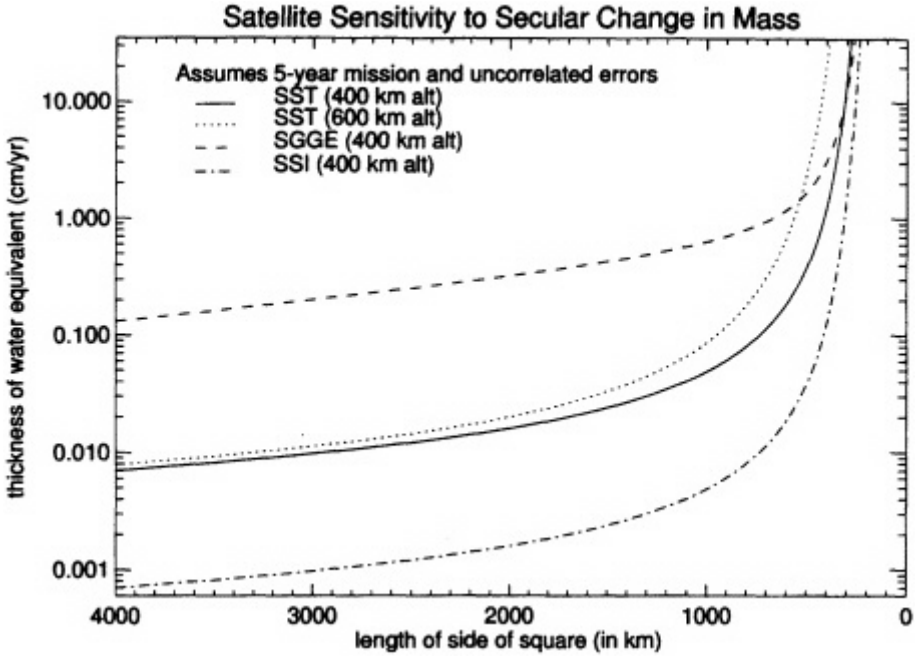

FIGURE B.1
Accuracy versus resolution for secular variations in the thickness of a disc of water, for four generic missions. We assumed a 5-year mission at an altitude of 400 km, which is probably realistic for SST and SSI, but is decidedly too long for an SGG mission, even at 400-km altitude. We denote the extended SGG mission as SGGE. The results here are used throughout the text to estimate the accuracies with which these missions could constrain various geophysical processes.

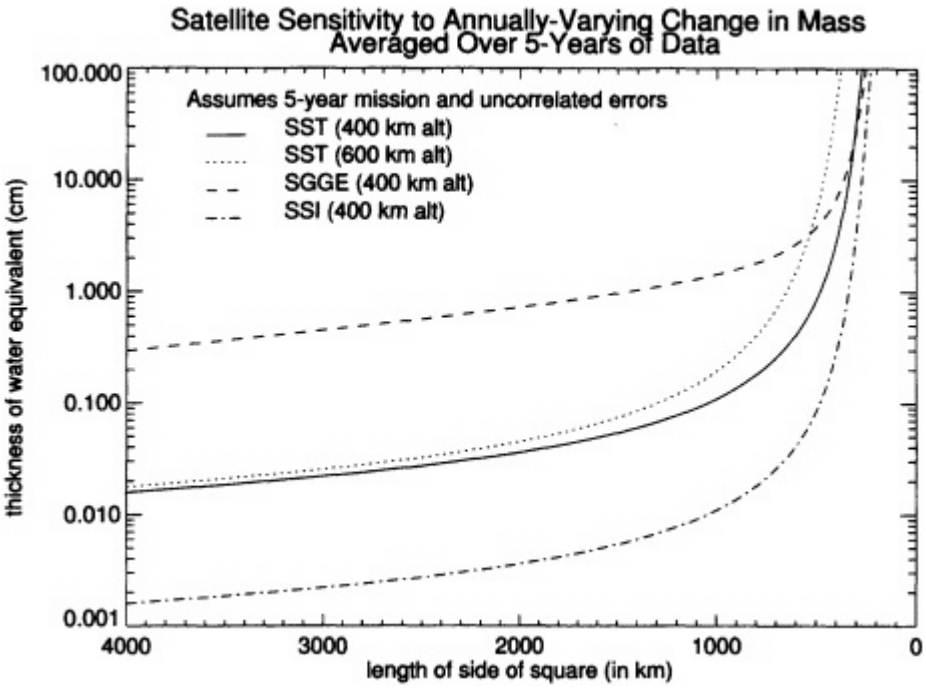

FIGURE B.2
Accuracy versus resolution for an annually-varying change in the thickness of a disc of water, averaged over 5 years, for four generic missions. The mission altitudes and durations are the same as in Figure B.1.

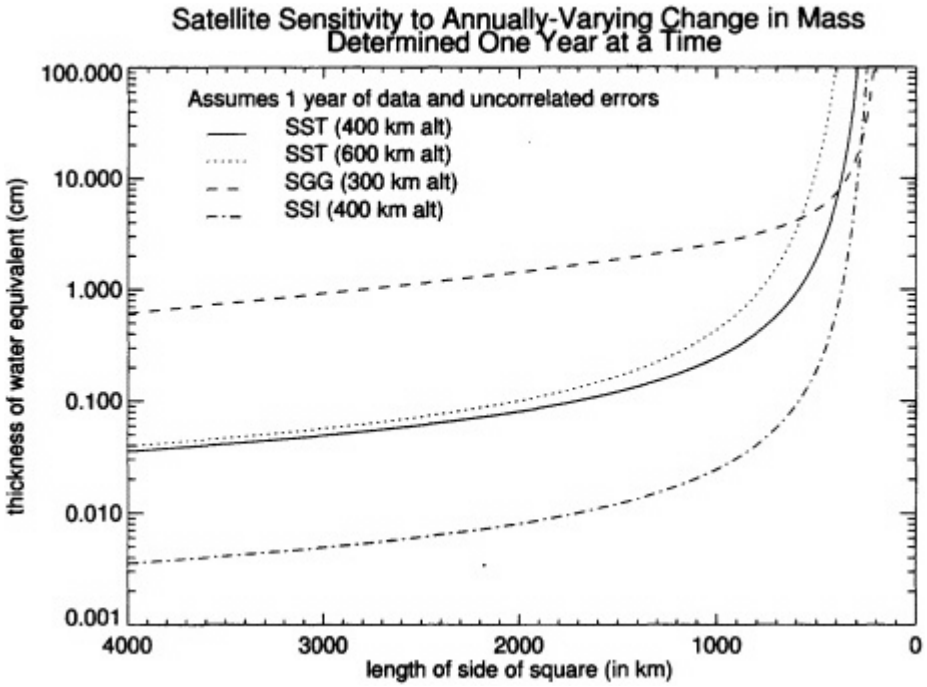

FIGURE B.3
Accuracy versus resolution for an annually-varying change in thickness of a disc of water, averaged over 1 year of data, for four generic missions. We assumed a 1-year mission and a 300-km altitude for SGG, since that is the most probable altitude for such a mission. We also include results for an SST mission at 600-km altitude to demonstrate the effects of an increase in altitude.

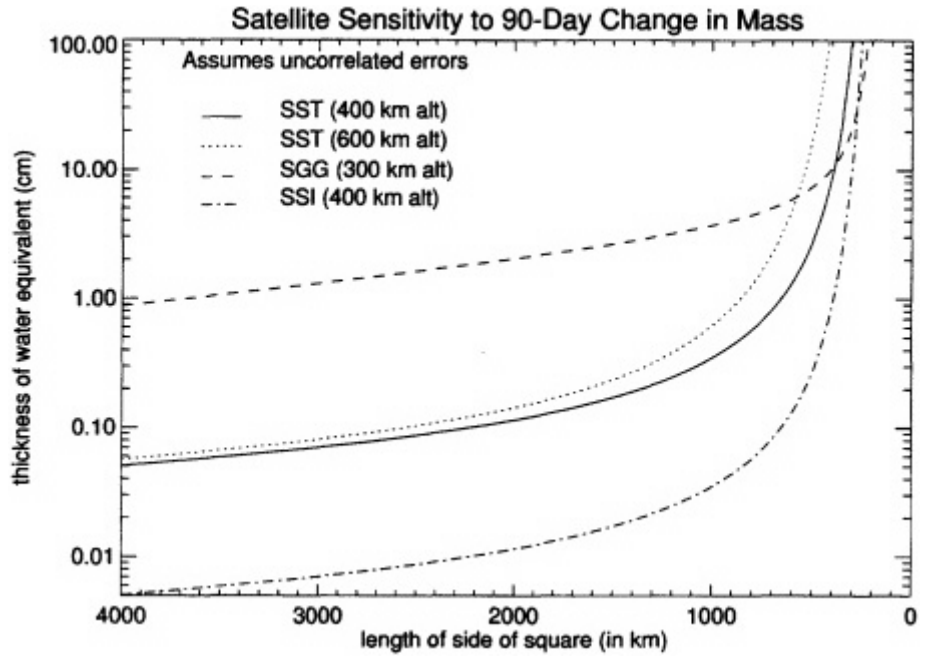

FIGURE B.4
Accuracy versus resolution for each 90-day value of the thickness of a disc of water for four generic missions. The mission altitudes are the same as in Figure B.3, but the values are calculated for a 90-day mission.

On the other hand, several important surface loads have geometries that cannot be characterized as discs. In those cases, we compute the geopotential coefficients by using estimates of the surface mass density as a function of latitude and longitude (i.e., $s(\theta, \phi)$) in (B2). Examples of these processes include global sea-level rise, oceanographic disturbances, atmospheric pressure variations, and continental water storage. The global sea-level rise was computed using the 5-minute topography of ETOPO-5 from Smith (1993) to determine the ocean/continent boundary. Oceanographic disturbances, such as deep ocean circulation, were determined using salinity, temperature, and sea-surface height from the Los Alamos POP general circulation model described by Dukowicz and Smith (1994), with model integration results provided by Frank Bryan at the National Center for Atmospheric Research. The effects of atmospheric pressure variations were calculated using the archived analysis fields of the National Centers for Environmental Prediction (formerly the National Meteorological Center) and ECMWF. Finally, temporal changes in continental water storage were calculated using a global soil-moisture data set from 1979-1993, generated as described by Huang et al. (1996) for a longer time period over the United States alone.

Finally, some processes, such as post-glacial rebound, cannot be represented as surface loads and their effects on the geoid must be modeled separately. Post-glacial rebound was modeled using the ICE-3G Pleistocene ice model of Tushingham and Peltier (1991) and the viscous-load Green's functions of Han and Wahr (1995). The viscous Green's functions were also used to estimate the visco-elastic response of the Earth to possible changes in Antarctic and Greenland ice since the Pleistocene. For example, we assumed that the Antarctic ice sheet has been melting at a steady rate (usually taken to be equivalent to 1 mm/yr of global sea-level rise) from time T in the past, until the present. We constructed a series of such models for different values of T. We then used the visco-elastic decay times and Green's functions from Han and Wahr (1995) to estimate the Earth's present-day visco-elastic response to each of these past changes in ice load. This allowed us to assess the problems of separating the effects of present-day changes in ice from the effects of the Earth's visco-elastic response to past events.

Acronyms

ACC	Antarctic Circumpolar Current
CIGAR	Consortium for Investigation on Gravity Anomaly Recovery
ECMWF	European Centre for Medium-Range Weather Forecasts
EGM96	Earth Geopotential Model (1996)
ENSO	El Niño/Southern Oscillation
ERS-1	European Remote Sensing Satellite-1
ESA	European Space Agency
GCIP	GEWEX Continental-Scale International Project
GCM	General Circulation Model
Geosat	Geodesy Satellite
GEWEX	Global Energy and Water Cycle Experiment
GLONASS	Global Navigation Satellite System
GPS	Global Positioning System
GPS/MET	GPS Meteorology Satellite
IPCC	Intergovernmental Panel on Climate Change
JGM	Joint Gravity Model
LAGEOS	Laser Geodynamics Satellite
NASA	National Aeronautics and Space Administration
NRC	National Research Council
PSD	Power Spectral Density
RMS	Root Mean Square
SAR	Synthetic Aperture Radar
SGG	Spaceborne Gravity Gradiometer
SGGE	Spaceborne Gravity Gradiometer Extended
SSI	Satellite to Satellite Interferometry
SST	Satellite to Satellite Tracking
TOPEX	Ocean Topography Experiment
WBC	Western Boundary Current
WOCE	World Ocean Circulation Experiment

References

Aagaard, K., and E.C. Carmack, 1989, The role of sea ice and other fresh water in the Arctic circulation: Journal of Geophysical Research, v. 94(C10), p. 14,485-14,498.

Balmino, G., and J.P. Barriot, 1991, Global recovery of the geopotential from satellite gravity gradiometry: A simulation: Symposium GM2, XXth International Union of Geodesy and Geophysics, General Assembly, Vienna.

Bechtel, T.D., D.W. Forsyth, V.L. Sharpton, and R.A.F. Grieve, 1990, Variations in effective elastic thickness of the North American lithosphere: Nature, v. 343, p. 636-638.

Bechtel, T.D., D.W. Forsyth, and C.J. Swain, 1987, Mechanisms of isostatic compensation in the vicinity of the East African Rift, Kenya: Geophysical Journal of the Royal Astronomical Society, v. 90(2), p. 445-465.

Behrendt, J.C., W.E. LeMasurier, A. Cooper, F. Tessensohn, A. Trehu, and D. Damaske, 1991, The West Antarctic rift system: A review of geophysical investigations: Contributions to Antarctic Research II, Antarctic Research Series, American Geophysical Union, v. 53, p. 67-112.

Bell, RE., and AB. Watts, 1986, Evaluation of the BGM-3 sea gravity meter system onboard R/V Conrad: Geophysics, v. 51(7), p. 1,480-1,493.

Bender, P.L., 1992, Integrated laser doppler method for measuring planetary gravity fields, *in* Colombo, O.L., ed., From Mars to Greenland: Charting Gravity with Space and Airborne Instruments: Springer-Verlag, New York, p. 63-72.

Bentley, C.R., and M.B. Giovinetto, 1991, Mass balance of Antarctica and sea level change, *in* Weller, G., CL. Wilson, and B.A.B. Severin, eds., Role of the Polar Regions in Global Change: Geophysical Institute Publication, University of Alaska, Fairbanks, p. 481-488.

Berner, E.K., and R.A. Berner, 1987, The Global Water Cycle: Geochemistry and Environment: Prentice Hall, Englewood Cliffs, 397 pp.

Bettadpur, S.V., 1993, A simulation study of high degree and order geopotential determination using satellite gravity gradiometry: Ph.D. Dissertation, University of Texas, Austin, 161 pp.

Bettadpur, S.V., and B.D. Tapley, 1996a, Accuracy assessments of dedicated geopotential mapping missions: Supplement to EOS, Transactions of the American Geophysical Union, v. 77(46), p. F140.

Bettadpur, S.V., and B.D. Tapley, 1996b, Assessments of future geopotential mapping missions: Supplement to EOS, Transactions of the American Geophysical Union, v. 77(17), p. S41.

Bills, B.G., and H.-J. Paik, 1996, GEOID mission: Gradiometer views of static and dynamic gravity signals: Supplement to EOS, Transactions of the American Geophysical Union, v. 77(17), p. S40.

Broecker, W.S., and T.-H. Peng, 1982, Tracers in the Sea: Eldigio Press, Palisades, p. 412-439.

Bromwich, D.H., F.M. Robasky, RA. Keen, and J.F. Bolzan, 1993, Modeled variations of precipitation over the Greenland ice sheetJournal of Climate, v. 6(7), p. 1,253-1,268.

Bromwich, D.H., F.M. Robasky, R.I. Cullather, and M.L. Van Woert, 1995, The atmospheric hydrologic cycle over the Southern Ocean and Antarctica from operational numerical analyses: Monthly Weather Review, v. 123(12), p. 3,518-3,538.

Brozena, J.M., 1991, GPS and airborne gravimetry: Recent progress and future plans: Bulletin Geodesique, v. 65(2), p. 116-121.

Calmant, S., and A. Cazenave, 1987, Anomalous elastic thickness of the oceanic lithosphere in the south-central Pacific: Nature, v. 328, p. 236-238.

Carton, J.A., and L. Miller, 1997, Atmosphere/ocean interactions and their role in decadal climate variability in the Atlantic: in preparation.

Cartwright, D.E., R. Spencer, and J.M. Vassie, 1987, Pressure variations on the Atlantic equator: Journal of Geophysical Research, v. 92(C1), p. 725-741.

Cathles, L.M., 1975, The Viscosity of the Earth's Mantle: Princeton University Press, Princeton, 386 pp.

Chao, B.F., and A.Y. Au, 1991, Temporal variation of the Earth's low-degree zonal gravitational field caused by atmospheric mass redistribution: 1980-1988: Journal of Geophysical Research, v. 94(B4), p. 6,569-6,575.

Chao, B.F., and R. Eanes, 1995, Global gravitational changes due to atmospheric mass redistribution as observed by the Lageos nodal residual: Geophysical Journal International, v. 122(3), p. 755-764.

Chao, B.F., and W.P. O'Connor, 1988, Global surface-water-induced seasonal variation in the Earth's rotation, and gravitational fields: Geophysical Journal International, v. 94, p. 263-270.

Chao, B.F., O.L. Colombo, and P.L. Bender, 1996, Global gravitational changes and the mission concept of TIDES: Supplement to EOS, Transactions of the American Geophysical Union, v 77(17), p. S41.

Chen, T.C., M.C. Yen, J. Pfaendtner, and Y.C. Sud, 1996, Annual variation of the global precipitable water and its maintenance: Observation and climate-simulation: Tellus, v. 48(A1), p. 1-16.

Chen, Q., D.H. Bromwich, and L Bai, 1997, Precipitation over Greenland retrieved by a dynamic method and its relation to cyclonic activity: Journal of Climatology, v. 10, in press.

CIGAR, 1990, Study on precise gravity field determination methods and mission requirements: Phase 2: Final Report: Prepared by Cisi ingenierie for the European Space Agency, v. 2.

CIGAR, 1996, Study of advanced reduction methods for spaceborne gravimetry data, and of data combination with geophysical parameters: Phase 4 . H. Sunkel, Project Manager.

Clark, T.A., D.R. Skillman, F.H. Bauer, J.R. O'Donnell, E.C. Pavlis, D.I. Liberman, and F. Bisiacci, 1996, COLIBRI: A low-cost spacecraft design for gravity change studies: Supplement to EOS, Transactions of the American Geophysical Union, v. 77(17), p. S40.

Davis, E.S., W.G. Melbourne, C. Reigber, B.D. Tapley, and M.M. Watkins, 1996, GRACE: An SST mission for gravity mapping: Supplement to EOS, Transactions of the American Geophysical Union, v. 77(17), p. S40.

Dickey, J.O., S.L. Marcus, and R. Hide, 1992, Global propagation of interannual fluctuations in atmospheric angular momentum: Nature, v. 357, p. 484-488.

Dong, D., R.S. Gross, and J.O. Dickey, 1996, Seasonal variations of the Earth's gravitational field: An analysis of atmospheric pressure, ocean tidal, and surface water excitation: Geophysical Research Letters, v. 23(7), p. 725-728.

Douglas, B.C., C.C. Goad, and F.F. Morrison, 1980, Determination of the geopotential from satellite-to-satellite tracking data: Journal of Geophysical Research, v. 85(B10), p. 5,471-5,480.

Dugan, J.T., and DA. Cox, 1994, Water-level changes in the High Plains aquifer—Predevelopment to 1993: U.S. Geological Survey, Water Resources Investigations Report 94-4157, 60 pp.

Dukowicz, J.K., and RD. Smith, 1994, Implicit free-surface method for the Bryan-Cox-Semtner ocean model: Journal of Geophysical Research, v. 99(C4), p. 7,991-8,014.

Dunne, T., and L.B. Leopold, 1978, Water in Environmental Planning: W.H. Freeman, San Francisco, 818 pp.

ESA, 1991, The solid-earth mission ARISTOTELES, in Mattock, C., ed., Proceedings of an International Workshop, Anacapri, Italy, September 23-24, 1991: ESA Special Publication329, 137 pp.

ESA, 1996, Gravity field and steady-state ocean circulation mission: Reports for Assessment; the Nine Candidate Earth Explorer Missions, ESA SP-1196(1), 77 pp.

Fischell, RE., and V.L. Pisacane, 1978, A drag-free lo-lo satellite system for improved gravity field measurements, *in* An International Symposium on the Application of Geodesy to Geodynamics: Proceedings of the 9th GEOP Conference, Reports of the Department of Geodetic Science and Surveying, Report 280, Ohio State University, Columbus.

Fitzgerald, P.G., 1994, Thermochronological constraints on post-Paleozoic tectonic evolution of the central Transantarctic Mountains, Antarctica: Tectonics, v. 13 (4), p. 818-836.

Forsyth, D.W., 1985, Subsurface loading and estimates of the flexural rigidity of continental lithosphere: Journal of Geophysical Research, v. 90, p. 12,623-12,632.

Forte, A.M., A.M. Dziewonski, and RL. Woodward, 1993, Aspherical structure of the mantle, tectonic plate motions, nonhydrostatic geoid, and topography of the core-mantle boundary, *in*Le Mouel, J.L, DE. Smylie, and T. Herring, eds., Dynamics of Earth's Deep Interior and Earth Rotation: Geophysical Monograph, v. 72, p. 135-166.

Forte, A.M., and J.X. Mitrovica, 1996, New inferences of mantle viscosity from joint inversion of long-wavelength mantle convection and post-glacial rebound data: Geophysical Research Letters, v. 23(10), p. 1,147-1,150.

Freund, LB., and D.M. Barnett, 1976, A two-dimensional analysis of surface deformation due to dip-slip faulting: Bulletin of the Seismological Society of America, v. 66(3), p. 667-675.

Frey, H., J. Abshire, B. Bills, J. Connerey, B. Johnson, R. Langel, F. Lerch, S. Nerem, E. Pavlis, D. Skillman, D. Smith, P. Taylor, and C. Voorhies, 1993, GAMES: A Gravity-And-Magnetics-Experiment-Satellite for oceanography and solid Earth science: Supplement to EOS, Transactions of the American Geophysical Union, v. 74(14), p. 97.

Fu, L.-L., EJ. Christensen, C.A. Yamarone Jr., M. Lefebvre, Y. Ménard, M. Dorrer, and P. Escudier, 1994. TOPEX/POSEIDON mission overview: Journal of Geophysical Research, v. 99(C12), p. 24,369-24,381.

Ganachaud, A., C. Wunsch, M.C. Kim, and B. Tapley, 1997, Combination of TOPEX/POSEIDON data with a hydrographic inversion for determination of the oceanic general circulation and its relation to geoid accuracy: Geophysical Journal International, v. 128(3), p. 708-722.

Gegout, P., and A. Cazenave, 1993, Temporal variations of the Earth gravity field for 1985-1989 derived from Lageos: Geophysical Journal International, v. 114(2), p. 347-359.

Giovinetto, M.B., 1964, The drainage systems of Antarctica: Accumulation, in Mellor, M., ed, Antarctic Snow and Ice Studies: American Geophysical Union, Antarctic Research Series, v. 2, p. 127-155.

Gleick, P.H., ed., 1993, Water In Crisis: Oxford University Press, New York, 473 pp.

Hager, B.H., and M.A. Richards, 1989, Long-wavelength variations in Earth's geoid; physical models and dynamical implications, *in*O'Nions, R.K., and B. Parsons, eds., Seismic Tomography and Mantle Circulation: Philosophical Transactions of the Royal Society of London, Series A, v. 328(1599), p. 309-327.

Han, D., and J. Wahr, 1995, The viscoelastic relaxation of a realistically stratified Earth, and a further analysis of post-glacial rebound: Geophysical Journal International, v. 120(2), p. 287-311.

Hasselmann, K., and R Giering, 1996, Impact of geoid on ocean circulation retrieval, Part 1: The global ocean circulation: Final Report, ESTEC Contract No. 11528/95/NL/CN, 26 pp.

Haxby, W.F., G.D. Karner, J.L. LaBrecque, and J.K. Weissel, 1983, Digital images of combined oceanic and continental data sets and their use in tectonic studies: EOS, Transactions of the American Geophysical Union, v. 64, p. 995-1,004.

Heiskanen, W.A., and H. Moritz, 1967, Physical Geodesy: W.H. Freeman and Co., San Francisco, 364 pp.

Holton, J.R, 1979, An Introduction to Dynamic Meteorology, 2nd edition: International Geophysics Series, v. 23, Academic Press, New York, 391 pp.

Huang, J., H.M. van den Dool, and K.P. Georgakakos, 1996, Analysis of model-calculated soil moisture over the United

States (1931-1993) and applications to long-range temperature forecasts: Journal of Climate, v. 9(6), p. 1,350-1,362.

IPCC, 1996, Climate Change 1995: Impacts, Adaptations and Mitigation of Climate Change: Scientific-Technical Analyses, Contribution of Working Group II to the Second Assessment, *in*Bruce, J., H. Lee, and E. Haites, eds., Report of the Intergovernmental Panel on Climate Change: Cambridge University Press, New York, 464 pp.

Isacks, B.L., 1988, Uplift of the Central Andean Plateau and bending of the Bolivian Orocline: Journal of Geophysical Research, v. 93(B4), p. 3,211-3,231.

Jackson, J.D., 1975, Classical Electrodynamics, 2nd edition: J. Wiley & Sons, New York, 848 pp.

James, T.S., and E.R. Ivins, 1995, Present-day Antarctic ice mass changes and crustal motion: Geophysical Research Letters, v. 22(8), p. 973-976.

Jeffreys, H., 1952, The Earth, Its Origin, History and Physical Constitution, 3rd edition: Cambridge University Press, Cambridge,420 pp.

Jekeli, C., 1981, Alternative methods to smooth the Earth's gravity field: Reports of the Department of Geodetic Science and Surveying, Report 327, Ohio State University, Columbus.

Jekeli, C., 1996, Methods to reduce aliasing in spherical harmonic analysis, *in*Rapp, RH., A.A. Cazenave, and RS. Nerem, eds., Global Gravity Field and Its Temporal Variations: International Association of Geodesy Symposium 116, Springer Verlag, New York, p. 121-130.

Jekeli, C., and RH. Rapp, 1980, Accuracy of the determination of mean anomalies and mean geoid undulations from a satellite gravity field mapping mission: Reports of the Department of Geodetic Science and Surveying, Report 307, Ohio State University, Columbus, 22 pp.

Jekeli, C., and T.N. Upadhyay, 1990, Gravity estimation from STAGE, a satellite-to-satellite tracking mission: Journal of Geophysical Research, v. 95(B7), p. 10,973-10,985.

Jin, Y., M.K. McNutt, and Y.S. Zhu, 1994, Evidence from gravity and topography data for folding of Tibet: Nature, v. 371, p. 669-674.

Jovanovitch, D.B., M.I. Husseini, and M.A. Chinnery, 1974, Elastic dislocations in a layered half-space; I. Basic theory and numerical methods: The Geophysical Journal of the Royal Astronomical Society, v. 39(2), p. 205-217.

Kahn, W.D., and F.O. von Bun, 1985, Error analyses for a gravity gradiometer mission: IEEE Transactions on Geoscience and Remote Sensing, v. GE-23(4), p. 527-530.

Kalnay, E., and 21 co-authors, 1996, The NCEP/NCAR 40-year reanalysis project: Bulletin of the American Meteorological Society, v. 77 (3), p. 437-471.

Karner, G.D., and A.B. Watts, 1982, On isostasy at Atlantic-type continental margins: Journal of Geophysical Research, v. 87(B4), p. 2,923-2,948.

Kaula, W.M., 1959, Statistical and harmonic analysis of gravity: Journal of Geophysical Research, v. 64, p. 2,401-2,421.

Kaula, W.M., 1963, Determination of the earth's gravitational field: Reviews of Geophysics, v. 1(4), p. 507-551.

Kaula, W.M., 1966, Global harmonic and statistical analysis of gravity, *in*Orlin, H., ed., Extension of Gravity Anomalies to Unsurveyed Areas, American Geophysical Union Monograph 9, p. 58-67.

Kaula, W.M., 1983, Inference of variations in the gravity field from satellite-to-satellite range rate: Journal of Geophysical Research, v. 88 (B10), p. 8,345-8,349.

Keating, T., P. Taylor, W. Kahn, and F. Lerch, eds., 1986, Geopotential Research Mission, Science, Engineering, and Program Summary: NASA Technical Memorandum 86240, Washington, D.C., 208 pp.

King, S.D., and G. Masters, 1992, An inversion for radial viscosity structure using seismic tomography: Geophysical Research Letters, v. 19, p. 1,551-1,554.

Kono, M., Y. Fukao, and A. Yamamoto, 1989, Mountain building in the Central Andes: Journal of Geophysical Research, v. 94(B4), p. 3,891-3,905.

Lambeck, K., P. Johnston, and M. Nakada, 1990, Holocene glacial rebound and sea-level change in NW Europe: Geophysical Journal International, v.103(2), p. 451-468.

Lemoine, F.G., E.C. Pavlis, S.M. Klosko, N.K. Pavlis, J.C. Chan, S. Kenyon, R. Trimmer, R. Salman, RH. Rapp, and R.S. Nerem, 1996, Latest results from the joint NASA GSFC and DMA gravity model project: Supplement to EOS, Transactions of the American Geophysical Union, v. 77(17), p. S41.

Levitus, S., and T. Boyer, 1994, World Ocean Atlas, Volume 4, Temperature: NOAA National Environmental Satellite, Data, and Information Service, Washington, D.C., 117 pp.

Levitus, S., R Burgett, and T.P. Boyer, 1994, World Ocean Atlas, Volume 3, Salinity: NOAA National Environmental Satellite, Data, and Information Service, Washington, D.C., 99 pp.

Lowry, A.R, and R.B. Smith, 1994, Flexural rigidity of the Basin and Range-Colorado Plateau-Rocky Mountain transition from coherence analysis of gravity and topography: Journal of Geophysical Research, v. 99(B10), p. 20,123-20,140.

MacRobert, T.M., 1967, Spherical Harmonics; an Elementary Treatise on Harmonic Functions, with Applications, 3rd edition: International Series of Monographs in Pure and Applied Mathematics, v. 98, Pergamon Press, New York, 349 pp.

Marchese, P.J., and A.L. Gordon, 1996, The eastern boundary of the Gulf Stream recirculation: Journal of Marine Research, v. 54(3), p. 521-540.

Marks, K.M., 1996, Resolution of the Scripps/NOAA marine gravity field from satellite altimetry: Geophysical Research Letters, v. 23(16), p. 2,069-2,072.

Masek, J.G., B.L. Isacks, T.L. Gubbels, and E.J. Fielding, 1994, Erosion and tectonics at the margins of continental plateaus: Journal of Geophysical Research, v. 99(B7), p. 13,941-13,956.

Masters, G., S. Johnson, G. Laske, and H. Bolton, 1996, A shear-velocity model of the mantle: Philosophical Transactions of the Royal Society of London, Series A, v. 354, p. 1,385-1,411.

McNutt, M.K., 1984, Lithospheric flexure and thermal anomalies: Journal of Geophysical Research, v. 89(B13), p. 11,180-11,194.

McNutt, M.K., M. Diament, and M.G. Kogan, 1988, Variations of elastic plate thickness at continental thrust belts: Journal of Geophysical Research, v. 93(B8), p. 8,825-8,838.

Meier, M.F., 1984, Contribution of small glaciers to global sea level: Science, v. 226(4681), p. 1,418-1,421.

Minster, J.F., and P. LeGrand, 1996, Impact of geoid on ocean circulation retrieval , Final Sub-contract Report: ESTEC Contract No. 11528/95/NL/CN.

Mitrovica J., and W.R. Peltier, 1992, Constraints on mantle viscosity from relative sea level variations in Hudson Bay: Geophysical Research Letters, v. 19(12), p. 1,185-1,188.

Mitrovica, J.X., and W.R Peltier, 1993, Present-day secular variations in the zonal harmonics of the Earth's geopotential: Journal of Geophysical Research, v. 98(B3), p. 4,509-4,526.

Mo, K.C., J.O. Dickey, and S.L. Marcus, 1997, Interannual fluctuations in atmospheric angular momentum simulated by the

National Centers for Environmental Prediction medium range forecast model: Journal of Geophysical Research, in press.
Morgan, S.H., and H.-J. Paik, eds., 1989, Superconducting Gravity Gradiometer Mission: NASA Technical Memorandum 4091, Washington, D.C., 35 pp.
NASA, 1987, Geophysical and Geodetic Requirements for Global Gravity Field Measurements, 1987-2000: Report of a Gravity Workshop, Colorado Springs, CO, NASA Geodynamics Branch, Division of Earth Science and Applications, Washington, D.C., 45 pp.
NASA, 1991, Solid Earth Science in the 1990s; Volume 2—Panel Reports: NASA Technical Memorandum 4256, v. 2, Washington, D.C., 296 pp.
NRC, 1979, Applications of a Dedicated Gravitational Satellite Mission: National Academy Press, Washington, D.C., 53 pp.
NRC, 1982, A Strategy for Earth Science from Space in the 1980's: Part I: Solid Earth and Oceans: National Academy Press, Washington, D.C., 99 pp.
NRC, 1986, Global Change in the Geosphere-Biosphere; Initial Priorities for an IGBP: National Academy Press, Washington, D.C., 91 pp.
NRC, 1994, The Ocean's Role in Global Change: National Academy Press, Washington, D.C., 85 pp.
NRC, 1995, Airborne Geophysics and Precise Positioning: Scientific Issues and Future Directions: National Academy Press, Washington, D.C., 111 pp.
Nerem, R.S., B.F. Chao, A.Y. Au, J.C. Chan, S.M. Klosko, N.K. Pavlis, and RG. Williamson, 1993a, Temporal variations of the Earth's gravitational field from satellite laser ranging to Lageos: Geophysical Research Letters, v. 20(7), p. 595-598.
Nerem, RS., B.F. Chao, J.C. Chan, S.M. Klosko, N.K. Pavlis, and RG. Williamson, 1993b, Temporal variations of the Earth's gravitational field: Measurement and geophysical modeling, Supplement to Annales Geophysicae, v. 11, p. C 110.
Nerem, RS., C. Jekeli, and W.M. Kaula, 1995, Gravity field determination and characteristics: Retrospective and prospective: Journal of Geophysical Research, v. 100(B8), p. 15,053-15,074.
Peltier, W.R, 1994, Ice age paleotopography: Science, v. 265, p. 195-201.
Peltier, W.R, 1985, The LAGEOS constraint on deep mantle viscosity; results from a new normal mode method for the inversion of viscoelastic relaxation spectra: Journal of Geophysical Research, v. 90(B1 1), p. 9,411-9,421.
Peltier, W.R, and X Jiang, 1996, Glacial isostatic adjustment and Earth rotation; refined constraints on the viscosity of the deepest mantle: Journal of Geophysical Research, v. 101(B2), p. 3,269-3,290.
Peltier, W.R., A.M. Forte, J.X. Mitrovica, and A.M. Dziewonski,1992, Earth's gravitational field; seismic tomography resolves the enigma of the Laurentian anomaly: Geophysical Research Letters, v. 19(15), p. 1,555-1,558.
Peixoto, J.P., and A.H. Oort, 1992, Physics of Climate: American Institute of Physics, New York, 520 pp.
Phipps Morgan, J., and P.M. Shearer, 1993, Seismic constraints on mantle flow and topography of the 660-km discontinuity: Evidence for whole-mantle convection: Nature, v. 365, p. 506-511.
Pisacane, V.L., J.C. Ray, J.L. MacArthur, and S.E. Bergeson-Willis, 1982, Description of the dedicated gravitational satellite mission (GRAVSAT): IEEE Transactions on Geoscience and Remote Sensing, v. GE-20(3), p. 315-321.
Press, W.H., S.A. Teukolsky, W.T. Vetterling, and B.P. Flannery, 1992, Numerical Recipes in FORTRAN; the Art of Scientific Computing, 2nd edition: Cambridge University Press, New York, 963 pp.
Rapp, RH., 1989, Signals and accuracies to be expected from a satellite gradiometer mission: Manuscripta Geodaetica, v. 14(1), p. 3642.
Rapp, RH., C. Zhang, and Y. Yi, 1996, Analysis of dynamic ocean topography using TOPEX data and orthonormal functions: Journal of Geophysical Research , v. 101(C10), p. 22,583-22,598.
Reigber, Ch., P. Schwintzer, Ph. Hartl, K.H. Ilk, K.F. Wakker, B.A.C. Ambrosius, and H. Leenman, 1987, Study of a satellite-to-satellite tracking gravity mission: ESA Contract Report ESTEC/6557/85/NL/PP(SC), Munich, 323 pp.
Reigber, Ch., Z. Kang, R König, and P. Schwintzer, 1996, CHAMP A minisatellite mission for geopotential and atmospheric research: Supplement to EOS, Transactions of the American Geophysical Union, v. 77(17), p. S40.
Ricard, Y., M. Richards, C. Lithgow-Bertelloni, and Y. LeStunff, 1993, A geodynamic model of mantle density heterogeneity: Journal of Geophysical Research, v. 98(B12), p. 21,895-21,909.
Richards, M.A., and B.H. Hager, 1984, Geoid anomalies in a dynamic Earth: Journal of Geophysical Research, v. 89(B7), p. 5,987-6,002.
Richards, M., Y. Ricard, and P. Bunge, 1995, Long-term rotational dynamics and mantle convection: International Union of Geodesy and Geophysics, General Assembly, Boulder, CO., v. 21, Week B, p. 22.
Rubincam, D.P., 1984, Postglacial rebound observed by Lageos and the effective viscosity of the lower mantle: Journal of Geophysical Research, v. 89(B2), p. 1,077-1,087.
Rummel, R., and EJ.O. Schrama, 1991, Two complementary systems on-board 'Aristoteles': Gradio and GPS: ESA Journal, v. 15(2), p. 135-139.
Rummel, R., and P. Schwintzer, 1994, A major STEP for Geodesy: Report of the STEP Geodesy Working Group, Munich/Potsdam.
Rummel, R., and M. van Gelderen, 1995, Meissl scheme-spectral characteristics of physical geodesy: Manuscripta Geodaetica, v. 20(5), p. 379-385.
Sabadini, R., and G. Spada, 1995, True polar wander, recent achievements: International Union of Geodesy and Geophysics, General Assembly, Boulder, CO., v. 21, Week B, p. 22.
Sabadini, R., D.A. Yuen, and P. Gasperini, 1988, Mantle rheology and satellite signatures from present-day glacial forcings: Journal of Geophysical Research, v. 93(B1), p. 437-447.
Saha, K, H. van den Dool, and S. Saha, 1994, On the annual cycle in surface pressure on the Tibetan Plateau compared to its surroundings: Journal of Climate, v. 7(12), p. 2,014-2,019.
Sandwell, D.T., 1992, Antarctic marine gravity field from high-density satellite altimetry: Geophysical Journal International, v. 109(2), p. 437-448.
Sandwell, D.T., and D.C. McAdoo, 1990, High-accuracy, high-resolution gravity profiles from two years of the Geosat Exact Repeat Mission: Journal of Geophysical Research, v. 95(C3), p. 3,049-3,060.
Sandwell, D.T., and W.H.F. Smith, 1997, Marine gravity anomalies from Geosat and ERS-1 altimetry: Journal of Geophysical Research, v. 102, p. 10,039-10,054.
Sansone, G., 1991, Orthogonal Functions, revised English edition: Dover, New York, 411 pp.
Savage, J.C., 1983, A dislocation model of strain accumulation and release at a subduction zone: Journal of Geophysical Research, v. 88(B6), p. 4,984-4,996.

Savage, J.C., 1984, Local gravity anomalies produced by dislocation sources: Journal of Geophysical Research, v. 89(B3), p. 1,945-1,952.

Schrama, E.J.O., 1991, Gravity field error analysis: Applications of Global Positioning System receivers and gradiometer on low orbiting platforms : Journal of Geophysical Research, v. 96(B12), p. 20,041-20,051.

Sclater, J.G., C. Jaupart, and D. Galson, 1980, The heat flow through oceanic and continental crust and the heat loss of the Earth: Reviews of Geophysics and Space Physics, v. 18(1), p. 269-311.

Semtner, A.J., and R.M. Chervin, 1992, Ocean general circulation from an eddy-resolving model: Journal of Geophysical Research, v. 97(C), p. 5,493-5,590.

Singh, S.J., 1970, Static deformation of a multilayered half-space by internal sources: Journal of Geophysical Research, v. 75(A17), p. 3,257-3,263.

Smith, W.H.F., 1993, On the accuracy of digital bathymetric data: Journal of Geophysical Research, v. 98(B6), p. 9,591-9,603.

Smith, W.H.F., and D.T. Sandwell, 1994, Elastic lithosphere thickness estimated from dense satellite altimetry and sparse shipboard bathymetry: Supplement to EOS, Transactions of the American Geophysical Union, v. 75(44), p. 154.

Smith, W.H.F., and D.T. Sandwell, 1995a, Marine gravity field from declassified Geosat and ERS-1 altimetry: Supplement to EOS, Transactions of the American Geophysical Union, v. 76(46), p. F156.

Smith, W.H.F., and D.T. Sandwell, 1995b, Oceanographic "pseudogravity" in marine gravity fields derived from declassified Geosat and ERS-I altimetry: Supplement to EOS, Transactions of the American Geophysical Union, v. 76(46), p. F151.

Smith, W.H.F., and D.T. Sandwell, 1995c, Global comparison of gravity anomalies measured by ships and derived from dense satellite altimetry: Supplement to EOS, Transactions of the American Geophysical Union, v. 76(17), p. S89.

Smith, W.H.F., H. Staudigel, A.B. Watts, and M.S. Pringle, 1989, The Magellan Seamounts: Early Cretaceous record of the South Pacific isotopic and thermal anomaly: Journal of Geophysical Research, v. 94(B8), p. 10,501-10,523.

Stammer, D., R Tokmakian, A. Semtner, and C. Wunsch, 1996, How well does a 1/4° global circulation model simulate the large-scale oceanic observations?: Journal of Geophysical Research, v. 101(C10), p. 25,779-25,811.

Subcommittee on Global Change Research, 1996, Our Changing Planet: The FY 1997 U.S. Global Change Research Program: Office of Science and Technology Policy, Washington, D.C., 162 pp.

Tapley, B.D., C.K. Shum, J.C. Ries, S.R. Poole, P.A.M. Abusali, RJ. Eanes, M.C. Kim, H.J. Rim, and B.E. Schutz, 1996, An improved Earth gravity field model: Supplement to EOS, Transactions of the American Geophysical Union, v. 77(17), p. S42.

Tapley, B.D., M.M. Watkins, J.C. Ries, G.W. Davis, R.J. Eanes, S.R. Poole, H.J. Rim, B.E. Schutz, C.K. Shum, RS. Nerem, F.J. Lerch, J.A. Marshall, S.M. Klosko, N.K. Pavlis, and R.G. Williamson, 1996, The Joint Gravity Model 3: Journal of Geophysical Research, v. 101 (B12), p. 28,029-28,049.

Titus, J.G., RA. Park, S.P. Leatherman, J.R. Weggel, M.S. Greene, P.W. Mausel, S. Brown, C. Gaunt, M. Trehan, and G. Yohe, 1991, Greenhouse effect and sea level rise: Potential loss of land and the cost of holding back the sea: Coastal Management, v. 19, p. 171-204.

Trenberth, K.E., 1981, Seasonal variations in global sea level pressure and the total mass of the atmosphere: Journal of Geophysical Research, v. 86(C6), p. 5238-5,246.

Trenberth, K.E., and C.J. Guillemot, 1994, The total mass of the atmosphere: Journal of Geophysical Research, v. 99(D1 1), p. 23,079-23,088.

Trupin, A.S., 1993, Effects of polar ice on the Earth's rotation and gravitational potential: Geophysical Journal International, v. 113(2), p. 273-283.

Tsimplis, M.N., and P.L. Woodworth, 1994, The global distribution of the seasonal sea level cycle calculated from coastal tide gauge data: Journal of Geophysical Research, v. 99(C8), p. 16,031-16,039.

Tushingham, A.M., and W.R. Peltier, 1991, ICE-3G; a new global model of late Pleistocene deglaciation based upon geophysical predictions of post-glacial relative sea level change: Journal of Geophysical Research, v. 96(B3), p. 4497-4523.

Van den Dool, H.M., and S. Saha, 1993, Seasonal redistribution and conservation of atmospheric mass in a general circulation model: Journal of Climate, v. 6(1), p. 22-30.

Van den Dool, H.M., J. Schemm, and S. Saha, 1995, On the climatological annual cycle in global mean atmospheric pressure and hydrology as revealed by NCEP/NCAR ReAnalysis: Proceedings of the 20th Climate Diagnostics Workshop, Seattle, October 23-27, 1995, 2 pp.

Van den Dool, H.M., S. Saha, J. Schemm, and J. Huang, 1996, Global climatology in motion: The (semi) diurnal variation of climatology and atmospheric tides in reanalysis: Proceedings of the 21st Climate Diagnostics and Prediction Workshop, Huntsville, Alabama

Visser, P.N.A.M., K.F. Wakker, and B.A.C. Ambrosius, 1994, Global gravity field recovery from the ARISTOTELES satellite mission: Journal of Geophysical Research, v. 99(B2), p. 2,841-2,851.

Wagner, C.A., 1983, Direct determination of gravitational harmonics from low-low Gravsat data: Journal of Geophysical Research, v. 88 (B12), p. 10,309-10,321.

Walsh, J.B., and J.R. Rice, 1979, Local changes in gravity resulting from deformation: Journal of Geophysical Research, v. 84(B1), p. 165-170.

Warrick, RA., C. Le Provost, M. Meier, J. Oerlemans, and P.L. Woodworth, 1996, Changes in sea level, *in*Houghten, J.T., L.G. Meira Filho, B.A. Callander, N. Harris, A. Kattenberg, and K. Maskell, eds., Climate Change 1995: The Science of Climate Change: Contribution of Working Group I to the Second Assessment Report of the Intergovernmental Panel on Climate Change: Cambridge University Press, New York, p. 359-405.

Watts, A.B., J.H. Bodine, and N.M. Ribe, 1980, Observations of flexure and the geological evolution of the Pacific Ocean basin: Nature, v. 283, p. 532-537.

Wessel, P., 1992, Thermal stresses and the bimodal distribution of elastic thickness estimates of the oceanic lithosphere: Journal of Geophysical Research, v. 97, p. 14,177-14,193.

Wessel, P., and A.B. Watts, 1988, On the accuracy of marine gravity measurements: Journal of Geophysical Research, v. 93(B 1), p. 393-413.

Willet, S.D., and C. Beaumont, 1994, Subduction of Asian lithospheric mantle beneath Tibet inferred from models of continental collision: Nature, v. 369, p. 642-645.

Woodworth, P.L., J.M. Vassie, C.W. Hughes, and M.P. Meredith, 1996, A test of the ability of TOPEX/POSEIDON to monitor

flows through the Drake Passage: Journal of Geophysical Research, v. 101(C5),p. 11,935-11,948.

World Resources Institute, 1990, World Resources 1990-91: Oxford University Press, New York, 383 pp.

Wunsch, C., 1996, The Ocean Circulation Inverse Problem: Cambridge University Press, New York, 442 pp.

Wunsch, C., and D. Stammer, 1997, Atmospheric loading and the oceanic "inverted barometer" effect: Review of Geophysics, v. 35, p. 79-107.

Yionoulis, S.M., and V.L. Pisacane, 1985, Geopotential research mission: Status report: IEEE Transactions on Geoscience and Remote Sensing, v. GE-23(4), p. 511-516.

Yoder, C.F., J.G. Williams, J.O. Dickey, B.E. Schutz, R.J. Eanes, and B.D. Tapley, 1983, Secular variations of Earth's gravitational harmonic J_2 coefficient from Lageos and nontidal acceleration of Earth rotation: Nature, v. 303, p. 757-762.

Yuen, D.A., R. Sabadini, and E.V. Boschi, 1982, Viscosity of the lower mantle as inferred from rotational data: Journal of Geophysical Research, v. 87(B13), p. 10,745-10,762.

Zuber, M.T., T.D. Bechtel, and D.W. Forsyth, 1989, Effective elastic thicknesses of the lithosphere and mechanisms of isostatic compensation in Australia: Journal of Geophysical Research, v. 94(B7), p. 9,353-9,367.